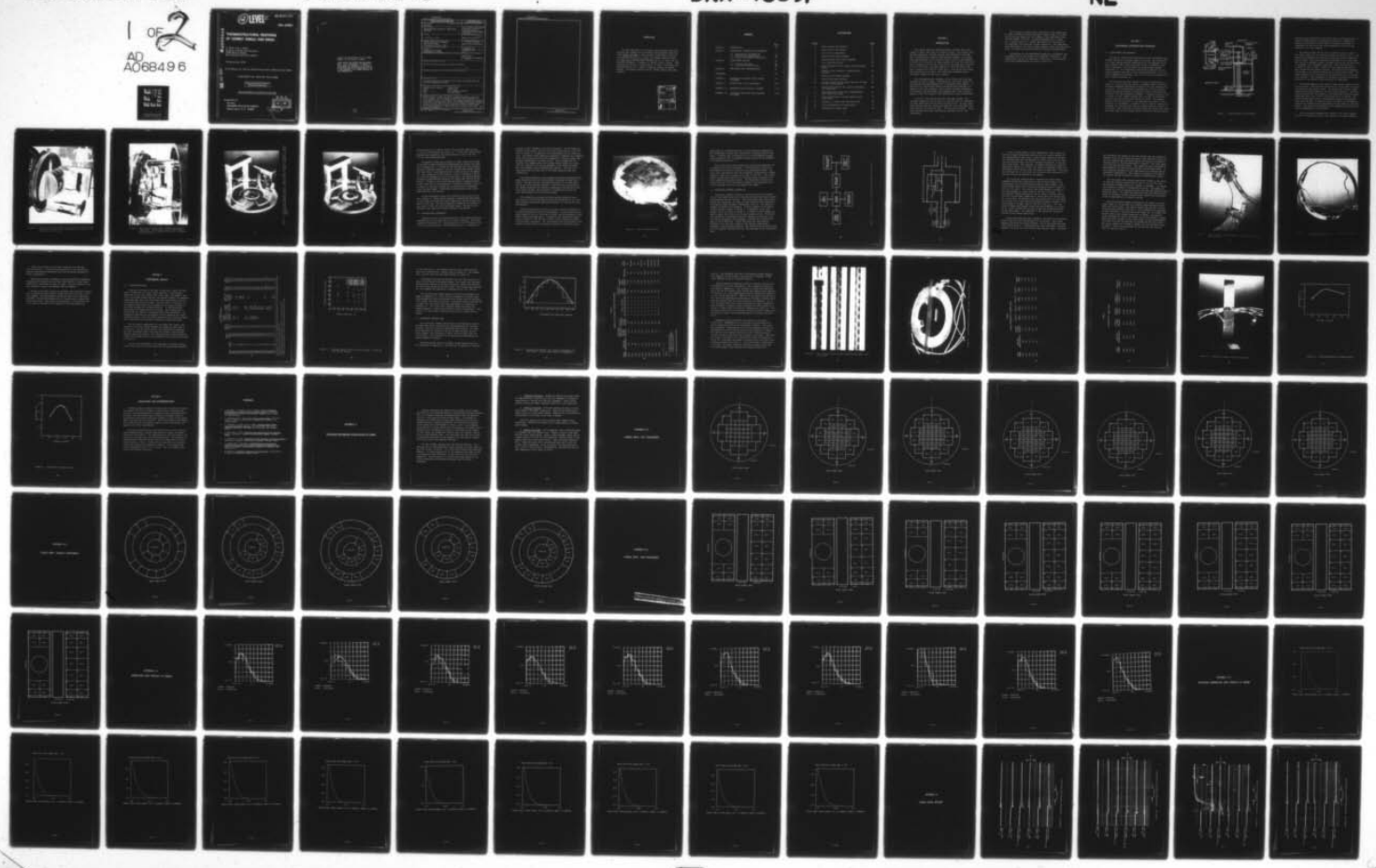
AD-A068 496 PHYSICS INTERNATIONAL CO SAN LEANDRO CALIF F/G 11/2
THERMOSTRUCTURAL RESPONSE OF CERMET ANNULI AND RINGS.(U)
NOV 78 E V BUCK, J SHEA DNA001-78-C-0068
UNCLASSIFIED PIFR-1148 DNA-4689F NL

1 OF 2
AD A068496



AD-E300 510

(12) LEVEL III

DNA 4689F

AD A068496

THERMOSTRUCTURAL RESPONSE OF CERMET ANNULI AND RINGS

V. Buck and J. Shea
Physics International Company
2700 Merced Street
San Leandro, California 94577

15 November 1978

Final Report for Period 15 December 1977—15 November 1978

CONTRACT No. DNA 001-78-C-0068

DDC FILE COPY

APPROVED FOR PUBLIC RELEASE;
DISTRIBUTION UNLIMITED.

THIS WORK SPONSORED BY THE DEFENSE NUCLEAR AGENCY
UNDER RDT&E RMSS CODE B342078464 N99QAXAH12301 H2590D.

Prepared for
Director
DEFENSE NUCLEAR AGENCY
Washington, D. C. 20305

DDC
RECEIVED
MAY 11 1979
B

79 04 04 026

Destroy this report when it is no longer needed. Do not return to sender.

PLEASE NOTIFY THE DEFENSE NUCLEAR AGENCY, ATTN: TISI, WASHINGTON, D.C. 20305, IF YOUR ADDRESS IS INCORRECT, IF YOU WISH TO BE DELETED FROM THE DISTRIBUTION LIST, OR IF THE ADDRESSEE IS NO LONGER EMPLOYED BY YOUR ORGANIZATION.

DNA PRINTING PLANT

UNCLASSIFIED

SECURITY CLASSIFICATION OF THIS PAGE *(When Data Entered)*

REPORT DOCUMENTATION PAGE		READ INSTRUCTIONS BEFORE COMPLETING FORM
1. REPORT NUMBER DNA 4689F	2. GOVT ACCESSION NO.	3. RECIPIENT'S CATALOG NUMBER
4. TITLE *(and Subtitle)* THERMOSTRUCTURAL RESPONSE OF CERMET ANNULI AND RINGS		5. TYPE OF REPORT & PERIOD COVERED Final Report for Period 15 Dec 77—15 Nov 78 6. PERFORMING ORG. REPORT NUMBER PIFR--1148
7. AUTHOR(s) V. Buck and J. Shea		8. CONTRACT OR GRANT NUMBER(s) DNA 001-78-C-0068
9. PERFORMING ORGANIZATION NAME AND ADDRESS Physics International Company 2700 Merced Street San Leandro, California 94577		10. PROGRAM ELEMENT, PROJECT, TASK AREA & WORK UNIT NUMBERS NWED Subtask N99QAXAH123-01
11. CONTROLLING OFFICE NAME AND ADDRESS Director Defense Nuclear Agency Washington, D.C. 20305		12. REPORT DATE 15 November 1978 13. NUMBER OF PAGES 106
14. MONITORING AGENCY NAME & ADDRESS*(if different from Controlling Office)*		15. SECURITY CLASS *(of this report)* UNCLASSIFIED 15a. DECLASSIFICATION/DOWNGRADING SCHEDULE

16. DISTRIBUTION STATEMENT *(of this Report)*

Approved for public release; distribution unlimited.

G27044

17. DISTRIBUTION STATEMENT *(of the abstract entered in Block 20, if different from Report)*

18. SUPPLEMENTARY NOTES

This work sponsored by the Defense Nuclear Agency under RDT&E RMSS Code B342078464 N99QAXAH12301 H2590D.

19. KEY WORDS *(Continue on reverse side if necessary and identify by block number)*

Thermostructural Response	Electron Beam
Cermet	Strain Gauge
Annuli	Quartz Pressure Transducer
Rings	High Speed Movie

20. ABSTRACT *(Continue on reverse side if necessary and identify by block number)*

Thermostructural response experiments have been performed on annuli and rings of cermet. Thermal loading was produced by energy deposition of a pulsed electron beam. The thermostructural response was monitored by strain gauges and a high speed movie camera. The loading conditions were determined from electron beam diagnostics and from quartz pressure transducer records. Specimens were subjected to doses ranging from 58 cal/gm to 440 cal/gm. Front surface material was removed with doses in excess of 100 cal/gm. One ring was fractured.

DD FORM 1 JAN 73 1473 EDITION OF 1 NOV 65 IS OBSOLETE

UNCLASSIFIED

SECURITY CLASSIFICATION OF THIS PAGE *(When Data Entered)*

PREFACE

The work described in this report was performed by Physics International Company for the Defense Nuclear Agency under contract DNA001-78-C-0068. The principal investigator at Physics International was Mr. E. V. Buck; the project supervisor was Dr. James Shea; and the chief engineer was Mr. A. York, who was assisted by Messrs. B. Burgess, G. Navarro, and G. Harvey. Also contributing were Mr. H. Hyatt and Mr. A. Dunn. The project was coordinated with Mr. R. Walz of Lockheed Missiles and Space Company. The project monitor was Mr. Donald Kohler, DNA, SPAS Division.

ACCESSION for
NTIS White Section
DDC Buff Section
UNANNOUNCED
JUSTIFICATION
BY
DISTRIBUTION/AVAILABILITY CODES
Dist. AVAIL. and/or SPECIAL
A

79 04 04 026

CONTENTS

		Page
SECTION 1	INTRODUCTION	5
SECTION 2	EXPERIMENTAL APPARATUS AND TECHNIQUES	7
	2.1 Experimental Configuration	7
	2.2 Electron Beam Diagnostics	14
	2.3 Structural Response Diagnostics	17
SECTION 3	EXPERIMENTAL RESULTS	25
	3.1 Electron Beam Data	25
	3.2 Structural Response Data	28
SECTION 4	CONCLUSIONS AND RECOMMENDATIONS	39
REFERENCES		40
APPENDIX A	TECHNIQUE FOR BONDING STRAIN GAUGES TO CERMET	A-1
APPENDIX B	FLUENCE MAPS, FLAT CALORIMETER	B-1.1
APPENDIX C-1	NORMALIZED DOSE PROFILES IN CARBON	C-1.1
APPENDIX C-2	CALCULATED NORMALIZED DOSE PROFILES IN CERMET	C-2.1

ILLUSTRATIONS

Figure		Page
1	Electron Beam Test Geometry	8
2	Front View of Ring Holder	10
3	Rear View of Ring Holder	11
4	Front View of Annulus Holder	12
5	Annulus Holder With Shields Removed	13
6	Flat Calorimeter Array	16
7	Block Diagram of Strain Gauge Instrumentation System	18
8	Bridge Circuit Schematic (Simplified for Clarity)	19
9	Annulus Strain Gauge Packages	22
10	Ring Strain Gauge Packages	23
11	Average Fluence Versus Radial Position in Beam for Four Mirror Ratios	27
12	Fluence Distribution Over Curved Calorimeter for Pulse 4344	29
13	Film Record from Pulse 4335, Approximately 5800 Frames per Second	32
14	Coning Deformation in Cermet Annulus from Pulse 4338	33
15	Fracture in Cermet Ring from Pulse 4349	36
16	Coning Deformation of Cermet Annuli	37
17	Distortion of Cermet Rings	38

SECTION 1

INTRODUCTION

This report describes thermostructural response tests performed on annuli and rings of a special cermet. The thermal loading was induced by a pulsed electron beam generated by the DNA OWL II accelerator at Physics International Company. The cermet test specimens were in the shape of annuli with an inner diameter of 10.16 cm (4.00 inch), an outer diameter of 15.24 cm (6.00 inch), and a thickness of 0.203 cm (0.080 inch); the rings had a width of 2.54 cm (1.00 inch), an outer diameter of 14.96 cm (5.89 inch), and a thickness of 0.206 cm (0.081 inch). The annuli were irradiated uniformly on one side. The rings were irradiated over a 180 degree segment of the outer surface.

The thermostructural responses of the annuli and rings were measured by strain gauges. Simultaneously, the front surface of the specimen was photographed with a high-speed movie camera. In addition, the stress wave loading conditions were measured on a separate flat test specimen, using a quartz pressure transducer. The electron beam environment was diagnosed with diode monitors, graphite-block calorimeters, and graphite-foil stack calorimeters.

A total of five annuli and five rings were tested. The fluences ranged from 9.7 cal/cm^2 to 55 cal/cm^2 and the corresponding peak doses were from 58 cal/gm to 440 cal/gm. At least some front surface material removal was observed in all specimens with peak doses of 100 cal/gm or more. One ring was fractured. Structural response data were successfully obtained from all ten experiments.

The structural response data collected in this program will be used by Lockheed Missiles and Space Company (LMSC) for modeling studies and comparison with computer code predictions under Contract DNA001-78-C-0134. Lockheed personnel (Mr. R. Walz, Mr. J. Fortun, and Mr. G. Yasui) participated in the design of the experiment and selection of test conditions. Test specimens were fabricated by the Union Carbide Company, under the supervision of Mr. B. Tokheim of Stanford Research Institute International.

Descriptions of the experimental apparatus, techniques, and procedures used in the program are presented in Section 2. The experimental results are described in Section 3, and the conclusions and recommendations are given in Section 4.

SECTION 2

EXPERIMENTAL APPARATUS AND TECHNIQUES

2.1 EXPERIMENTAL CONFIGURATION

The OWL II electron beam generator was used to produce rapid thermal loading of the cermet annuli and rings. The accelerator is a pulse charged system, consisting of an oil-immersed 1/3-MJ Marx generator and a water-insulated coaxial transmission line pulse transformer, which provides the pulse-forming network (Reference 1). The accelerator configuration employed for the testing reported here had a 120-ns pulse-forming line, a 1.8 ohm output impedance transformer, and a 22.9-cm (9 inch) diameter circular cathode (Reference 2).

The electron beam test geometry is shown schematically in Figure 1. The fixtures are similar to hardware used in previous structural response experiments on annuli and rings (References 3, 4, and 5). The electron beam is generated by a field emission cathode and passes through a transmission anode (0.013-mm-thick titanium) into the experimental chamber. A graphite aperture with a 20.3-cm (8 inch) inside diameter and a second 0.013-mm-thick titanium foil are located just behind the anode. The graphite absorbs the intense portion of the beam that originates at the perimeter of the cathode. A magnetic lens is used to control and transport the electron beam from the cathode emission surface to the target. This produces an electron beam that retains the cross-sectional shape of the cathode, while the area of the beam varies

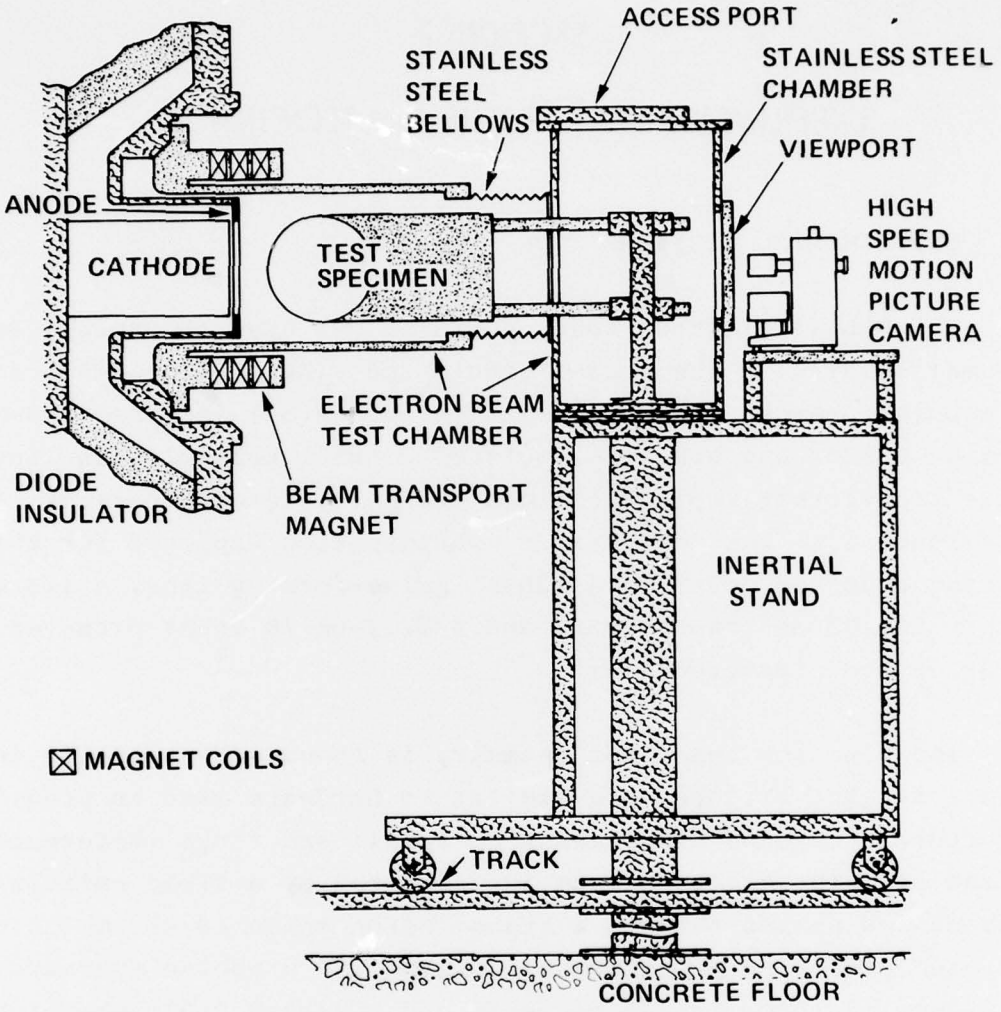


Figure 1 Electron beam test geometry.

inversely with the magnetic lens ratio; hence, the beam fluence is directly proportional to the magnetic lens ratio. Fluence uniformity is controlled to first order by dishing the cathode to compensate for the bow of the anode produced by the 1-torr gas pressure in the test chamber.

The target holder for the ring is shown in Figures 2 and 3. The target holder for the annulus is shown in Figures 4 and 5. The annulus was suspended at three points from small clips attached to elastic bands. The clips contacted the annulus on its inner edge. The ring was suspended by small Y-shaped clips at the top and bottom (+ 90-degree and - 90-degree locations). The clips were also attached to elastic bands. Tension of the bands was adjusted by pegs located behind graphite shields. The entire target apparatus was mounted on an inertial stand bolted to the concrete floor. The target apparatus was isolated from the accelerator by a stainless-steel bellows. This arrangment is necessary to prevent shock waves generated in the machine from disturbing the experiment.

The pulsed magnetic field used for beam control exerts a force on the annulus. The direction of the force is such that the annulus is pushed into the target holder. To restrain the annulus, rubber bumpers were placed between it and the holder apparatus. When the electron beam fires, the magnetic field intensity will have reached a maximum; hence, the force on the annulus is at a minimum. The strain records show that any disturbances caused by the magnetic field were too small to measure; hence, the effect of the magnetic field on the dynamic strain measurements of the annuli is not significant. The ring was not affected by the magnetic field since its axis is perpendicular to the field.

The strain-gauge packages were located on the top (0 degree) and left (90 degree) sectors of the annulus. The gauge packages

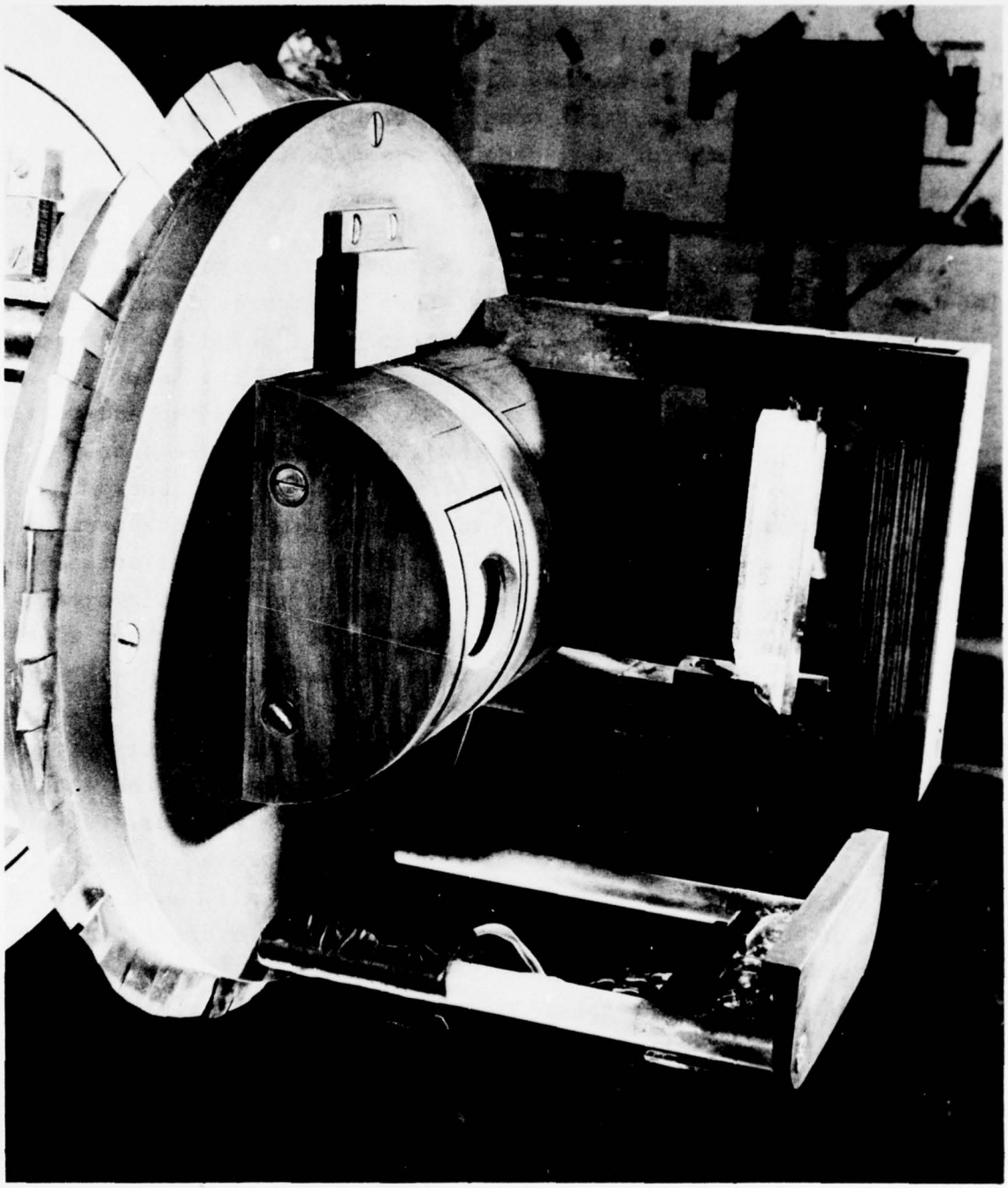


Figure 2 Front view of ring holder. Ring at center. Quartz gauge specimen in center of left calorimeter. Mirror on right with lights at bottom.

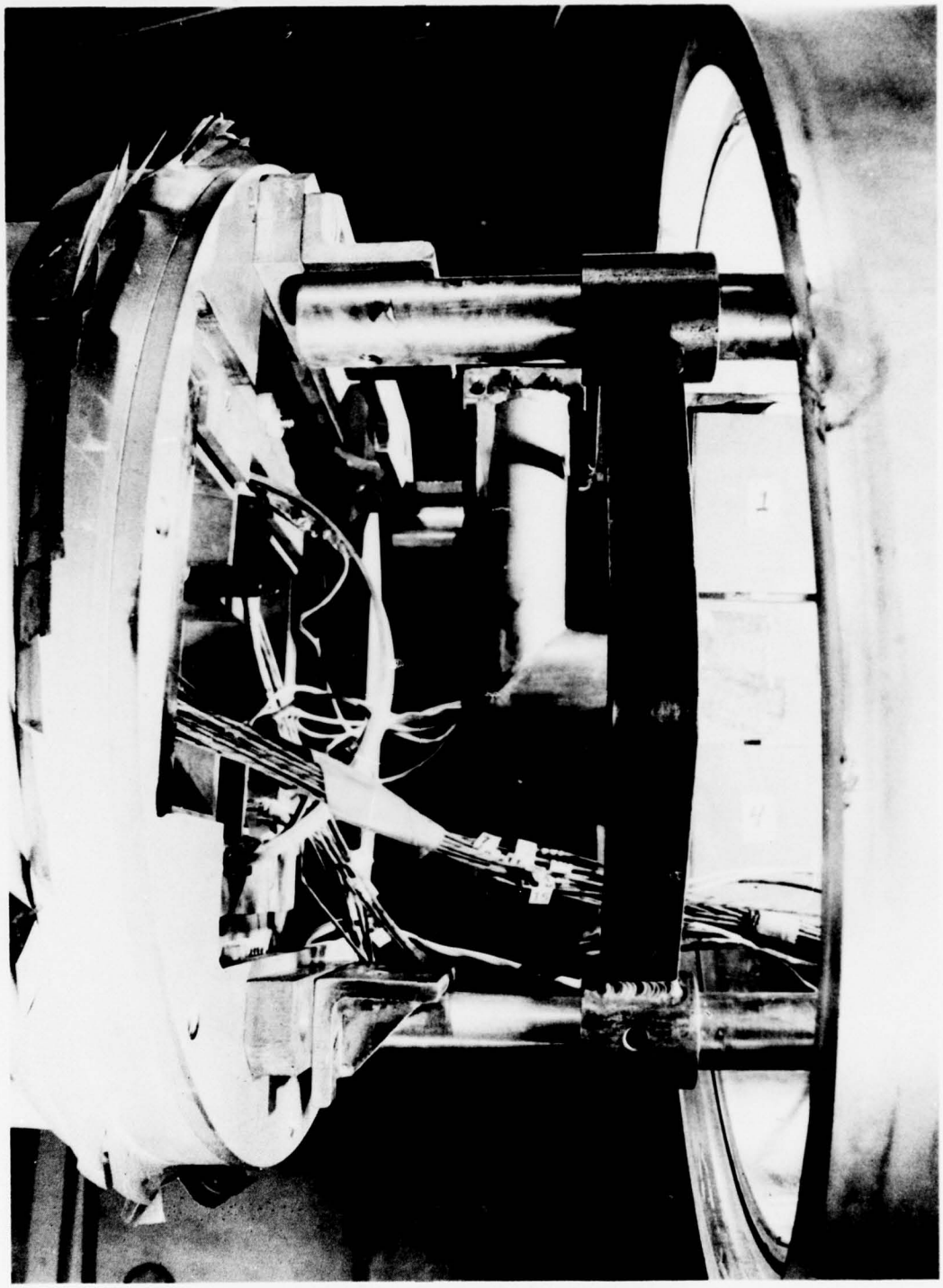


Figure 3 Rear view of ring holder. Thermocouple leads in foreground. Strain gauge leads in background. Strain gauge noise cancellation loops in numbered boxes on right.

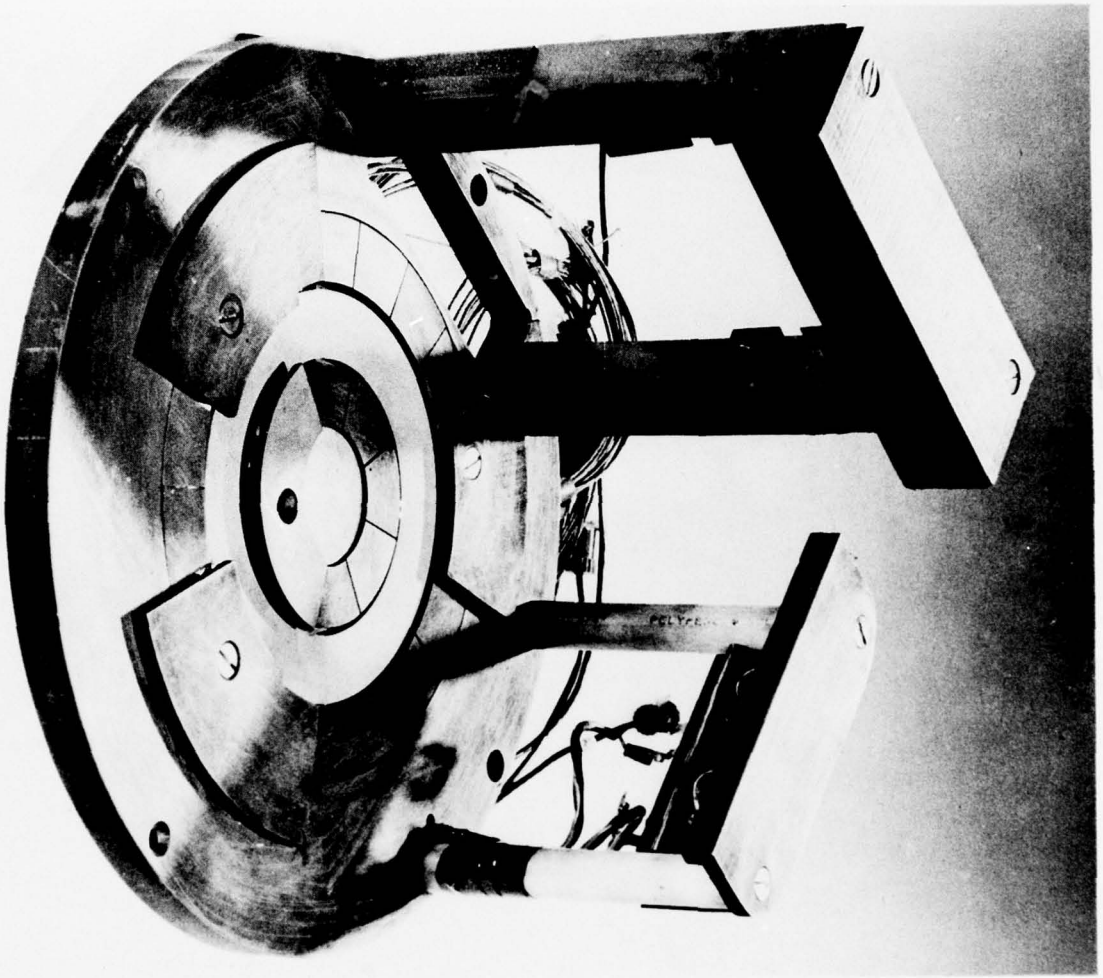


Figure 4 Front view of annulus holder. Quartz gauge specimen in center. Strain gauge packages protected by shields on left. Camera viewport at upper right.

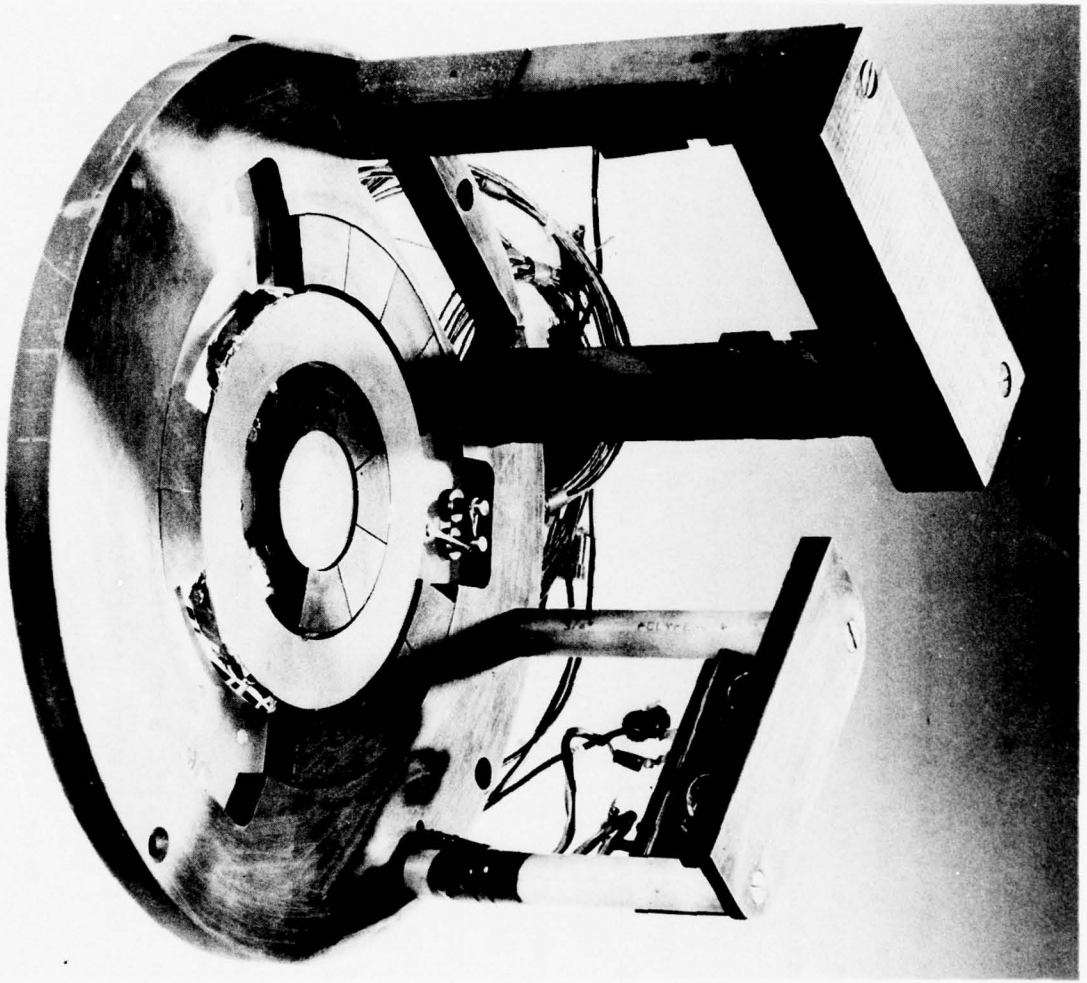


Figure 5 Annulus holder with shields removed. Strain gauge packages on left. One of three elastic bands in position on right.

were protected by a graphite shield that extended approximately 2.5 mm over the annulus (see Figure 2). On the ring, strain-gauge packages were located on the inner surface at -90, 0, 45, 90, 135, and 180 degree positions.

Calorimeter blocks were arranged in rings inside and outside the annulus to make simultaneous measurement of fluence and structural response data. A coupon of the test material with a quartz pressure transducer bonded to the rear surface was mounted inside the inner ring of calorimeter blocks, at the center of the apparatus. The coupon was in the shape of a disk, of diameter 5.08 cm (2 inch) and thickness 0.112 cm (0.044 inch). The quartz pressure transducer simultaneously measured the stress-time history of the annulus. Finally, a mirror was mounted behind a graphite shield on the right side of the apparatus. The mirror provided a view of a segment of the front surface of the annulus for a high-speed motion picture camera. Illumination was provided by two quartz lamps mounted at the bottom.

Curved calorimeter blocks were mounted on both sides of the ring (Figure 3). These blocks enabled a simultaneous measurement of the fluence distribution versus radius with the structural response of the ring. The quartz pressure transducer was located in the center of the left side calorimeter array. The mirror was mounted on the right with lights mounted at the bottom.

2.2 ELECTRON BEAM DIAGNOSTICS

Diagnostics used in characterization of the electron beam were employed both in the diode and at the target location. The diode diagnostics consisted of a voltage monitor, a set of $\dot{B}$ probes, and a set of current monitors. The voltage monitor is a capacitive

voltage divider embedded in the diode insulator. The $\dot{B}$ probes are magnetic field sensors and have an output proportional to the time rate of change of the magnetic field associated with the diode current. The diode current monitors consisted of Rogowski coil segments, which are $\dot{B}$ probes with built-in integrators. Thus the output was directly proportional to diode current. Four $\dot{B}$ probes and two Rogowski coil segments were on the anode plate located on a diameter just inboard of the inside diameter of the diode insulator. Two full Rogowski coils surrounded the cathode: one was in the anode plate and the other was in the anode extension near the cathode tip.

The diode diagnostics were recorded with Tektronix RM7912 transient digitizers and fast oscilloscopes (typically 150-MHz bandwidth). The data analysis includes correction of the input data for any RC and L/R slumps inherent in the monitors, correction of the voltage waveforms for inductive components, calculation of the accelerator voltage, and calculation of quantities such as the total beam energy and mean electron energy.

The acceleration voltage and diode current waveforms were used directly in the PIElD Monte Carlo Code (Reference 6) to calculate electron beam energy deposition profiles for correlation with measurements.

The beam diagnostics used at the target location consisted of fluence and deposition profile calorimeters. On data shots the primary diagnostic used at the target location was the peripheral calorimeter arrays described above. A separate flat calorimeter array, shown in Figure 6, was used for initial fluence mapping and determining fluence uniformity. The calorimeters were constructed of ATJ graphite blocks mounted on fiberglass boards with aluminum screws.

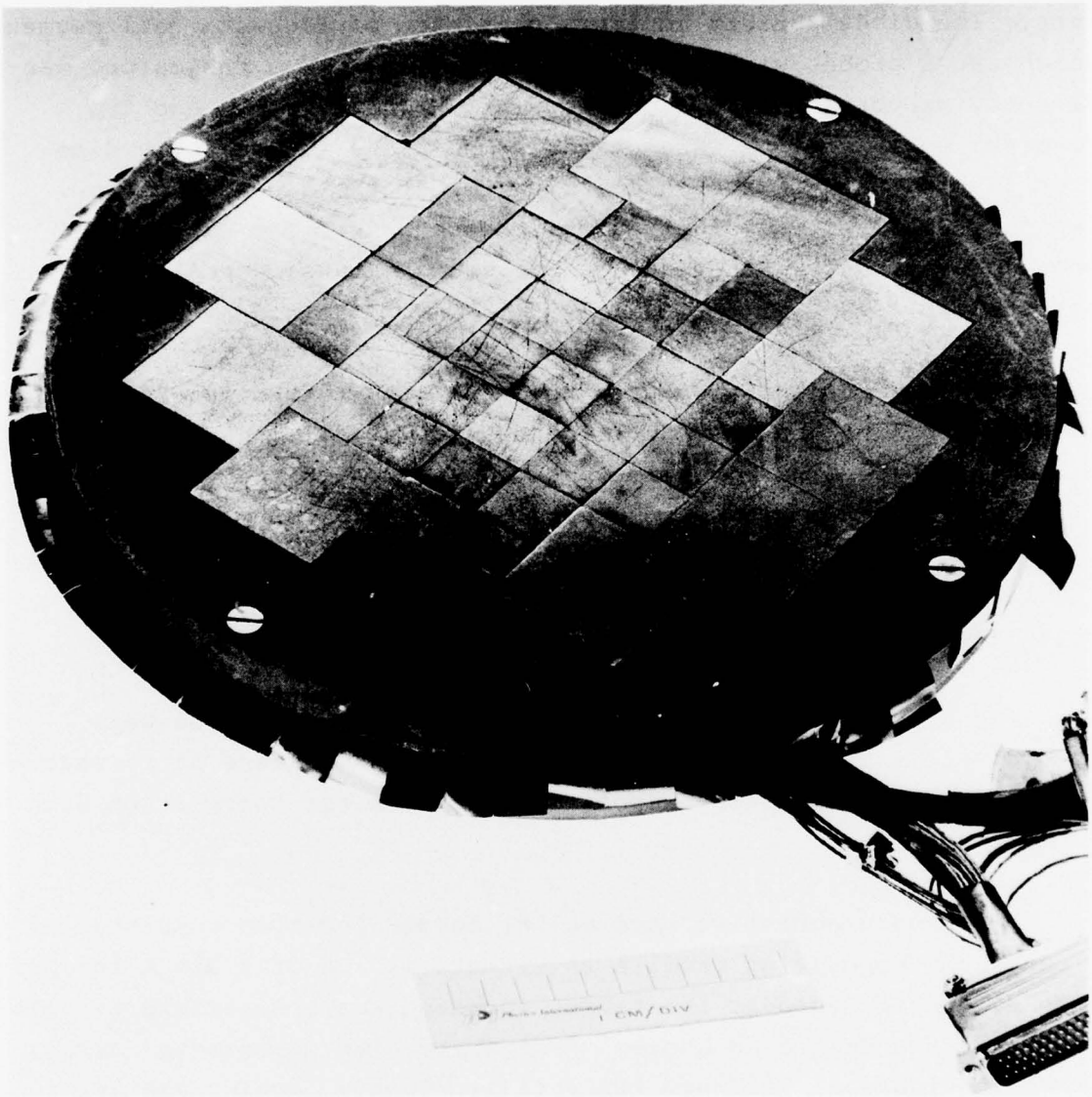


Figure 6 Flat calorimeter array.

Each block was instrumented with an iron-constantan thermocouple. The thermocouple signals were recorded by a scanning digital voltmeter. Fluences were calculated with a PI mini-computer program, using polynomial fits to handbook enthalpy curves for ATJ graphite and aluminum (Reference 7).

The electron beam energy deposition profile was measured with a graphite foil stack calorimeter. The foils were 0.5-mm-thick ATJ graphite foils held in position by polyethylene blocks. The foils were instrumented with iron-constantan thermocouples, clamped against a copper tab attached to an edge of each foil. The thermocouple signals were read out with the same scanning digital voltmeter system described previously. The deposition profiles were calculated with a PI mini-computer program using polynomial fits to the enthalpy curves for ATJ graphite and copper.

2.3 STRUCTURAL RESPONSE DIAGNOSTICS

Structural response induced by pulsed electron beam irradiation of the cermet annuli and rings was measured using strain gauges and high-speed motion pictures. The strain gauge data acquisition system was essentially the same as used during previous experiments on aluminum rings and annuli (References 4 and 5). The system is capable of handling six channels. A block diagram of one channel of this system is shown in Figure 7. A schematic of the basic bridge circuit is shown in Figure 8. A common dc power supply was used to apply 20.0 volts of dc to each bridge circuit. The system was calibrated by switching precision resistors in parallel with the active and passive strain gauges. Considerable attention was paid to noise reduction. Double shielding was used wherever possible, with the inner shield of each channel single-point grounded to the amplifier chassis. The other shield, which enclosed all six channels, extended from the test specimen to the electronics rack.

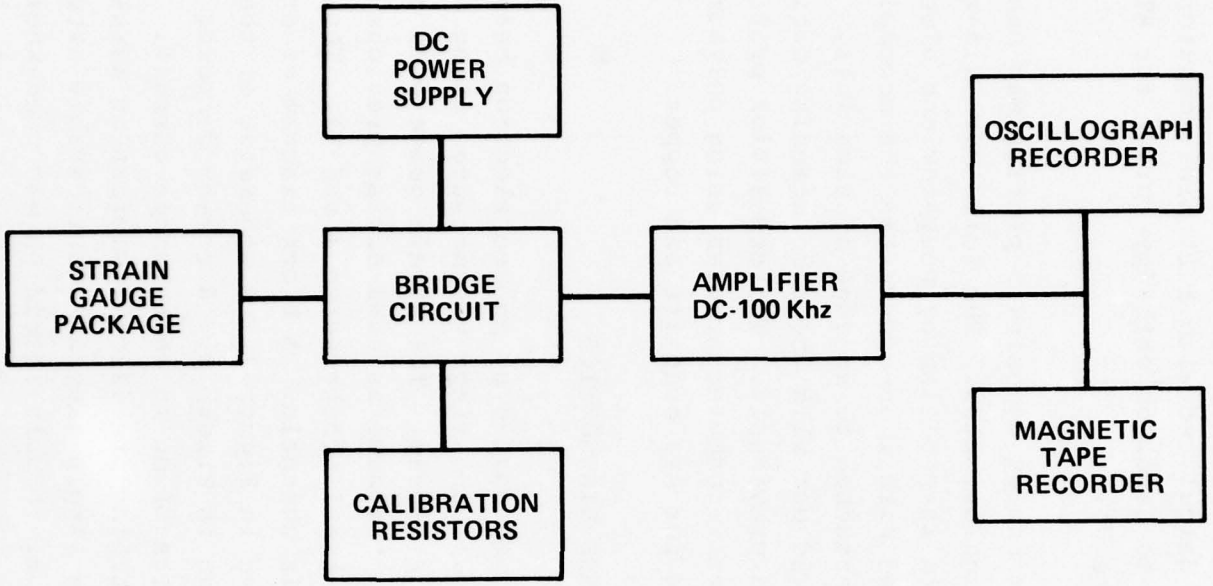


Figure 7 Block diagram of strain gauge instrumentation system.

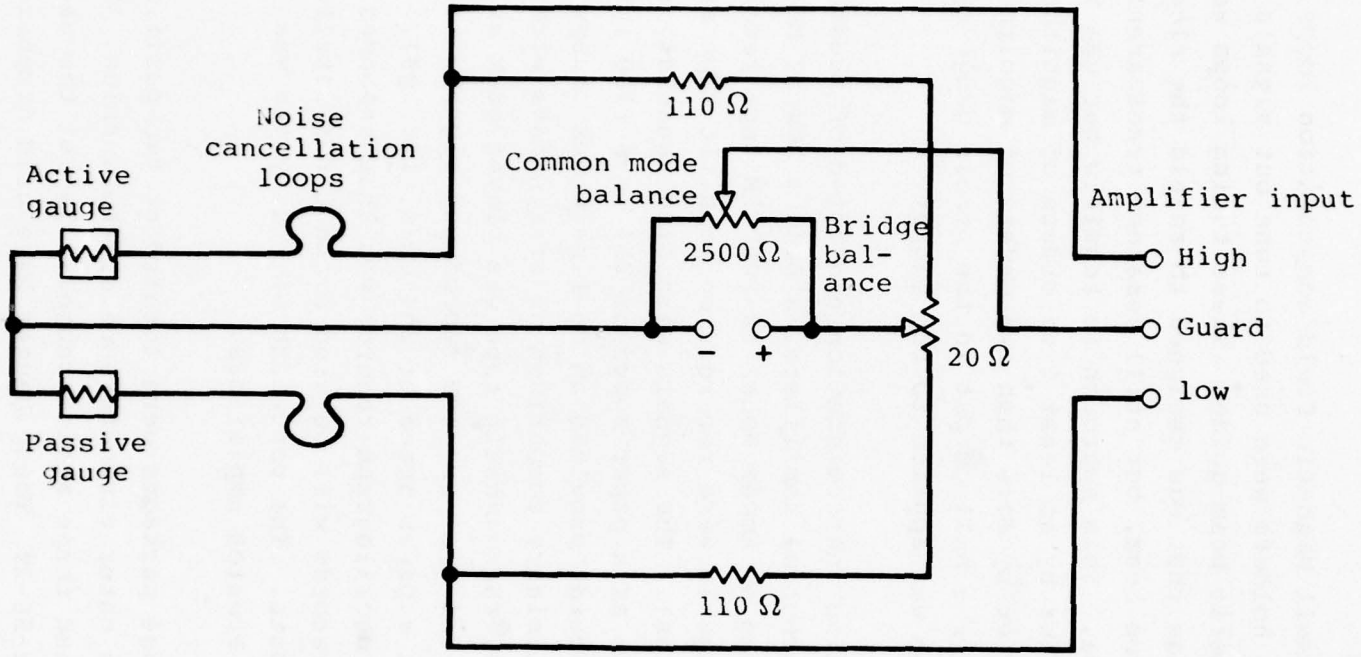


Figure 8 Bridge circuit schematic (simplified for clarity).

A set of small magnetic field compensation loops located behind the target holders were used to tune out signals induced by the pulsed magnetic beam guide. These tuning loops were enclosed in a Faraday cage that was designed to shield the electrical noise from the electron beam, but still remained transparent to the magnetic beam guide. This approach is feasible because the relevant frequencies differ by at least five orders of magnitude (hence the skin depths differ by more than two orders of magnitude). The loops were adjusted for a null output in the strain gauge system while a 60-cycle voltage was applied to the magnet.

The recording instrumentation consisted of Preston Model 8300XWB-B differential amplifiers, a Bell & Howell Model 5-134 oscillograph, and an Ampex Model FR-2000 FM tape recorder. The strain gauge signals were recorded on magnetic tape at a speed of 305 cm/s (120 ips). The signals were simultaneously recorded on the oscillograph at a paper speed of 254 cm/s (100 ips). The oscillograph records provided an on-line check of system performance and a preliminary comparison of strain data with predictions. At a later date, the magnetic tape was played back at a tape speed of 9.5 cm/s (3-3/4 ips) and the reproduced signals recorded on the oscillograph at a paper speed of 254 cm/s (100 ips). The time scale on these oscillograph records was thus expanded by a factor of 32. These records will be used by LMSC for detailed analysis of the strain data. The bandwidth of the system was limited to 100 kHz by the Preston amplifiers.

Strain gauge packages were located at two positions 90 degrees apart along the outer circumference of the annulus. Each gauge package contained three active gauges. Two of the gauges were BLH type FAE-12S-12-S6-2. These gauges have grid dimensions of approximately 3.18 mm by 3.18 mm and have long integral leads. One gauge

was located at the center of the rear surface and was oriented to measure strain in the radial direction. The other was located on the rear surface near the outer edge of the annulus, oriented to measure strain in the circumferential direction. The third gauge was a BLH type FAE-18-12-S6-1. This gauge has grid dimensions of approximately 4.76 mm by 0.64 mm and has long integral leads. It was originally designed for the experiments with aluminum annuli described in Reference 4. This gauge was mounted on the edge of the annulus and was oriented to measure circumferential strain.

For the cermet ring, strain gauges were located at the center of the inner surface at positions of -90, 0, 45, 90, 135, and 180 degrees (0 degree position is nearest to cathode). All gauges were oriented to measure circumferential strain. The gauges employed at the 0 and 45 degree positions were BLH type FAE-12S-12-S6-2, described above. The remaining gauges were BLH type FAE-12S-12-S6. These are standard, general purpose strain gauges with grid dimensions of approximately 3.18 mm by 3.18 mm.

Each strain gauge channel consisted of two gauges, an active gauge bonded to the specimen and a passive gauge mounted directly above the active gauge. The passive gauges were mounted on small stainless-steel plates which were in turn attached to the specimen by soft foam pads. Stainless steel was chosen for its roughly comparable density and thermal properties to cermet. The passive gauge comprised one leg of the bridge circuit and served to cancel spurious signals induced in the active gauge by the pulsed magnetic field used to guide the beam and the pulsed electron beam itself. The entire package was covered by copper foil for additional noise shielding. Strain gauge packages for the annulus and ring are shown in Figures 9 and 10.

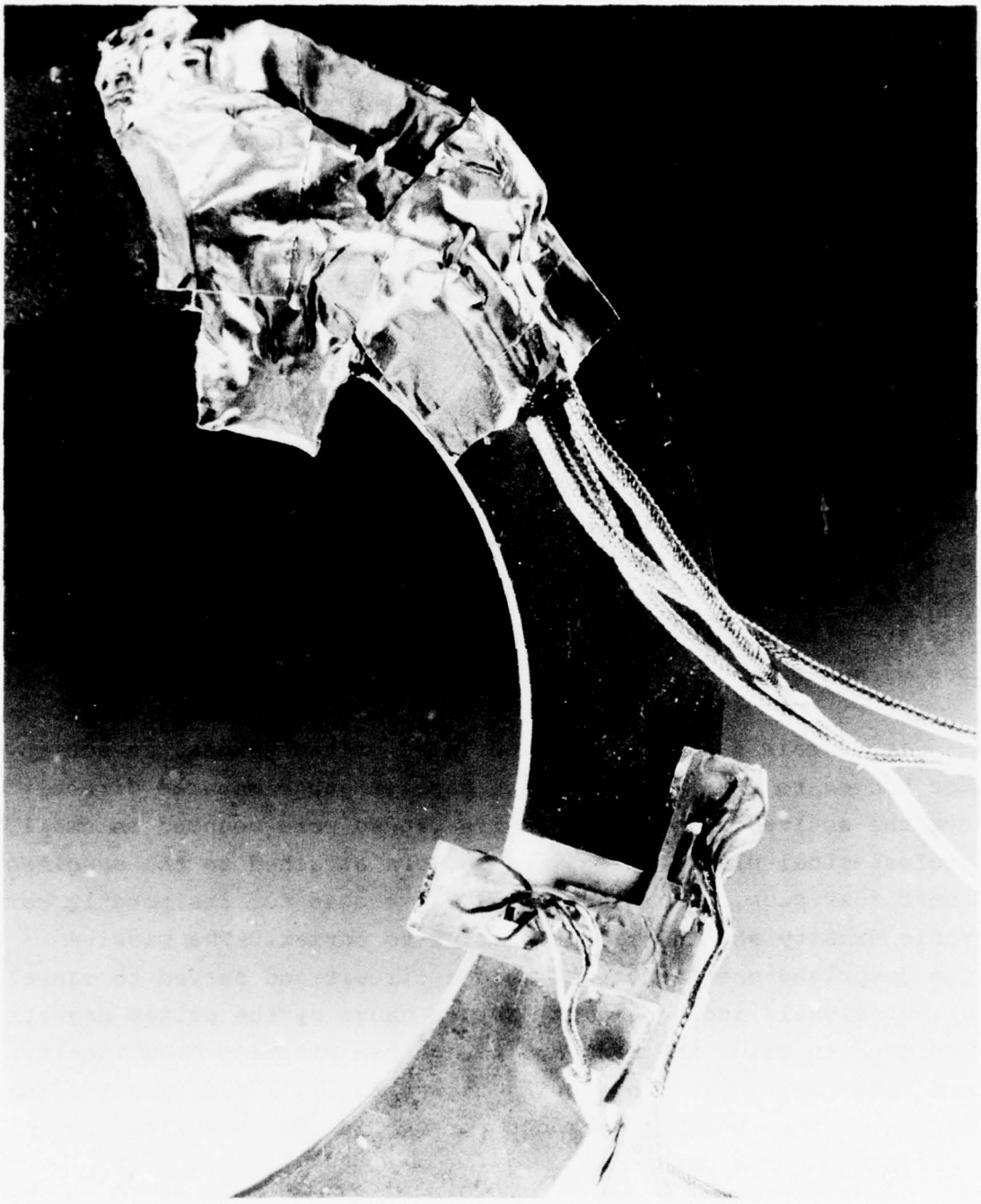


Figure 9 Annulus strain gauge packages. Copper tape removed from lower package.

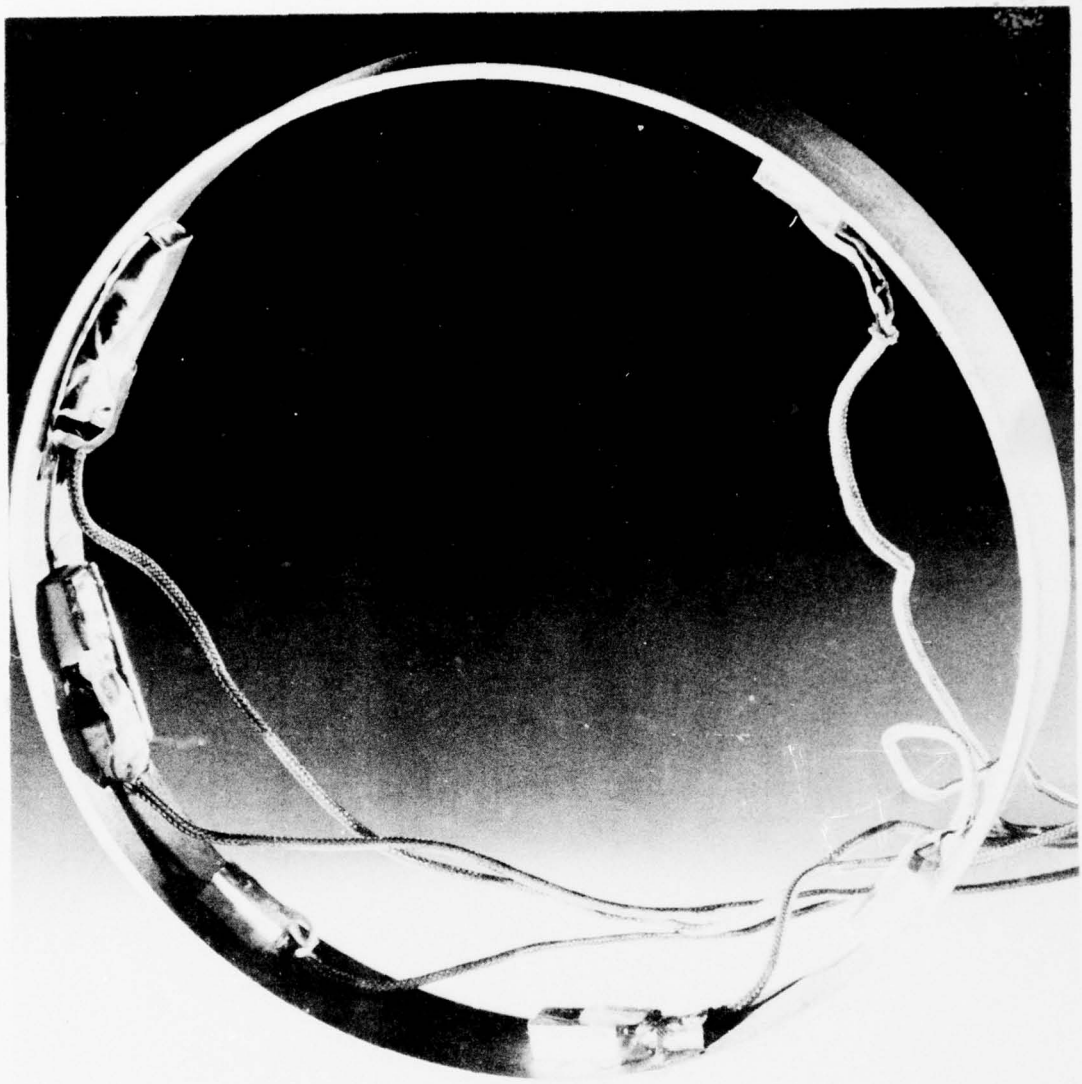


Figure 10 Ring strain gauge packages. Zero-degree package at 10 o'clock position.

Gauges were bonded to the cermet specimens with BLH type EPY-150 adhesive. A step-by-step description of the surface preparation and bonding techniques used with the cermet specimens is given in Appendix A.

The quartz pressure transducers were manufactured by Specialty Engineering Associates and were type 31250-250-500. These transducers have a read time of about 1.1 μsec. They were bonded to the disc coupons of cermet with Epocast type 202 cement.

Motion of the front region of the annuli and rings was recorded with a high-speed motion picture system mounted at the rear of the test chamber. The photographic record was taken with a Red Lakes Lab Model 1C 2051E Hycam operating at a framing rate of about 6000 frames per second. The camera was enclosed by a 2.5-cm-thick lead box in order to minimize X-ray fogging of the high-speed film.

SECTION 3

EXPERIMENTAL RESULTS

3.1 ELECTRON BEAM DATA

Data were collected at the OWL II Facility in April of 1978. Table 1 summarizes the useful shots obtained in this program. Tabulated are the shot number, the target type, the magnetic lens ratio, the anode-cathode spacing, the average fluence, the measured normalized peak dose, the calculated total diode energy, and the calculated mean electron energy. The lens ratio is the ratio of the magnetic beam guide field strength at the target location to the field strength at the anode location. It was adjusted by positioning the magnet and/or the target. The fluences were measured by the graphite calorimeters described previously. The normalized peak dose was calculated from the graphite foil stack calorimeter data. The total diode energy and mean electron energy were calculated from the diode voltage and current waveforms.

For the annulus experiments at the higher lens ratios, the fluence at the quartz gauge specimen was slightly higher than at the annulus. The correction factor was determined by examining the flat calorimeter data from shots with similar anode-cathode spacings and mirror ratios. The average fluence versus radius for several shots employing the flat calorimeter array has been plotted in Figure 11.

For the ring experiments, the difference in fluence incident on the ring (which is at the center) and the quartz gauge specimen

TABLE 1
OVERALL DATA SUMMARY

Pulse	Target[1]	Magnetic Lens Ratio	Anode-Cathode Spacing (cm)	Average Fluence at Annulus Location (cal/cm^2)	Average Fluence at Center (cal/cm^2))	Normalized Peak Dose ($cal/gm/cal/cm^2$)	Total Diode Energy (kJ)	Mean Electron Energy (MeV)
4307	DD	0.297	2.0			2.94	57.6	0.91
4308	C	0.297	2.0	10.4	10.7		21.8	0.95
4310	C	0.297	1.8	30.0	30.0		60.5	0.90
4311	DD	0.297	1.8			2.69	53.6	1.09
4312	A	0.297	1.8	9.7	10(4)		23.1	0.98
4318	DD	0.297	1.8			2.95	20.0	0.98
4319	DD	0.297	1.7			2.93	39.3	0.86
4320	DD	0.297	1.7			3.21	36.6	0.79
4322	DD	0.297	1.4			3.39	65.4	0.77
4325	C	0.297	1.2	25.5	29.8		53.6	0.71
4327	A	0.297	1.1	30.7	36(4)		59.4	0.69
4329	DD	0.297	1.1			3.12	94.9	0.78
4333	C	0.143	1.2	16.5	16.0		73.7	0.66
4334	A	0.143	1.2	10.8	11(4)		43.0	0.78
4335	A	0.143	1.2	21.8	22(4)		93.1	0.78
4337	C	0.343	1.2	43.3	50.2		74.3	0.76
4338	A	0.343	1.2	52(3)	60(3,4)		90.6	0.73
4339	C	0.200	1.2	32.4	33.6		81.0	0.75
4341	CC	0.195	1.2		17.0		58.3	0.68
4342	CC	0.195	1.2		26.7		81.9	0.72
4343	R	0.195	1.2		10.5		33.6	0.60
4344	R	0.206	1.2		22.7		77.2	0.76
4345	DD	0.206	1.2			3.80	54.1	0.59
4346	CC	0.343	1.2		52.5		90.2(2)	0.81(2)
4347	R	0.343	1.2		28.0		58.9	0.73
4348	R	0.308	1.2		37.6		81.8	0.69
4349	R	0.356	1.2		54.8		95.0	0.83
4350	DD	0.231	1.2			3.67	94.0	0.77
4351	DD	0.231	1.2			3.72	91.8	0.72

(1) A--annulus, R--ring, C--flat calorimeter, CC--curved calorimeter, DD--foil stack depth-dose calorimeter.

(2) Estimated value--no diode voltage record.

(3) Value obtained by scaling previous two shots--no calorimetry record.

(4) Value has been adjusted to reflect fluence variation with radius in beam.

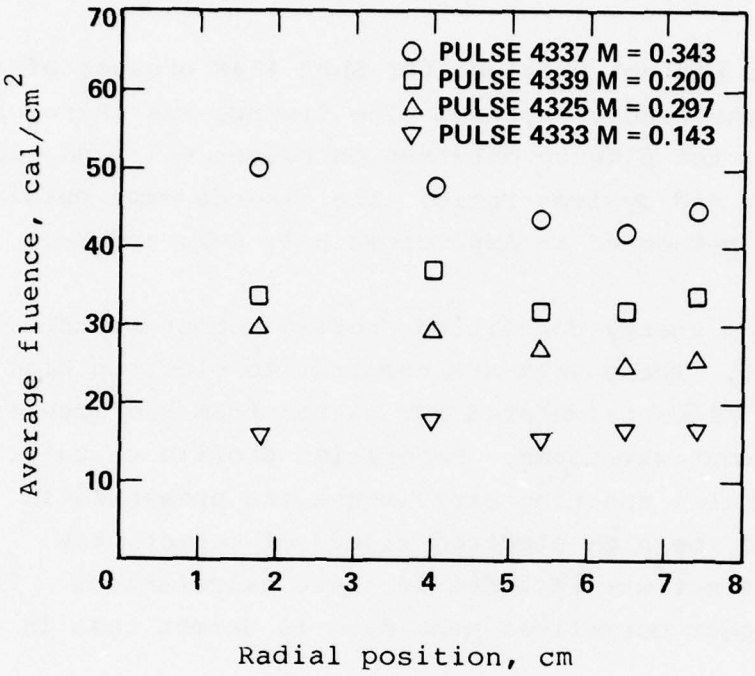


Figure 11 Average fluence versus radial position in beam for four mirror ratios.

is not significant. The fluence variation with circumferential position is plotted for a typical shot in Figure 12. For comparison, a cosine curve has also been plotted in Figure 12.

Calorimetry data was not obtained for Shot 4338 because of an error in setting up the readout system. The fluence was therefore determined by scaling the fluence obtained on pulses 4335 and 4337 by total diode energy and by lens ratio. The fluence maps obtained for this program are presented in Appendices B-1, B-2, and B-3.

The electron beam energy deposition profile measurements are shown in Appendix C-1. These data are compared to electron beam energy deposition profiles calculated for carbon from the acceleration voltage and current waveforms. Deposition profile calculations in cermet for the annulus and ring experiments are presented in Appendix C-2. Due to the high electron albedo of cermet, the albedo suppression effect was included in these calculations. This results in a much higher normalized peak dose in cermet than in carbon.

3.2 STRUCTURAL RESPONSE DATA

The structural response data pulses are summarized in Table 2. The peak dose levels indicated were determined from the fluences of Table 1 and the calculated normalized dose profile. The table also indicates the success or failure of data recovery for the strain gauges, the occurrence of spall, and its effect upon the film records. Also tabulated is the peak stress measured by the quartz pressure transducer.

The oscillograph records of dynamic strain obtained on-line are reproduced in Appendix D. The data are in general of excellent

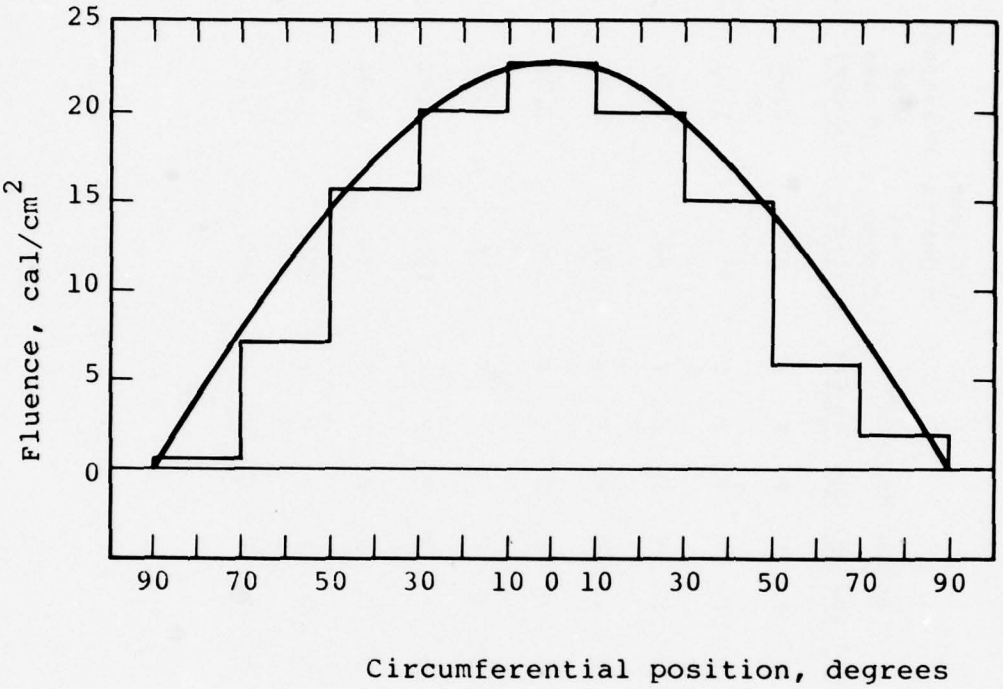


Figure 12 Fluence distribution over curved calorimeter for pulse 4344. Cosine curve shown for comparison.

TABLE 2

SUMMARY OF STRUCTURAL RESPONSE EXPERIMENTS

Pulse Number	Specimen Identification	Calculated Normalized Peak Dose (cal/gm/cal/cm^2)	Peak Dose in Annulus or Ring (cal/gm)	Strain Records[1] Ch1	Ch2	Ch3	Ch4	Ch5	Ch6	Peak Dose in Quartz Gauge Coupon (cal/gm)	Measured Peak Stress (kbars)	Spallation	Film Record
4312	27A	6.0	58	F	F	F	F	F	F	60	0.48	No	Yes
4327	22A	9.6	294	F	F	F	F	F	F	350	1.12	Yes	Obscured
4334	26A	7.8	84	N	F	F	F	F	F	86	0.54	No	Yes
4335	21	8.0	174	F	F	F	F	F	F	176	0.80	Yes	Yes
4338	14	8.4	440	P	F	F	N	F	F	500	2.91	Yes	Obscured
4343	29-1	10.2	106	F	F	F	F	F	F	106	0.58	Slight	Yes
4344	29-2	8.1	181	F	F	F	F	F	F	181	0.97	Yes	Obscured
4347	29-7	8.8	254	F	F	F	F	F	F	254	0.94	Yes	Obscured
4348	29-8	9.4	350	F	F	F	F	F	F	350	1.08	Yes	Obscured
4349	29-3	7.1	390	P[2]	F	F	F	F	F	390	1.27	Yes	Obscured

Notes:

(1) F--Full data recovery
P--Partial data recovery
N--Data not recovered

(2) Ring fractured under gauge

quality. The expanded time scale oscillograph records obtained from playback of the magnetic tape have been forwarded to LMSC under separate cover for detailed analysis.

Quartz pressure transducer records of excellent quality were obtained for all of the experiments. The transducer records are reproduced in Appendix E. The records for pulses 4338 and 4349, which are for the highest doses tested, have double peaks separated by about 0.1 μs. High-speed motion picture records were obtained for all of the experiments. However, at the higher fluence levels, the view of the specimen was obscured by intensely brilliant spall material ejected from the front surface of the specimen. In the film for pulse 4335, with a dose just above the spall threshold, spall material is clearly visible leaving the front surface of an annulus. Frames from this film are reproduced in Figure 13. Also visible in this film is the arrival of debris from the diode region. The debris is seen to arrive approximately 12 ms after the beam fired.

Permanent coning distortion was induced in the annuli (Figure 14). Measurements of the deviation from flatness at 4 points around each annulus are presented in Table 3. The rings were flattened. Measurements of the ring diameters parallel and perpendicular to the electron beam axis are presented in Table 4. The ring of pulse 4349 was fractured at the 0 degree position (Figure 15) and is therefore not included in the table. The degree of coning of the annuli as a function of fluence is plotted in Figure 16. Similarly the degree of distortion of the rings versus fluence is plotted in Figure 17. Both curves show a peak around 25 cal/cm^2. At higher fluences, spallation removes energy and relieves stresses, thus reducing the residual distortion.

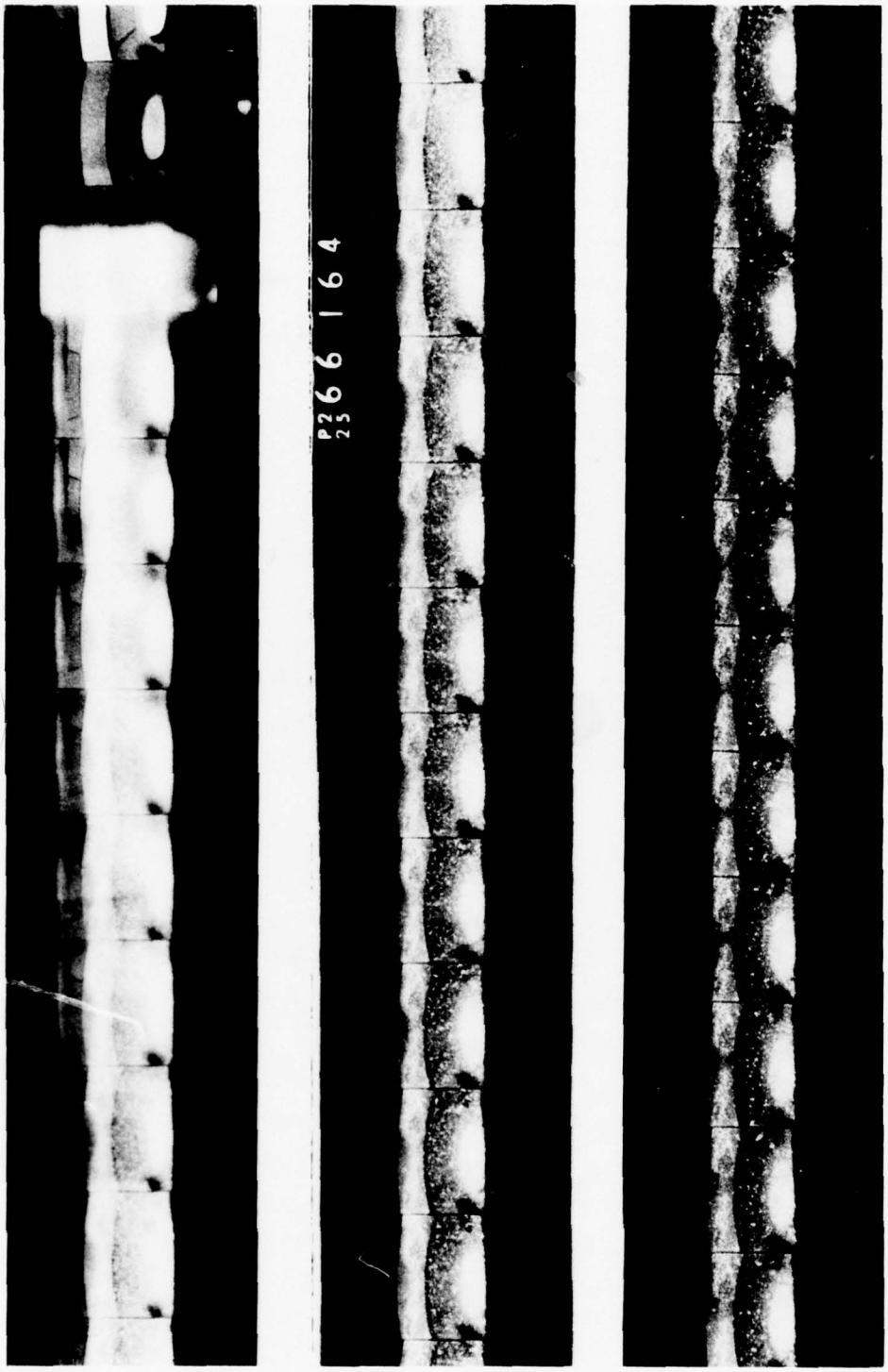


Figure 13 Film record from pulse 4335, approximately 5800 frames per second.

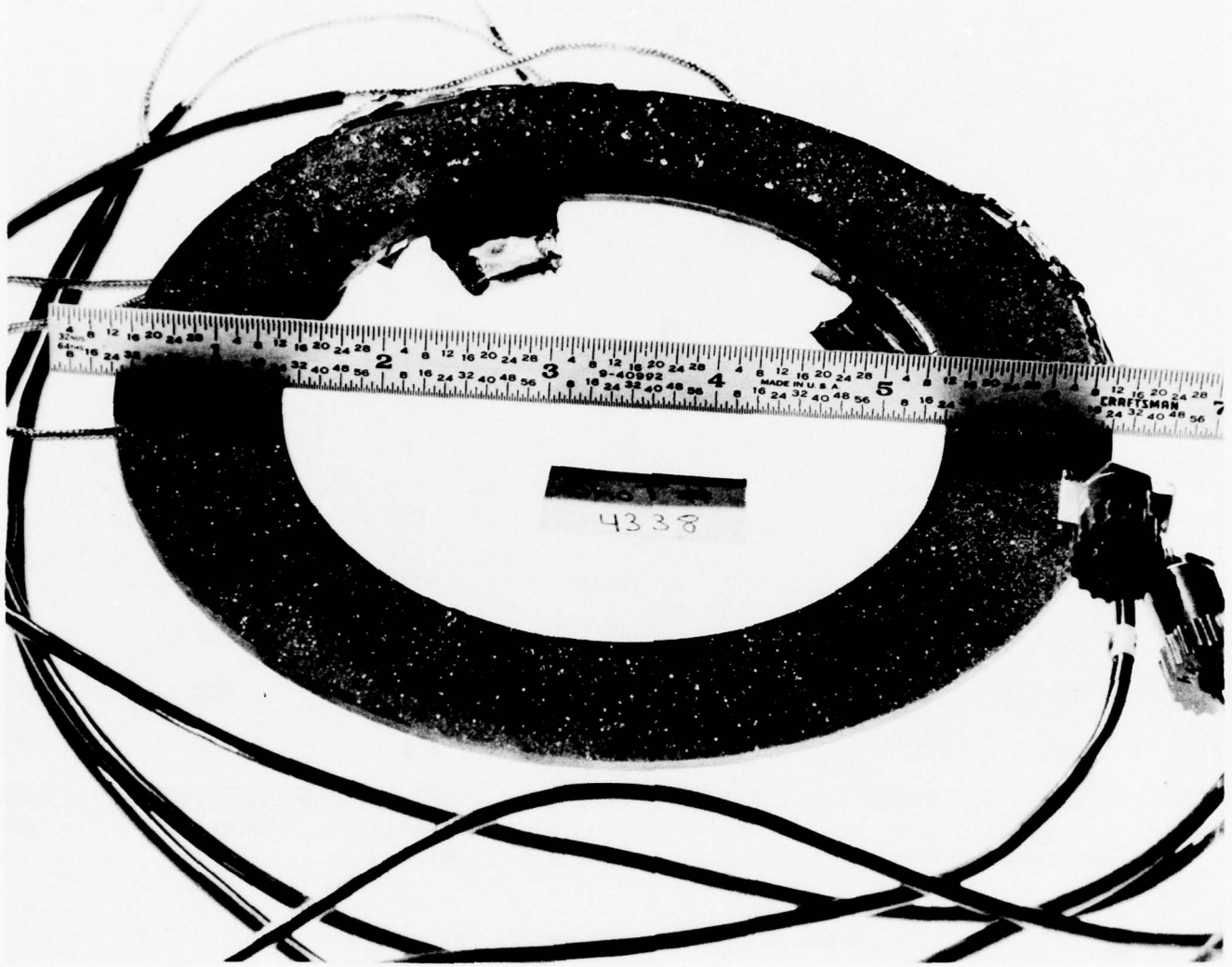


Figure 14 Coning deformation in cermet annulus from pulse 4338.

TABLE 3

CONING DEFORMATION OF CERMET ANNULI

Pulse Number	Specimen Identification	Average Fluence (cal/cm^2)	Position 1 (mm)	Position 2 (mm)	Position 3 (mm)	Position 4 (mm)	Average (mm)
4312	27A	9.7	1.27	0.97	1.02	0.97	1.06
4327	22A	30.7	1.83	1.47	1.60	1.78	1.67
4334	26A	10.8	1.19	0.97	1.02	0.97	1.04
4335	21	21.8	1.91	1.30	1.60	1.47	1.57
4338	14	52.0	1.47	1.09	1.42	1.50	1.37

TABLE 4

DEFORMATION OF CERMET RINGS

Pulse Number	Specimen Identification	Fluence at Center (cal/cm^2)	Diameter Parallel (cm)	Diameter Perpendicular (cm)	Difference (cm)
4343	29-1	10.5	14.88	15.00	0.12
4344	29-2	22.7	14.86	15.05	0.19
4347	29-7	28.0	14.85	15.03	0.18
4348	29-8	37.6	14.90	15.00	0.10



Figure 15 Fracture in cermet ring from pulse 4349.

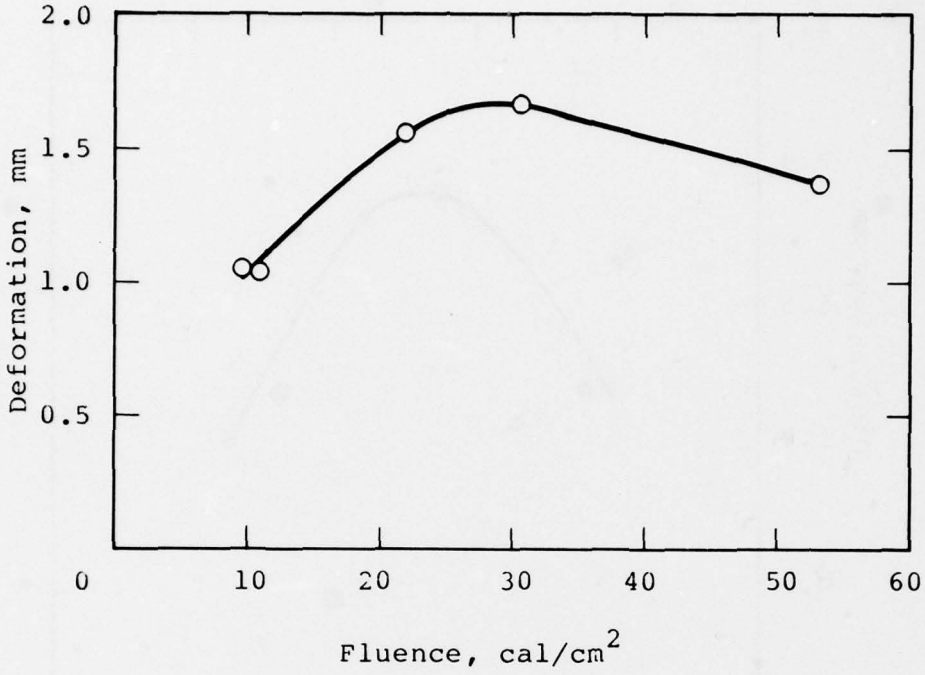


Figure 16 Coning deformation of cermet annuli.

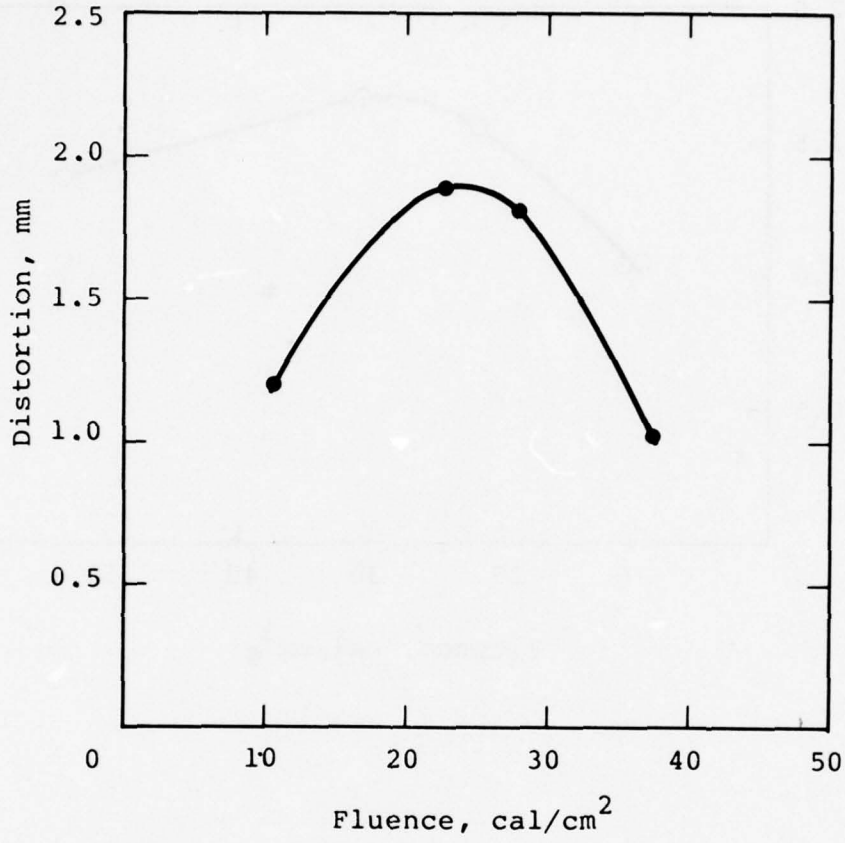


Figure 17 Distortion of cermet rings.

SECTION 4

CONCLUSIONS AND RECOMMENDATIONS

Thermostructural response data have been successfully obtained from annuli and rings of cermet, irradiated by an electron beam. The data include measurements of dynamic strain, high-speed motion pictures, and simultaneous quartz pressure transducer records. Substantial front-surface spall was produced in many of the experiments, and one ring was fractured. The electron beam was diagnosed with diode monitors, peripheral graphite block calorimeters, and graphite foil stack calorimeters.

The good reliability and high data recovery rate of electron beam thermostructural response experiments has again been demonstrated by this program. The adaptability of the techniques to new materials and shapes has also been demonstrated. This program has substantially increased the data base on an important new structural material: cermet. These data are essential for successful theoretical modeling of structural response. We recommend continued experimental work in this field, with more complex geometries and advanced materials.

REFERENCES

1. K. Nielsen, G. Frazier, and P. Spence, OWL II Generator Enhancement and Electron Beam Characterization, PIFR-464 and DNA-3414F, Physics International Company, San Leandro, CA (Unpublished).

2. K. Childers and C. Stallings, OWL II Diode Study, PIFR-788 (Draft), Physics International Company, San Leandro, CA (Unpublished).

3. K. Childers, V. Buck, and J. Shea, Carbon-Carbon Thermal Structural Response Testing, AFWL-TR-74-330, Air Force Weapons Laboratory, Kirtland Air Force Base, NM, October 1975.

4. V. Buck and J. Shea, Aluminum Ring Thermostructural Response Study, PIFR-930-1, Physics International Company, October 1976.

5. V. Buck and J. Shea, Thermostructural Response of Aluminum Annuli, PIFR-930-2, Physics International Company, January, 1978.

6. J. Reaugh and L. Behrmann, Documentation of the Physics International Monte Carlo Electron Transport Computer Code, PIIR-9-71, Physics International Company, San Leandro, CA, January 1971.

7. A. Mazzella, Graphite Calorimeter Calibrations, PIIR-22-68-V, Physics International Company, 1968.

APPENDIX A

TECHNIQUE FOR BONDING STRAIN GAUGES TO CERMET

Several techniques for bonding strain gauges to the cermet specimens were investigated before a satisfactory bond was achieved. The first attempts employed Micromeasurements Type 610 adhesive, which is a heat-curing solvent-thinned epoxy. It produces an extremely thin bond, and has been used successfully in previous thermostructural response experiments on aluminum and titanium. Strain gauges were test-bonded to cermet, first in the standard technique with a single application of adhesive, and second, with a cured pre-coat of adhesive to help fill the pores in the cermet. In both cases, the gauges were found to peel off readily, indicating an unsatisfactory bond. The difficulty may have been caused by excessive absorption of the adhesive into the cermet, leaving too little left at the bonding interface.

The next attempt employed BLH Type EPY-150 adhesive. This adhesive may be room temperature cured overnight, or heat cured for one hour at 66° C (150° F). It is much more viscous than type 610 adhesive. A single application of this adhesive was found to give a satisfactory bond; therefore, it was chosen for use with this experiment. The following is a step by step description of the surface preparation and bonding technique used for cermet specimens:

1. Underwater Abrading: Abrade the gauging area under water for approximately 5 minutes with 220 grit sandpaper, followed by approximately 3 minutes with 320 grit sandpaper. After drying, lightly burnish the gauge alignment marks with a ball point pen.

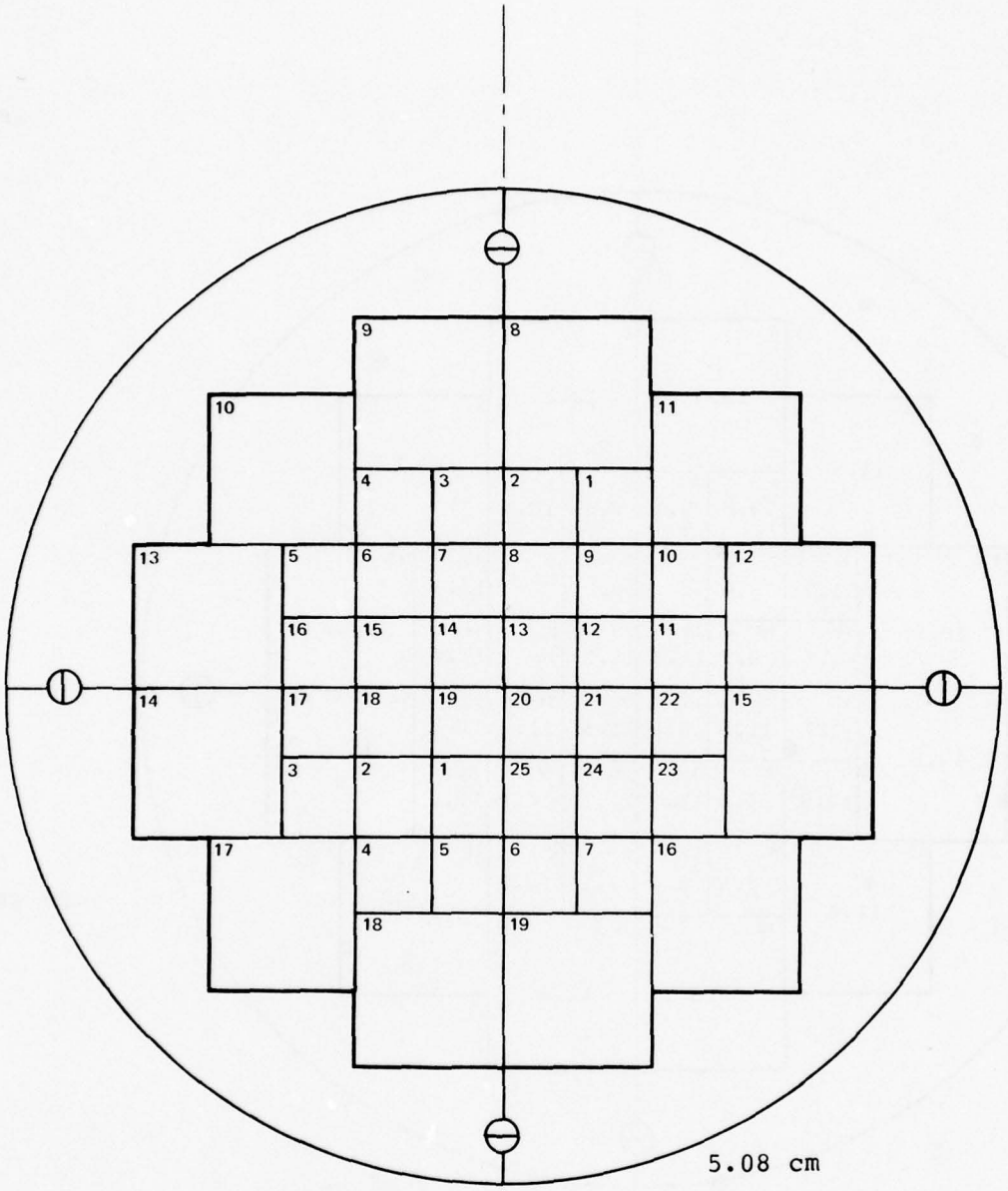
2. Chemical Cleaning: Scrub the gauging area with a cotton swab soaked in BLH Metal Conditioner. Wipe off the liquid with a single swipe of a clean gauze sponge. Repeat until no particles or discoloration can be seen on the swab or sponge.

Scrub the gauging area with a cotton swab soaked in BLH Neutralizer. Wipe off the liquid with a single swipe of a clean gauze sponge.

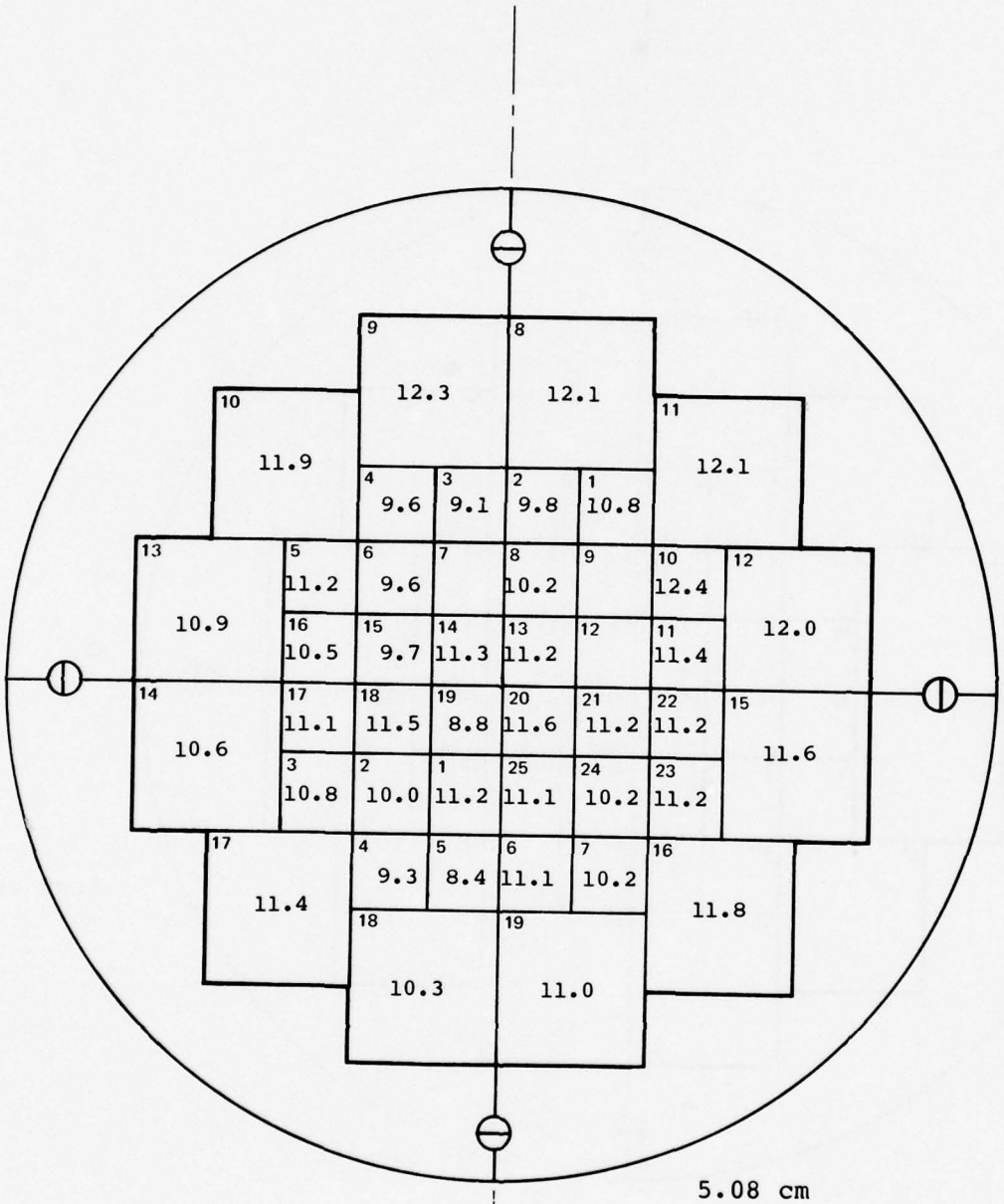
3. Bonding the Gauge: Use transparent tape to hold the gauge in alignment over the gauging area. Prepare a batch of BLH Type EPY-150 strain gauge cement. Using a clean spreader (which can be a small piece of 0.25 mm [10 mil] polyester), spread cement on the gauging area and on the gauge itself. Lower the gauge into position. Clamp the gauge with a silicone gum pad over a 0.025 mm (1 mil) Teflon separater. Place the work in an oven and cure at 66° C (150° F) for one hour. Alternatively, the bond may cure at room temperature for at least 12 hours.

APPENDIX B-1

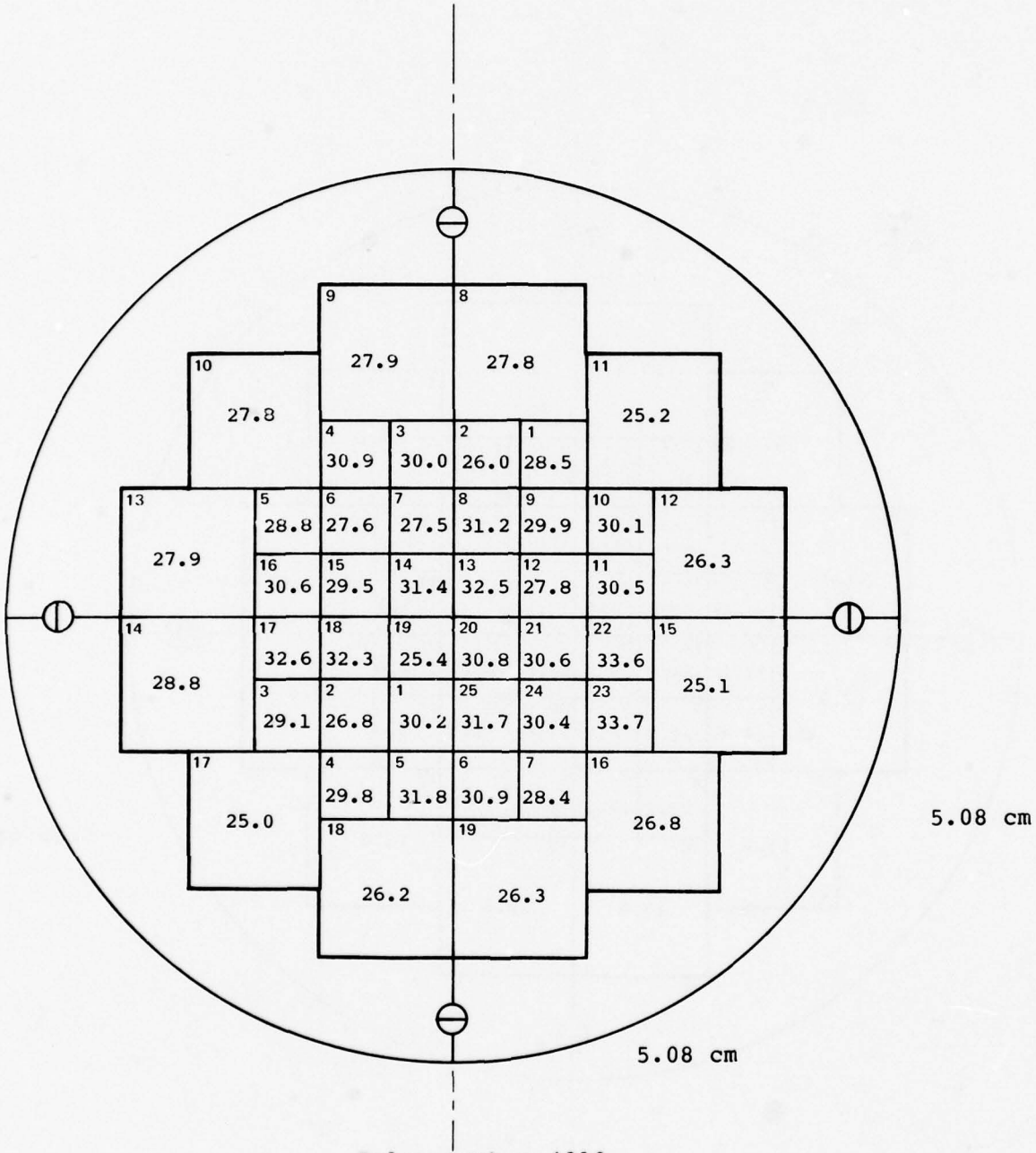
FLUENCE MAPS, FLAT CALORIMETER



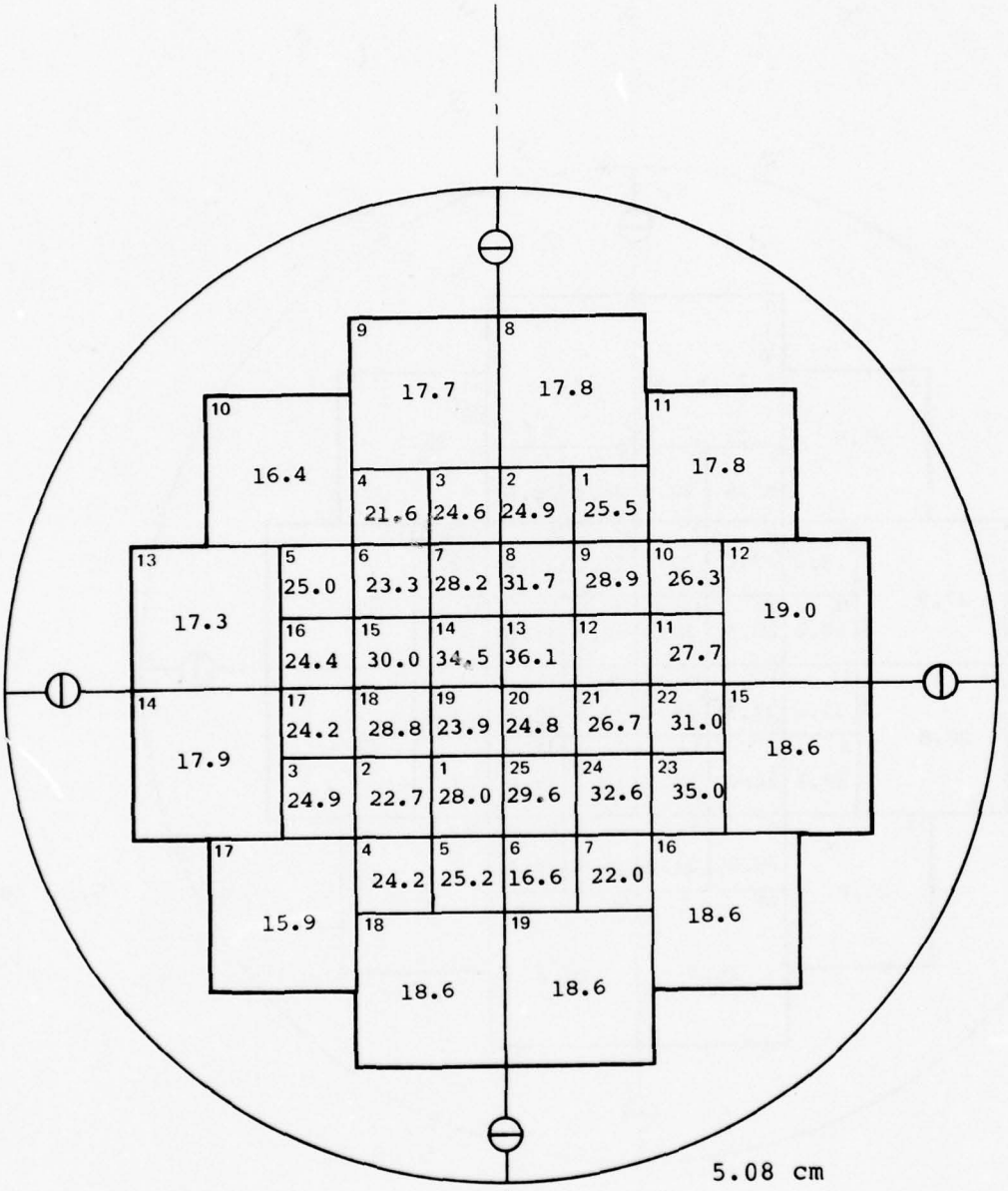
Pulse number 4444



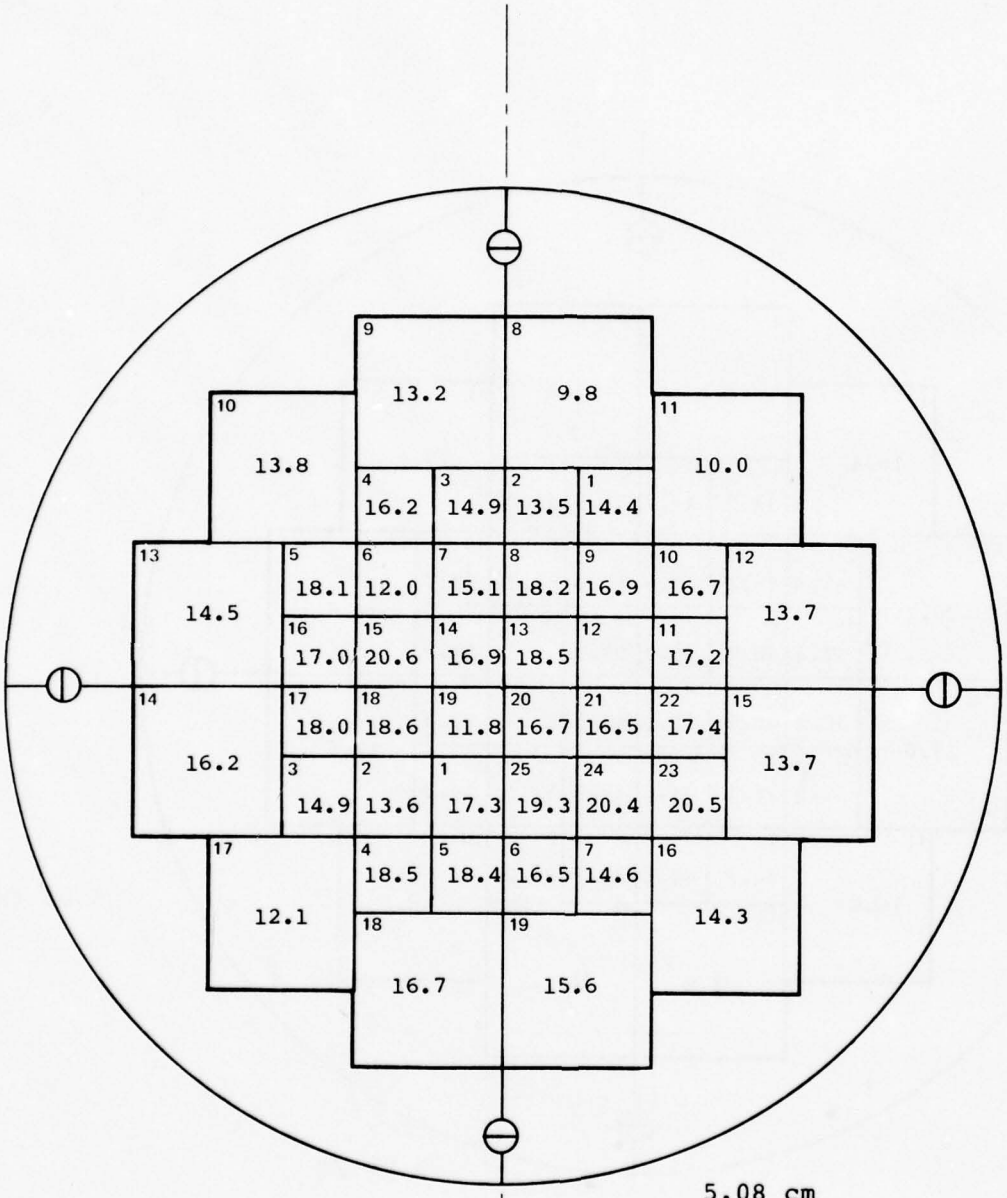
Pulse number 4308



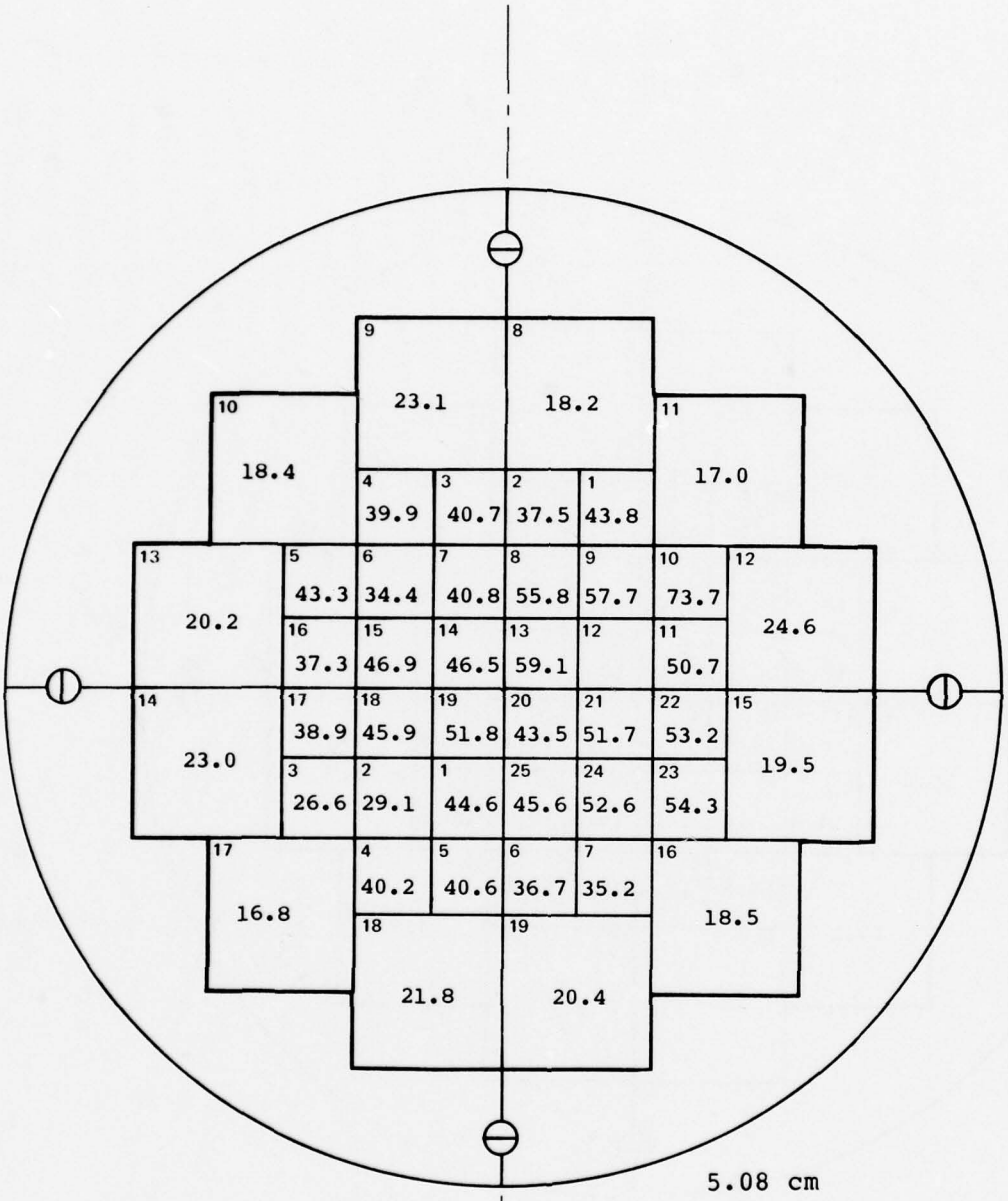
Pulse number 4310



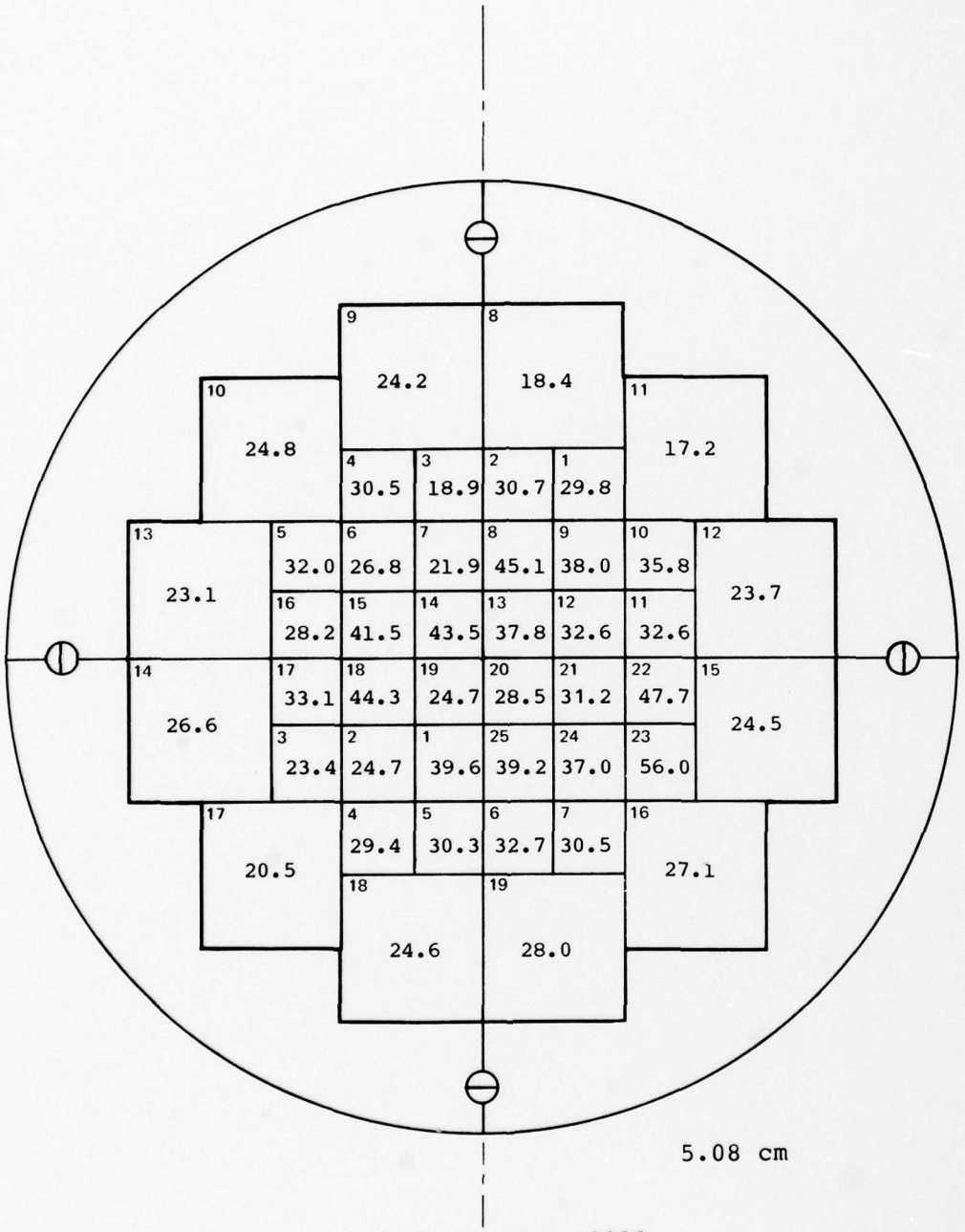
Pulse number 4325



Pulse number 4333



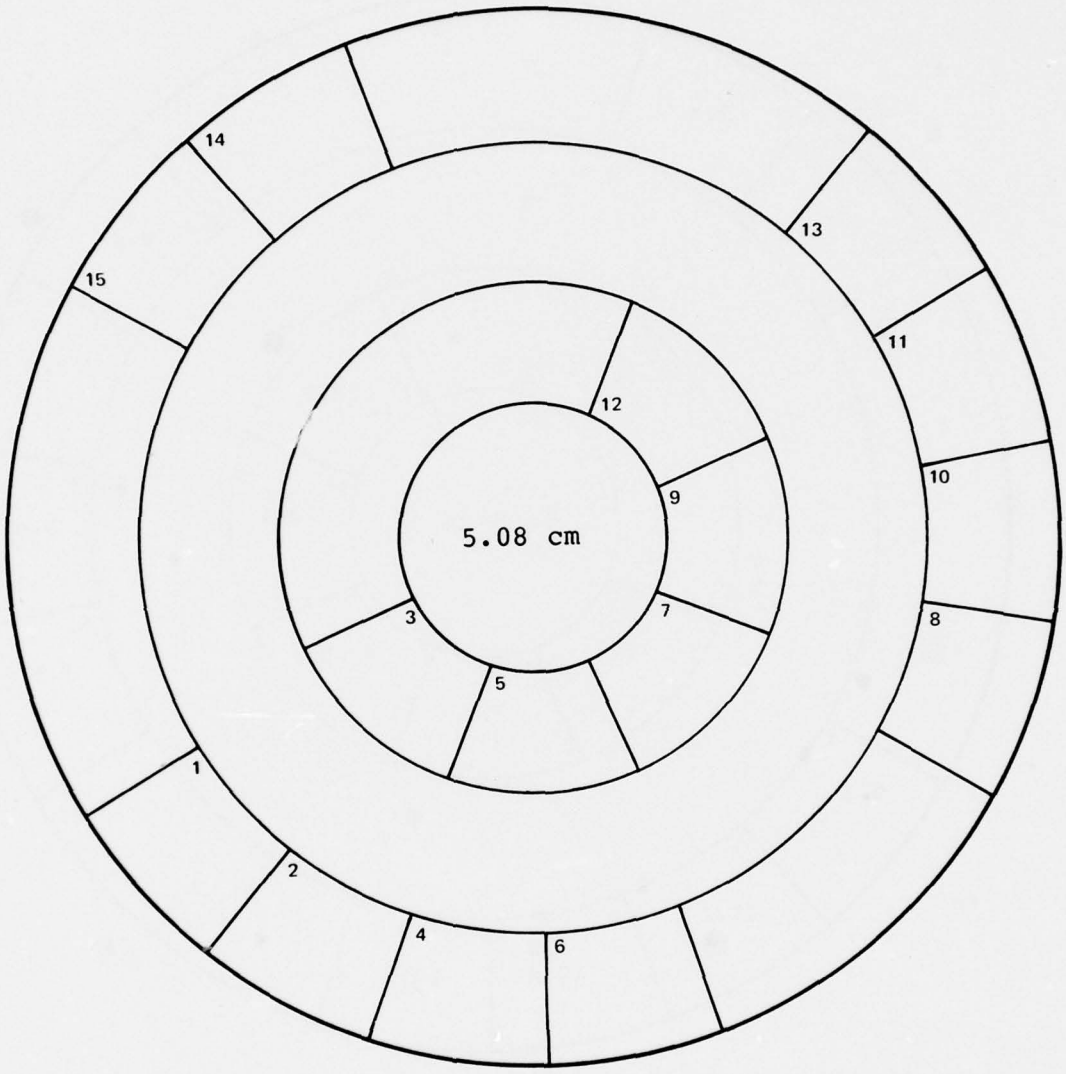
Pulse number 4337



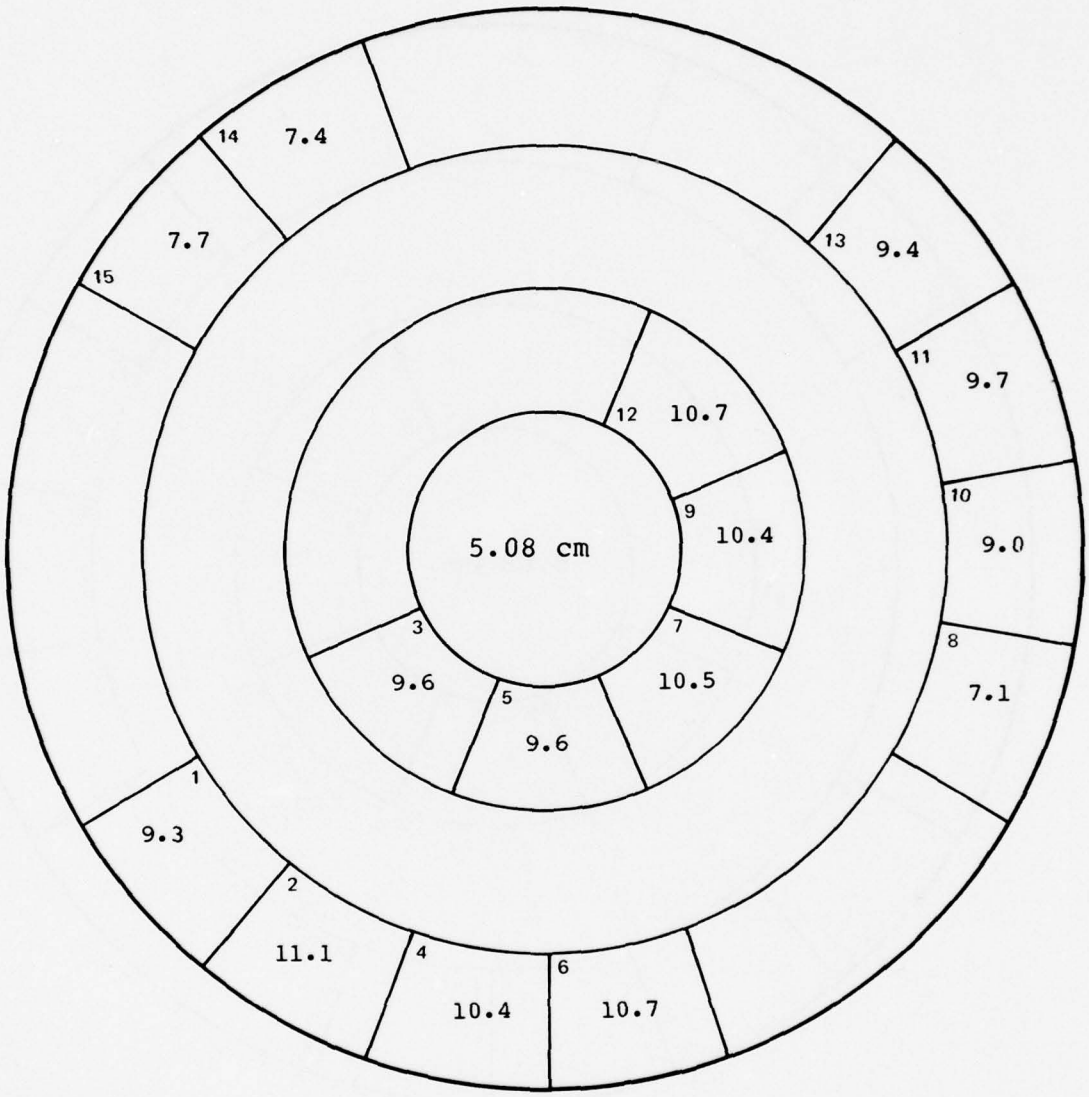
Pulse number 4339

APPENDIX B-2

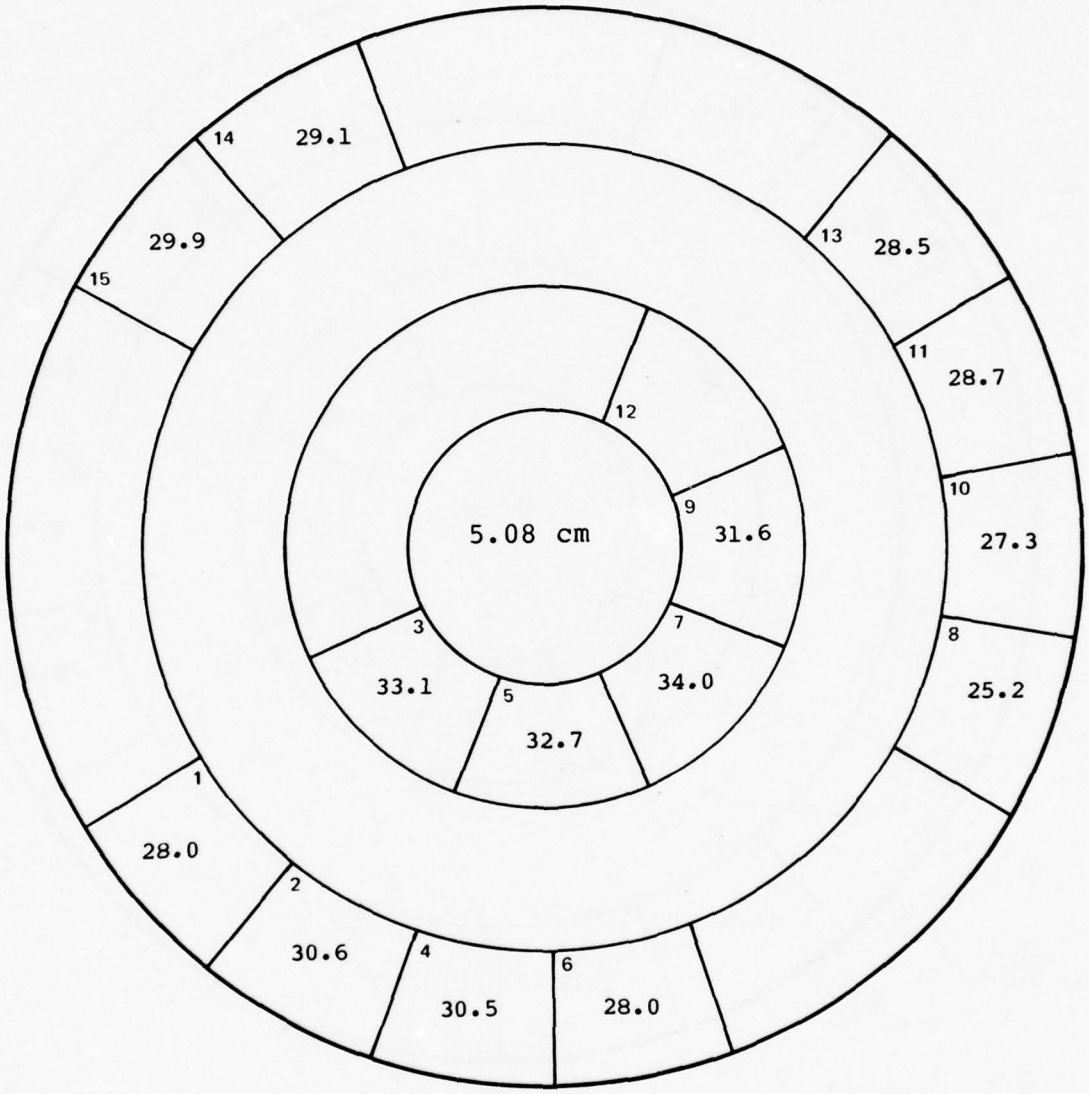
FLUENCE MAPS, ANNULUS EXPERIMENTS



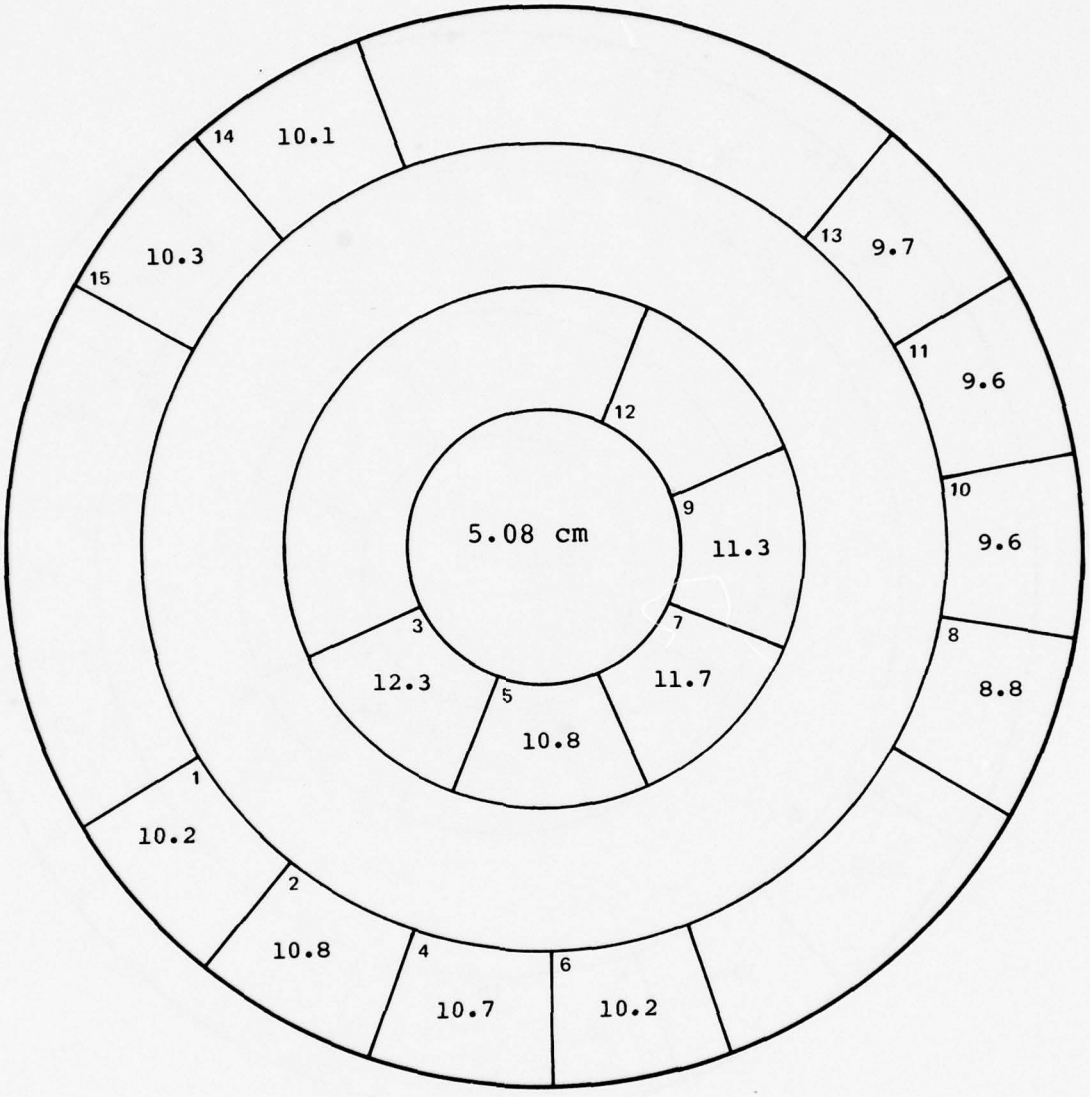
Pulse number 1234



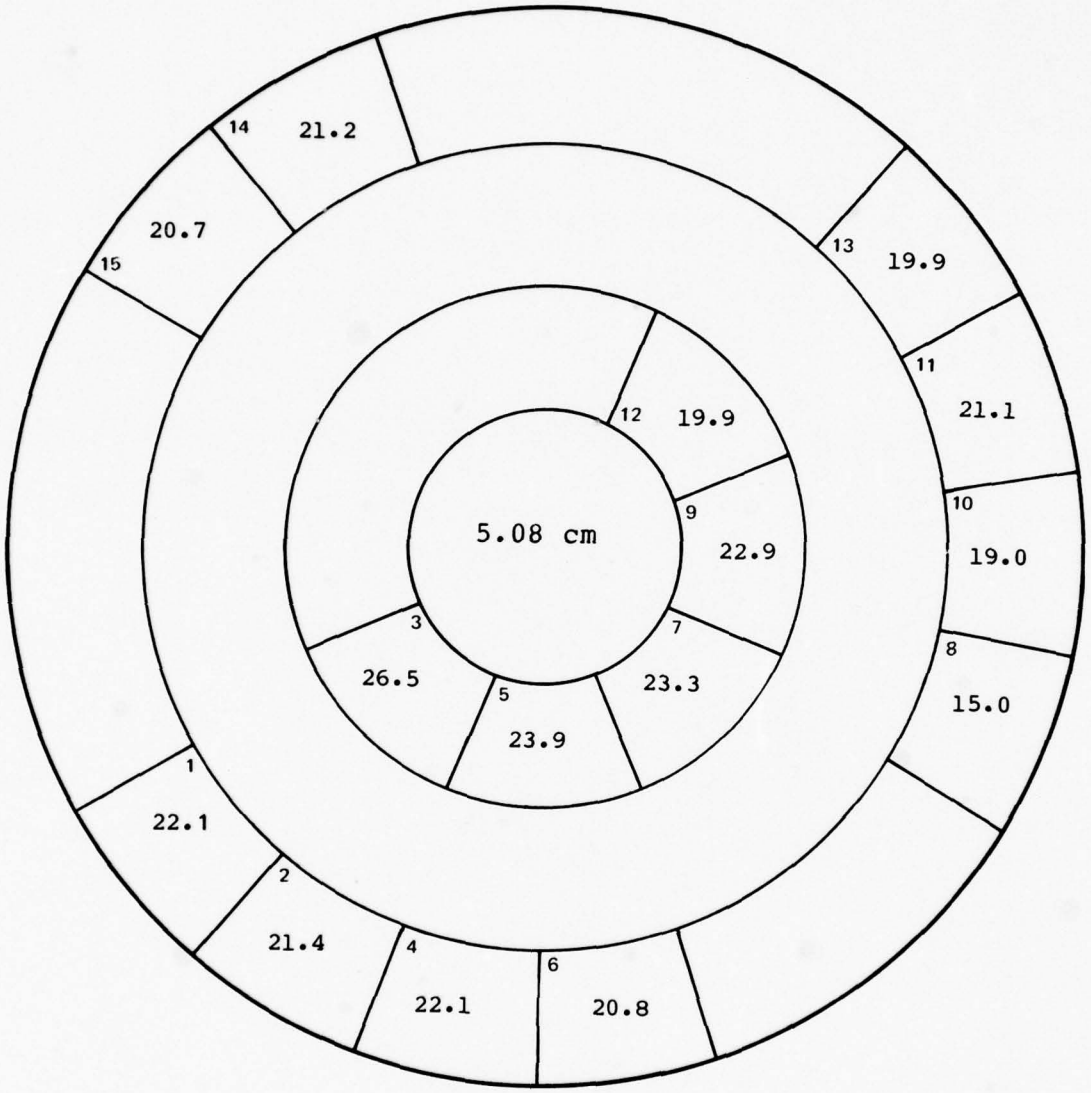
Pulse number 4312



Pulse number 4327



Pulse number 4334

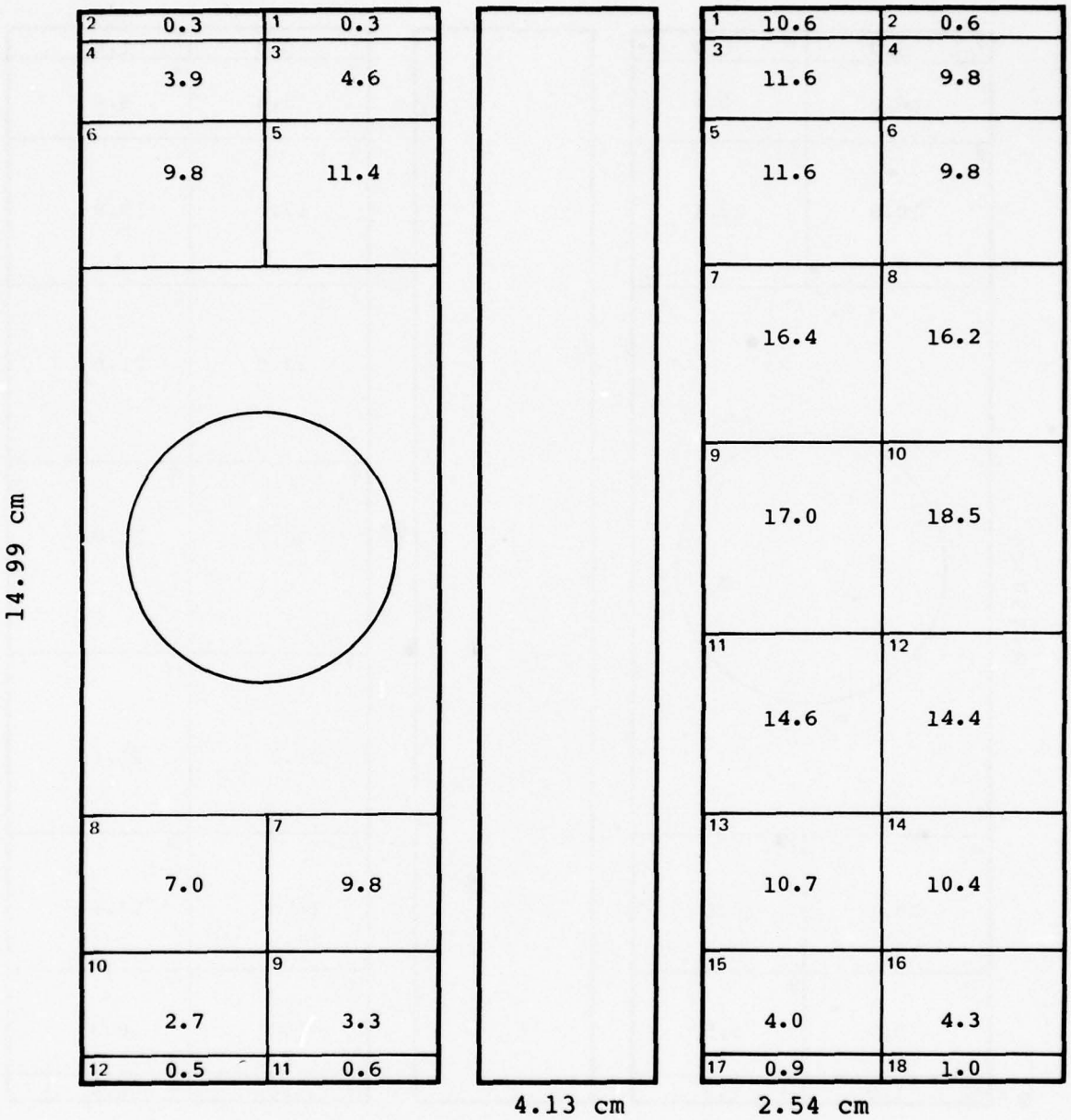


Pulse number 4335

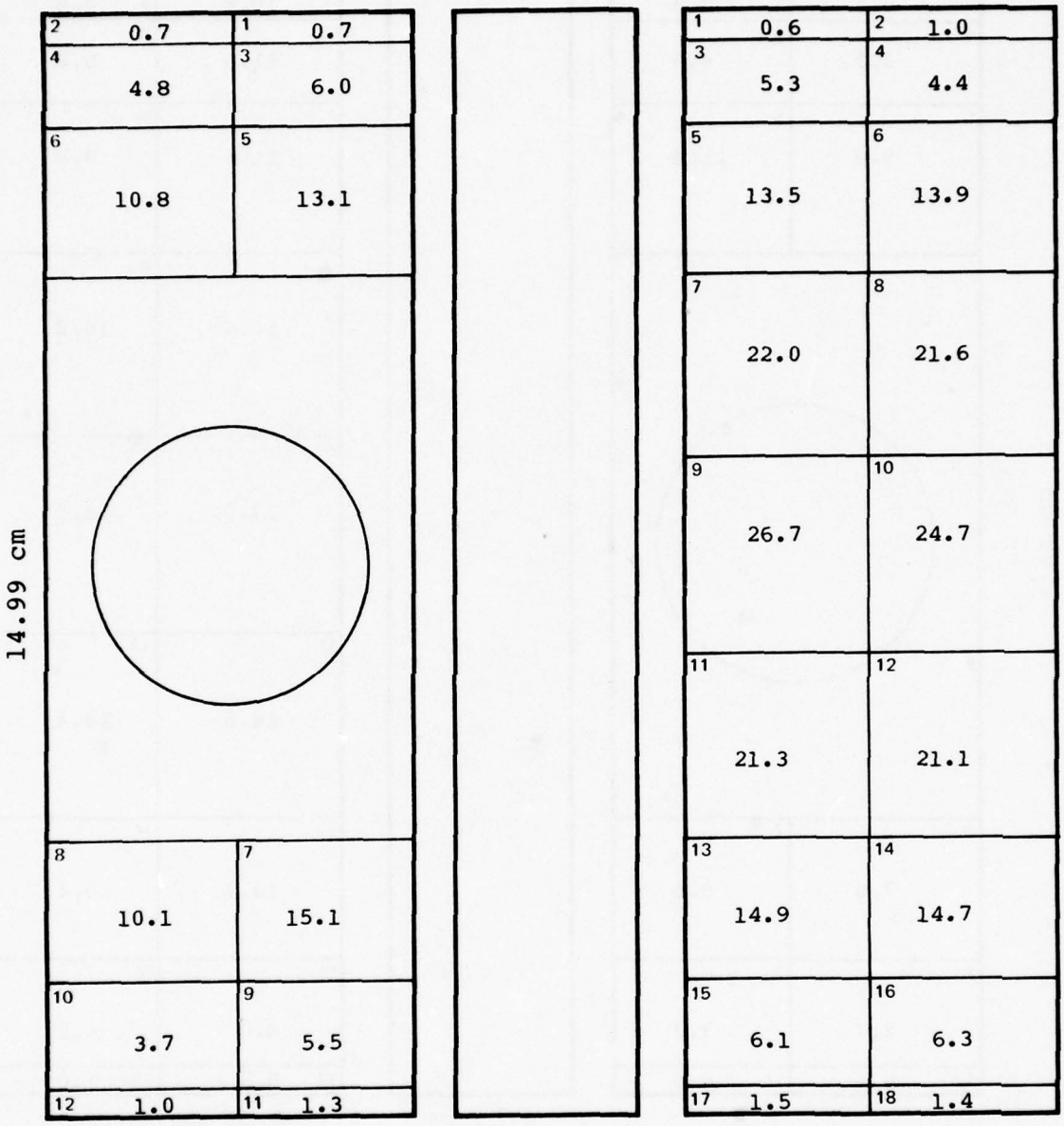
APPENDIX B-3

FLUENCE MAPS, RING EXPERIMENTS

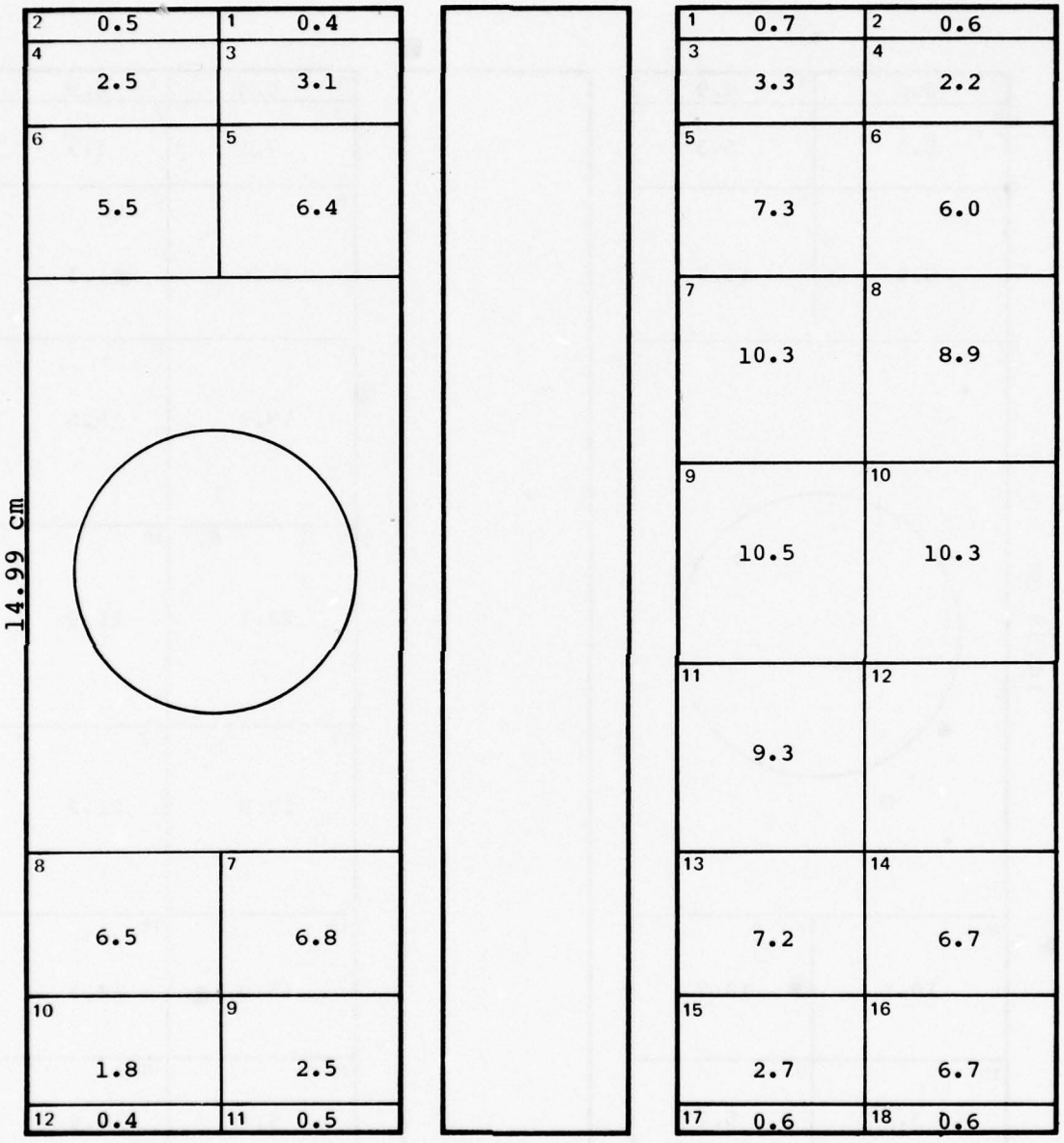
PRECEDING PAGE BLANK - NOT FILMED



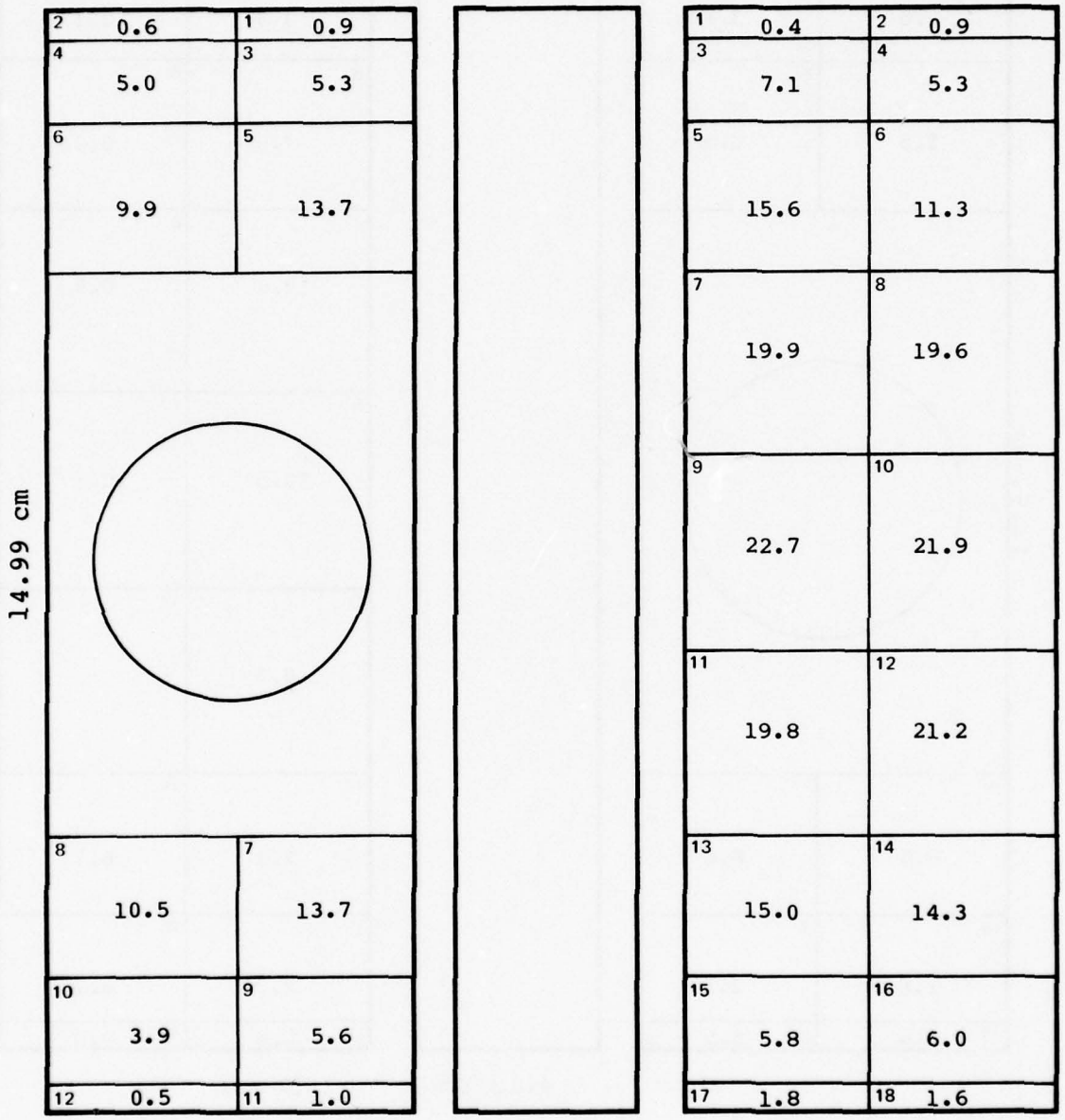
Pulse number 4341



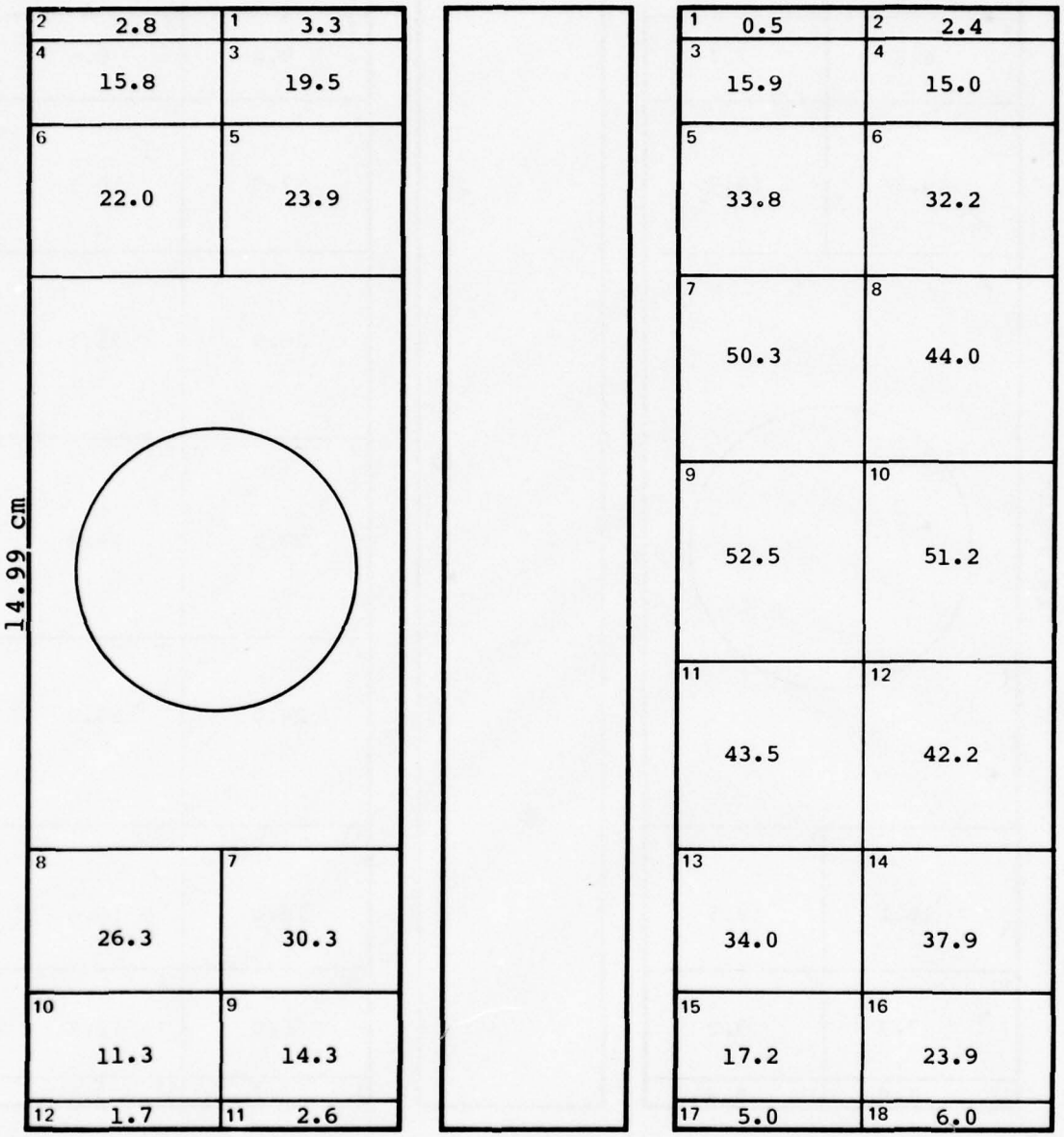
Pulse number 4342



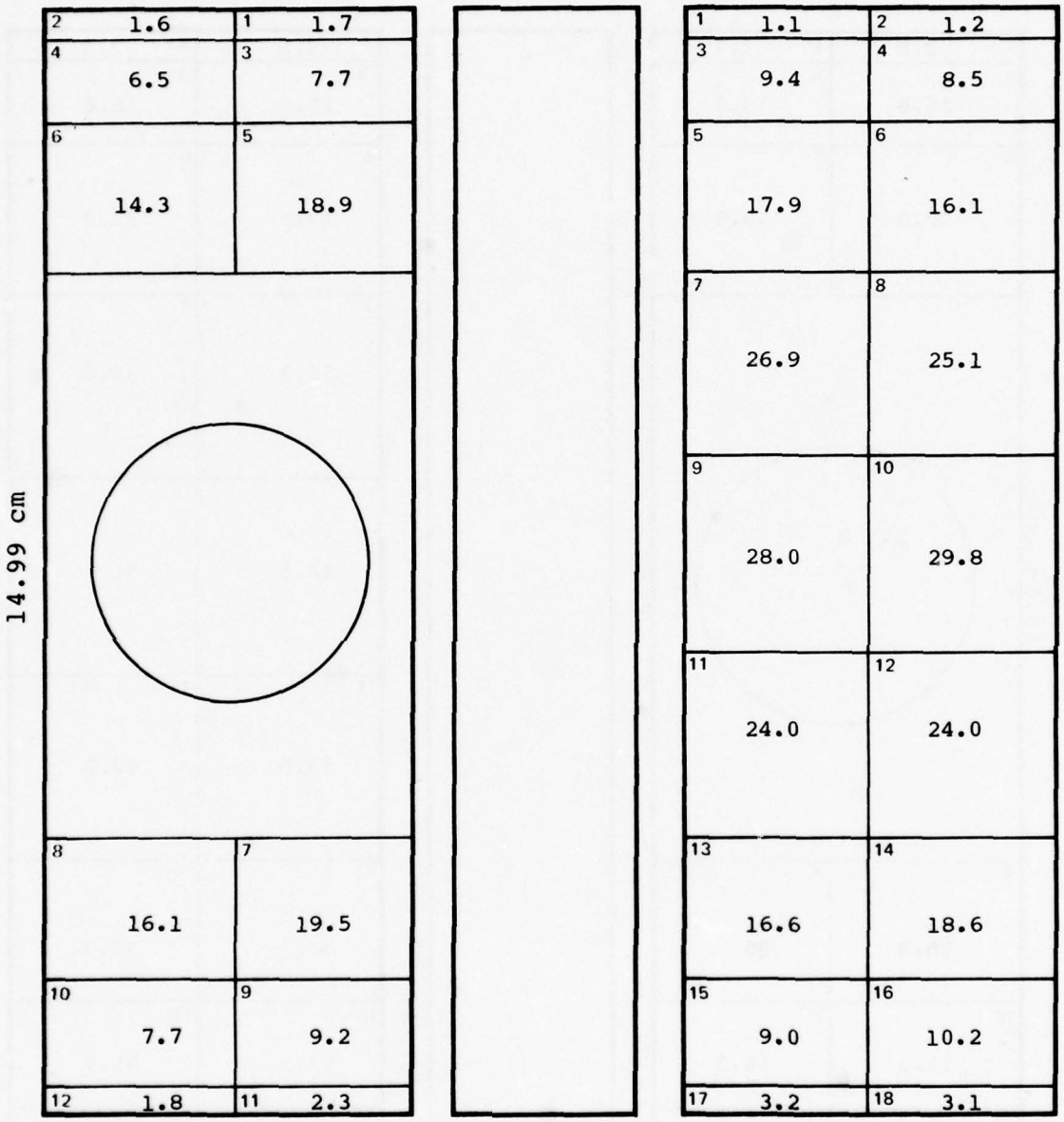
Pulse number 4343



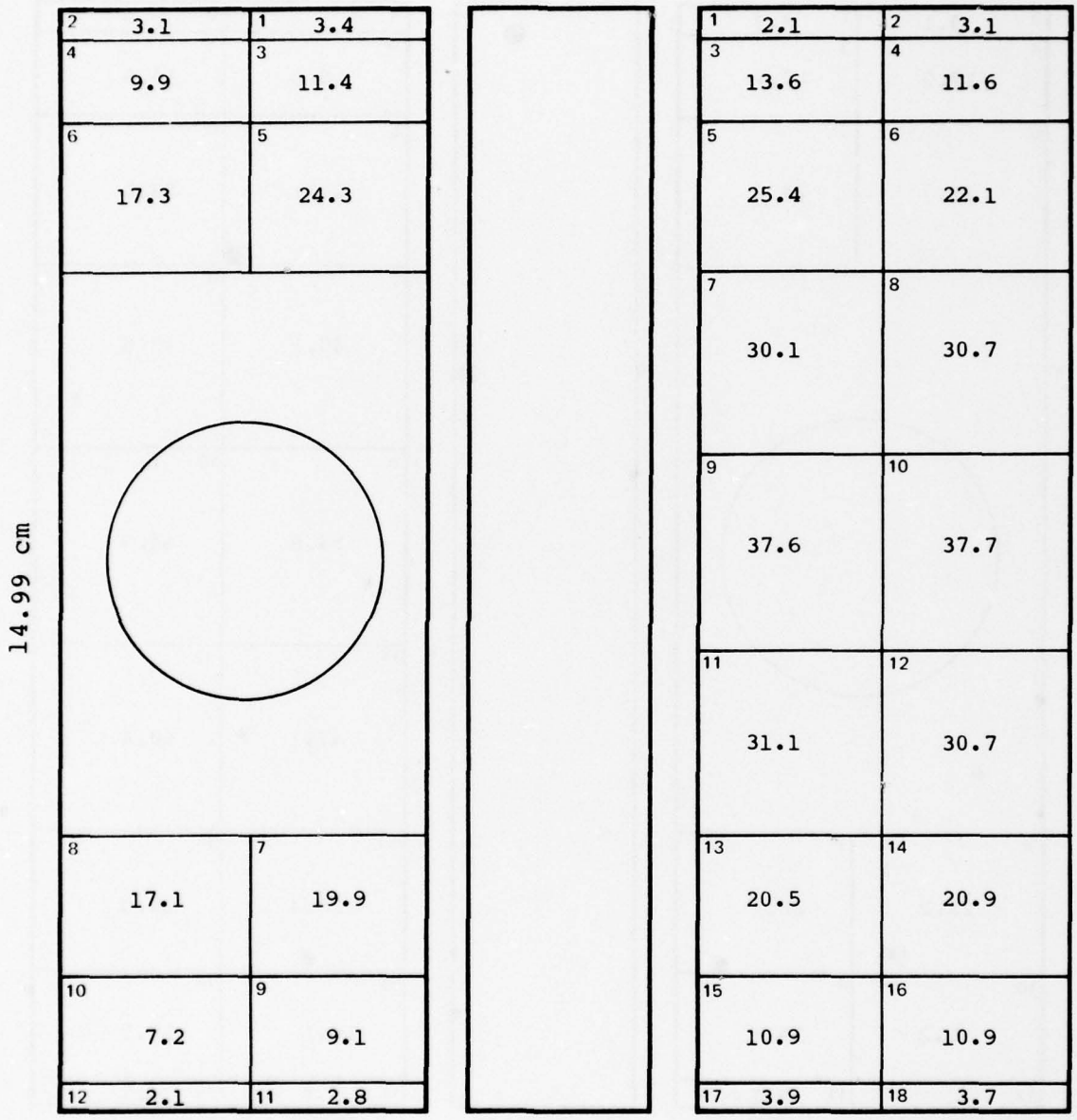
Pulse number 4344



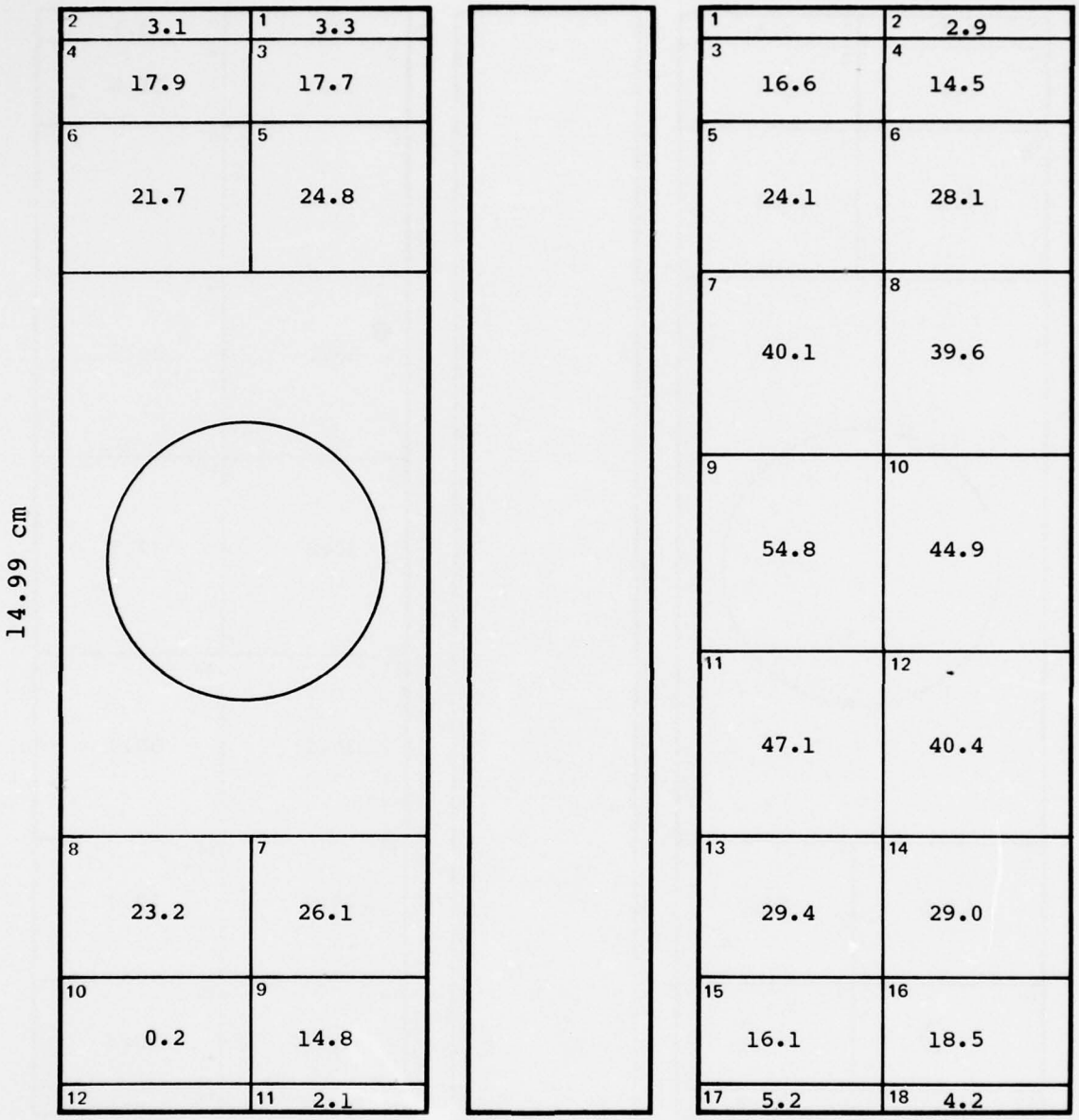
Pulse number 1234



Pulse number 4347



Pulse number 4348



Pulse number 4349

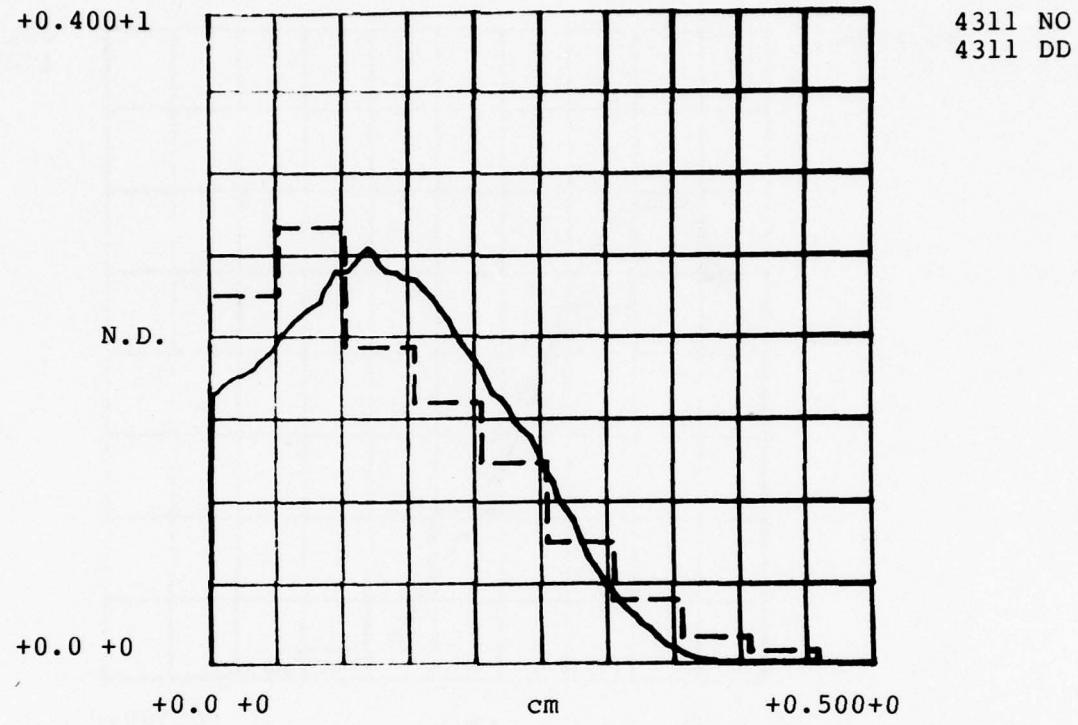
APPENDIX C-1

NORMALIZED DOSE PROFILES IN CARBON



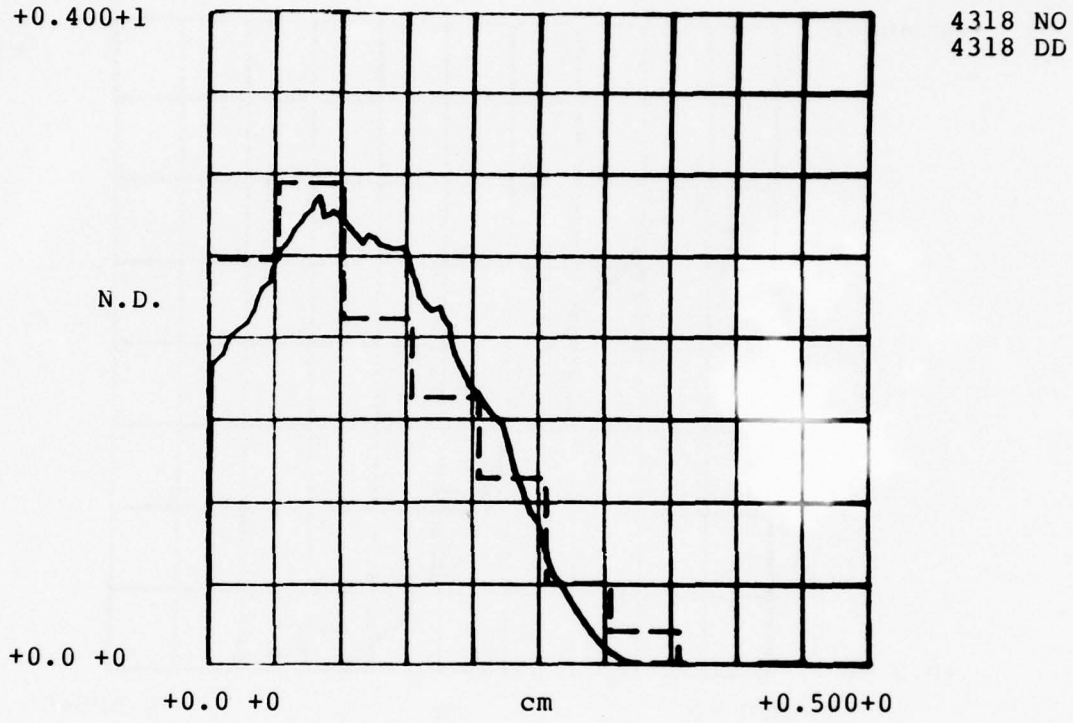
Dashed - Measured

Solid - Calculated



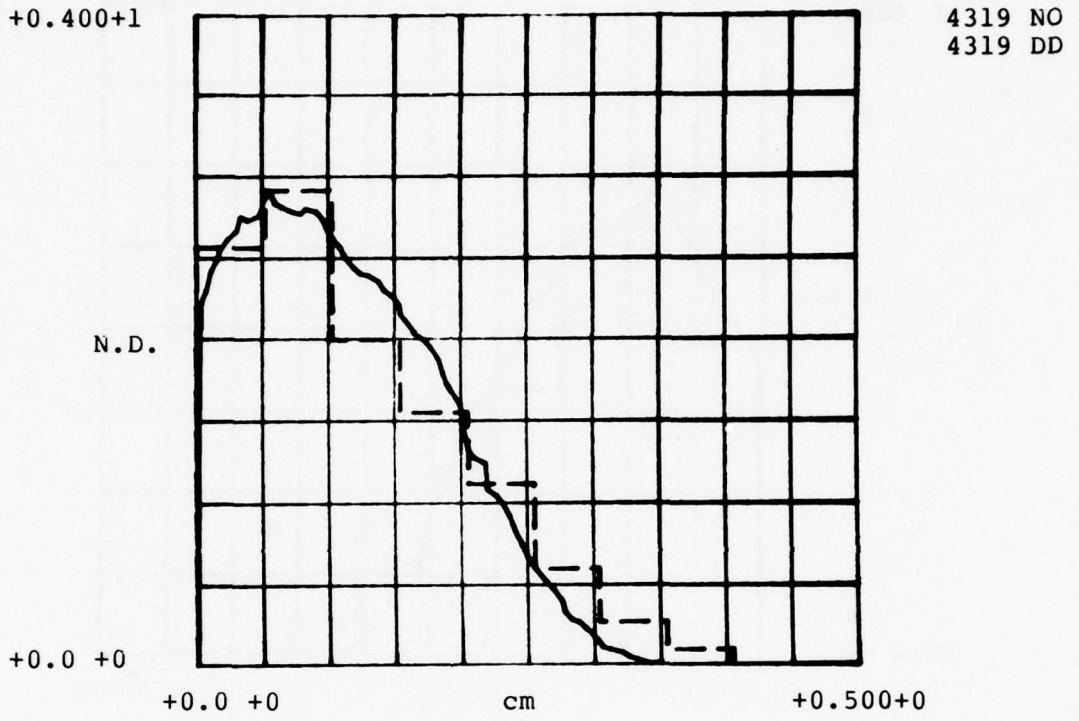
Dashed - Measured

Solid - Calculated



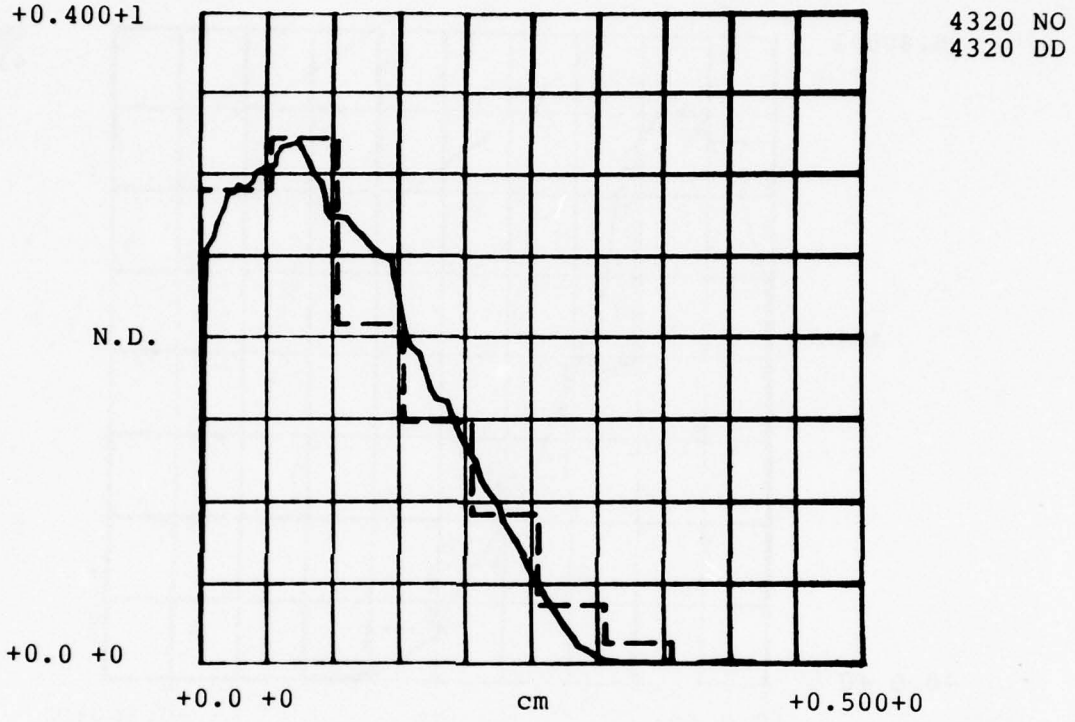
Dashed - Measured

Solid - Calculated



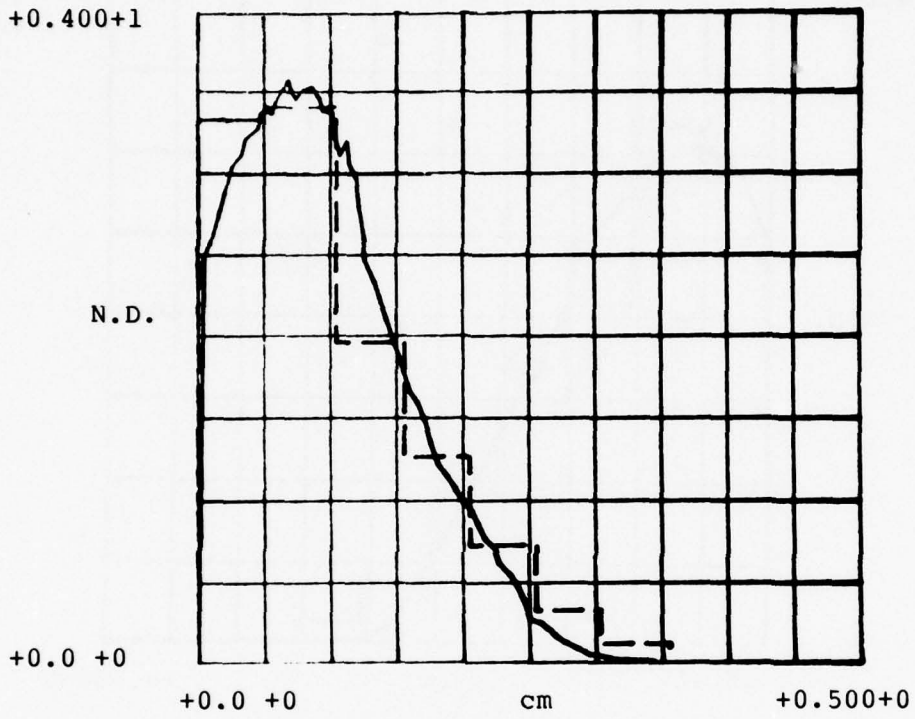
Dashed - Measured

Solid - Calculated



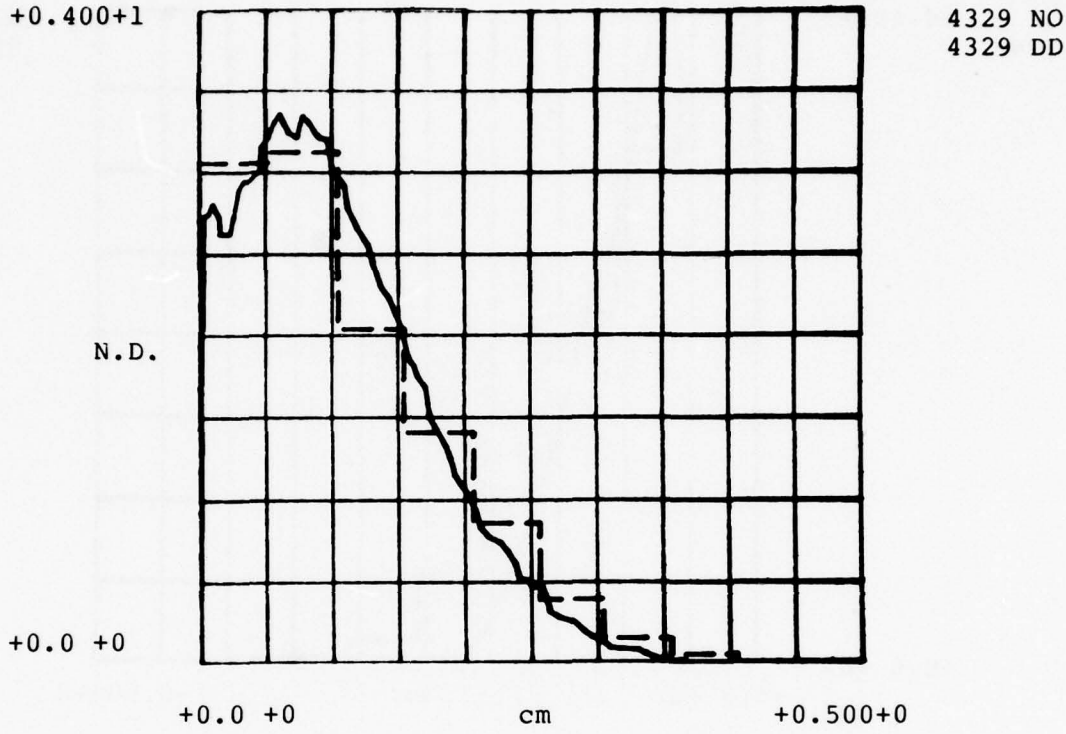
Dashed - Measured

Solid - Calculated

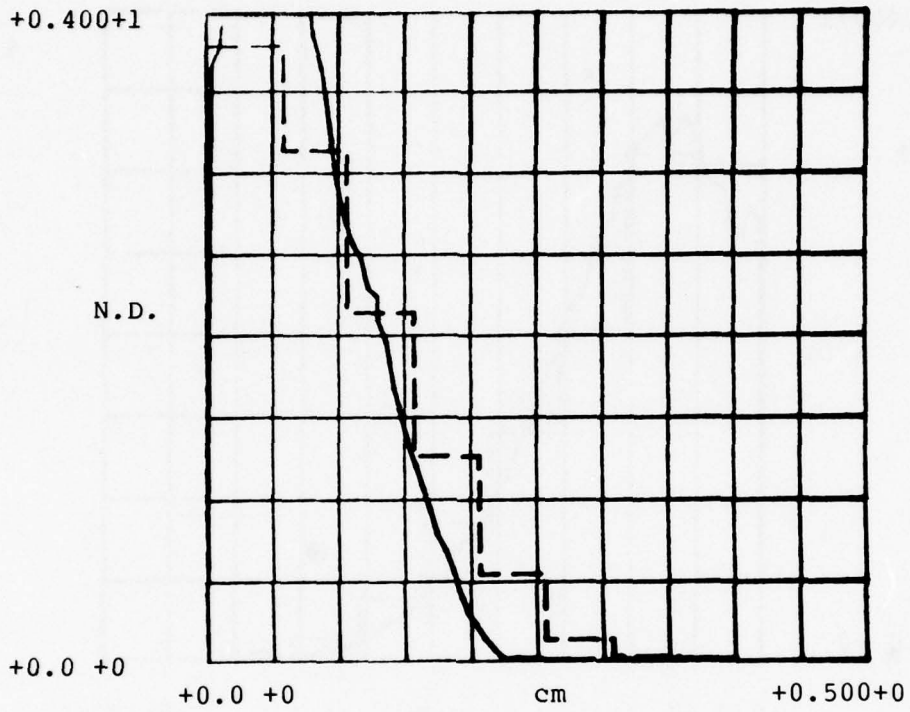


Dashed - Measured

Solid - Calculated

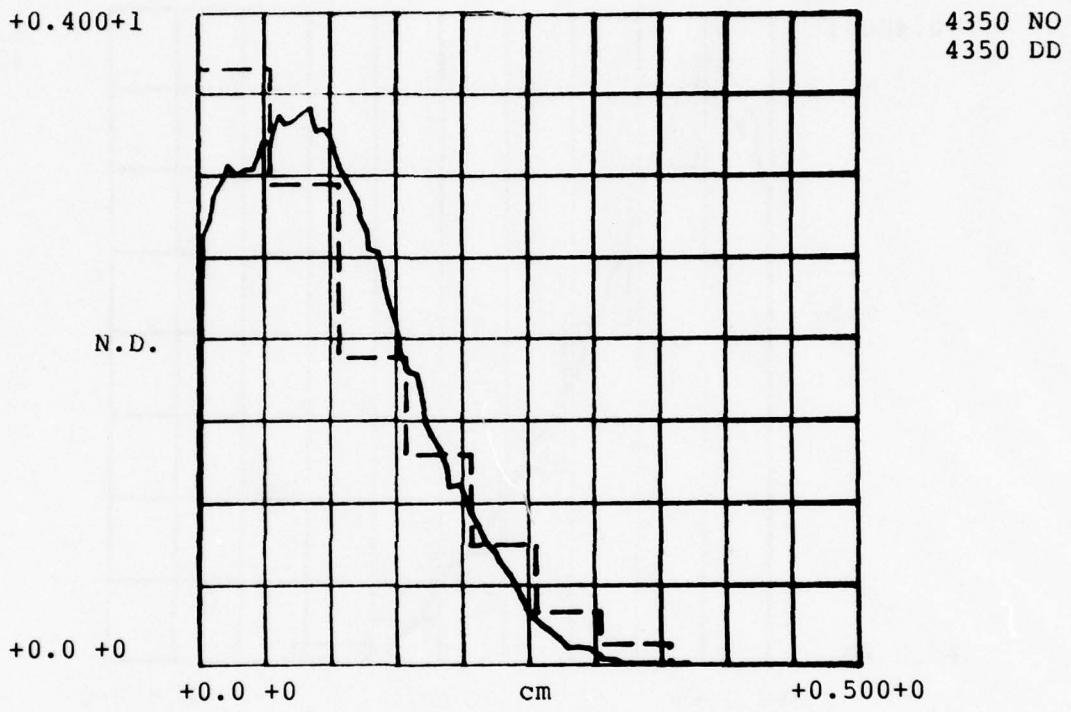


Dashed - Measured
Solid - Calculated



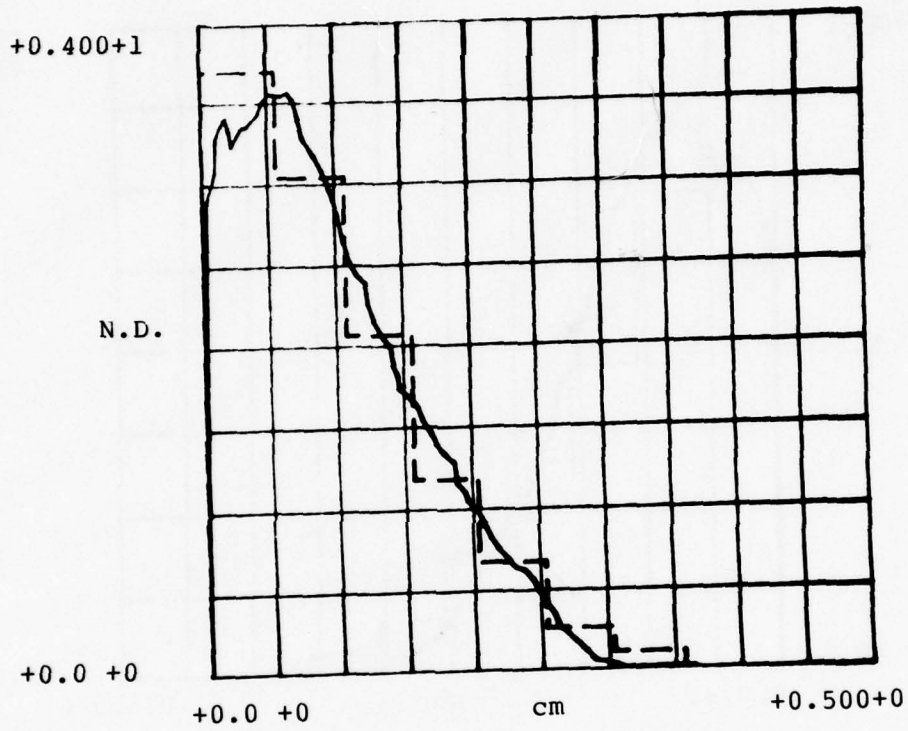
Dashed - Measured

Solid - Calculated



Dashed - Measured

Solid - Calculated



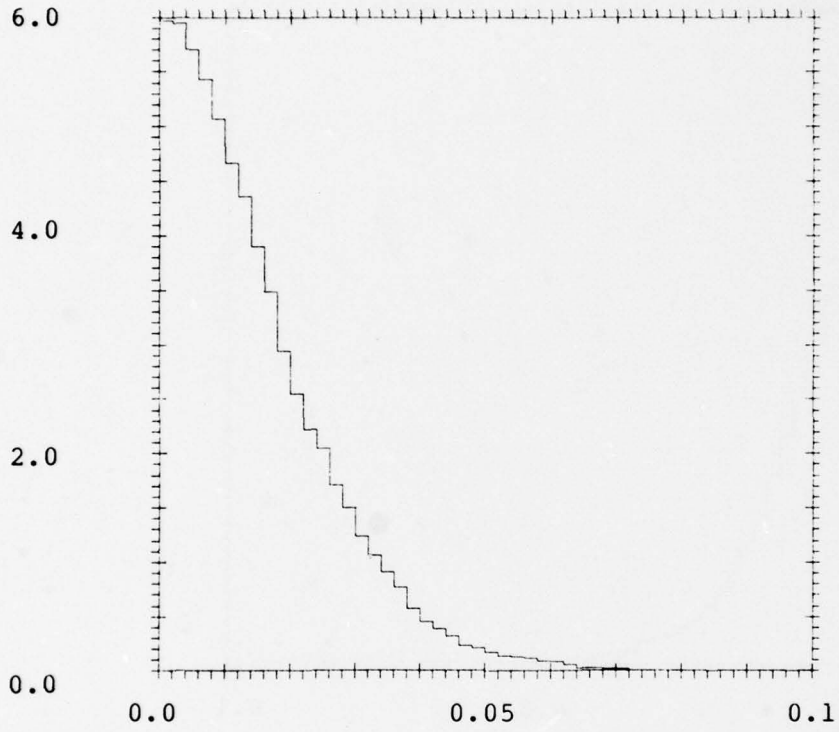
Dashed - Measured

Solid - Calculated

APPENDIX C-2

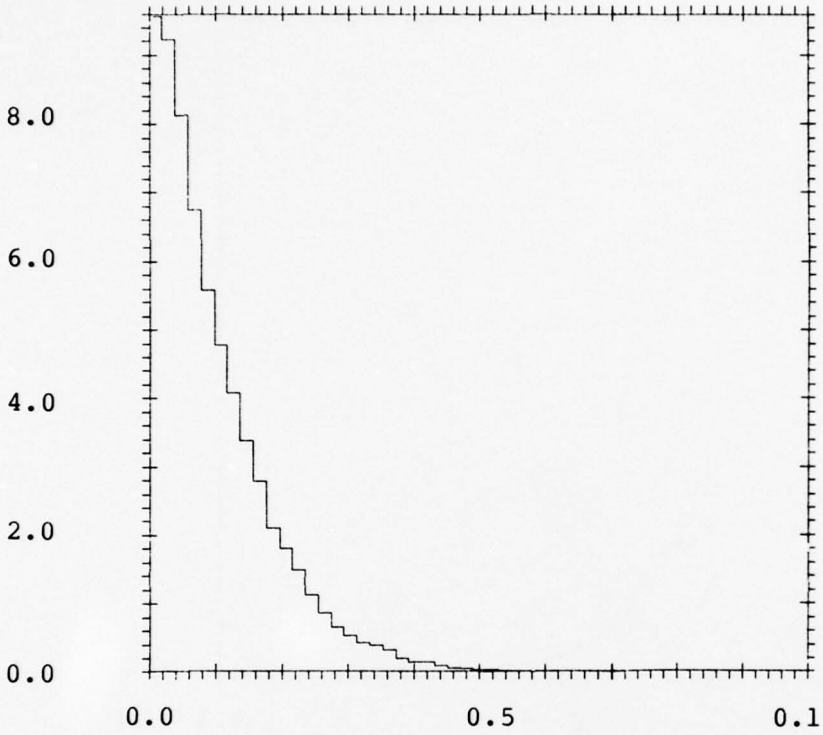
CALCULATED NORMALIZED DOSE PROFILES IN CERMET

Pulse 4312 into Cermet RHO = 7.22

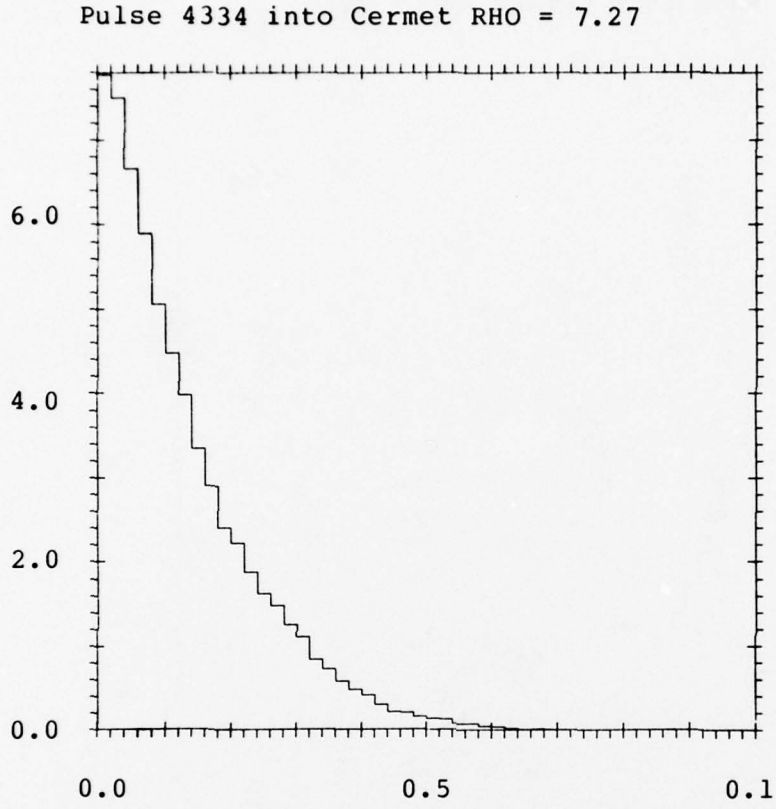


PIEld E Dep. Versus Depth, cos = 0.100E+01, Emean = 0.982E+00

Pulse 4327 into Cermet RHO = 7.33

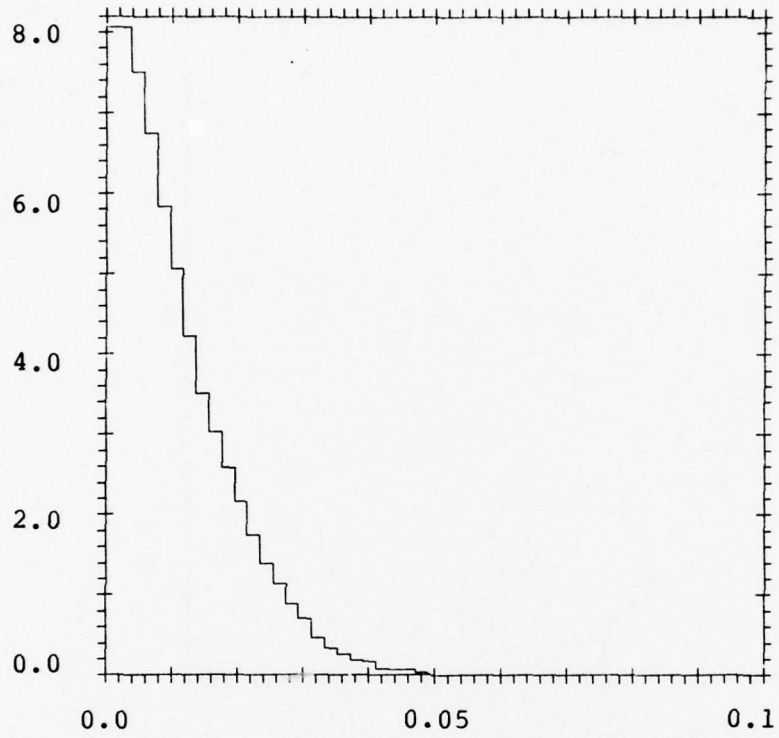


PIEld E Dep. Versus Depth, cos = 0.100E+01, Emean = 0.685E+00



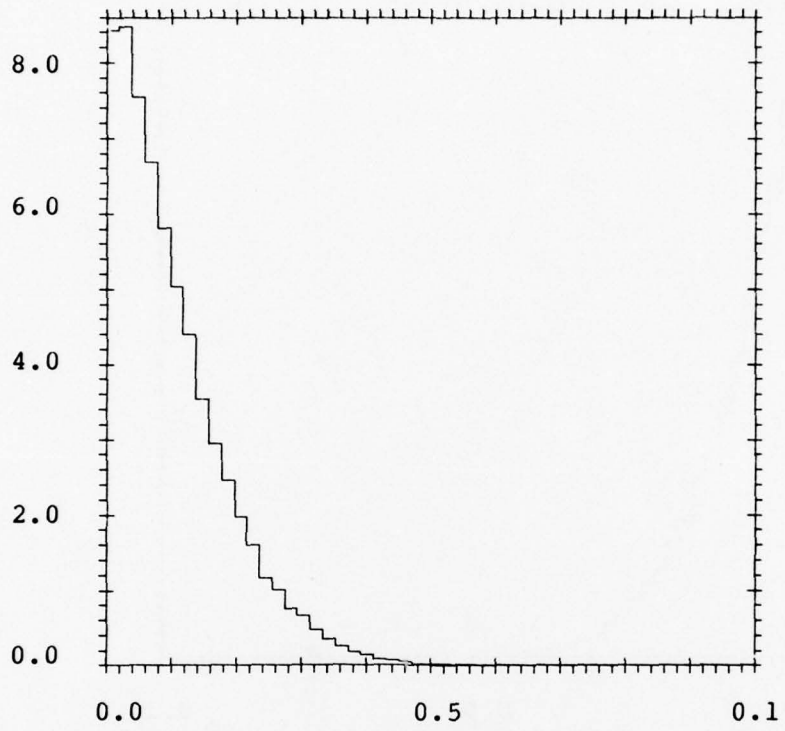
PIEld E Dep. Versus Depth, cos = 0.100E+01, Emean = 0.809E+00

Pulse 4335 into Cermet RHO = 7.37



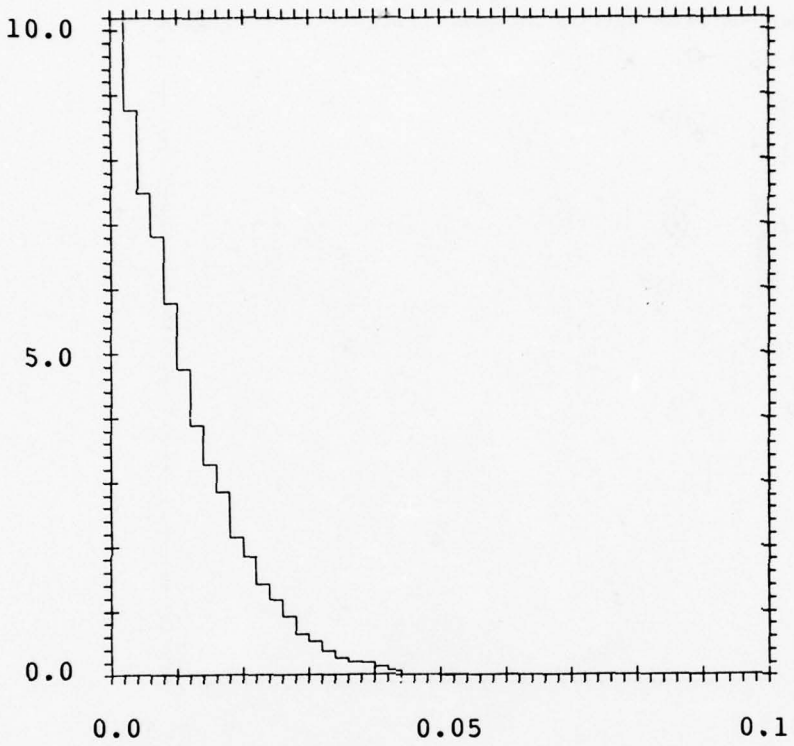
PIEld E Dep. Versus Depth, cos = 0.100E+01, Emean = 0.777E+00

Pulse 4338 into Cermet RHO = 7.39



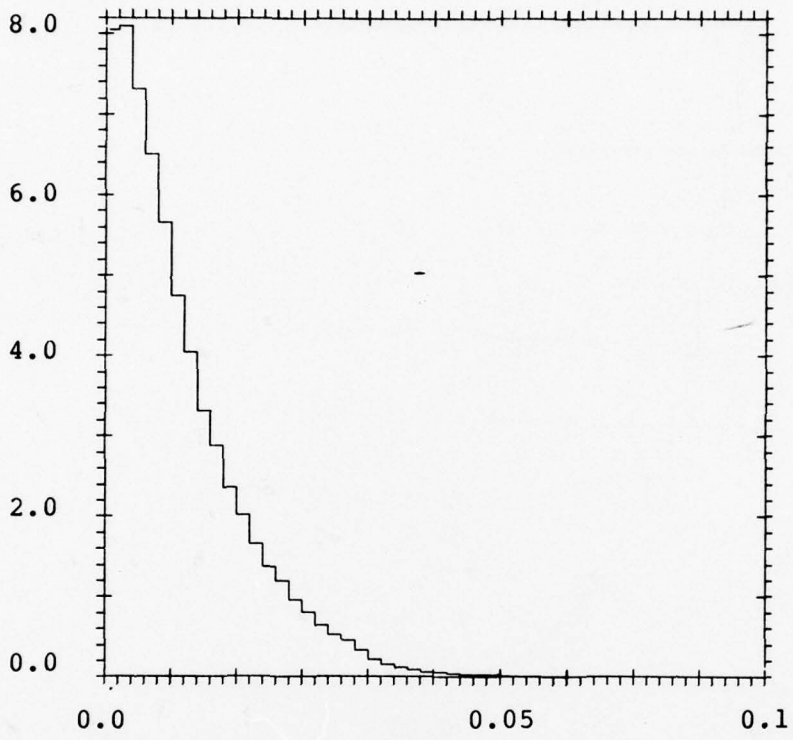
PIEld E Dep. Versus Depth, cos = 0.100E+01, Emean = 0.737E+00

Pulse 4343 into Cermet RHO = 7.29



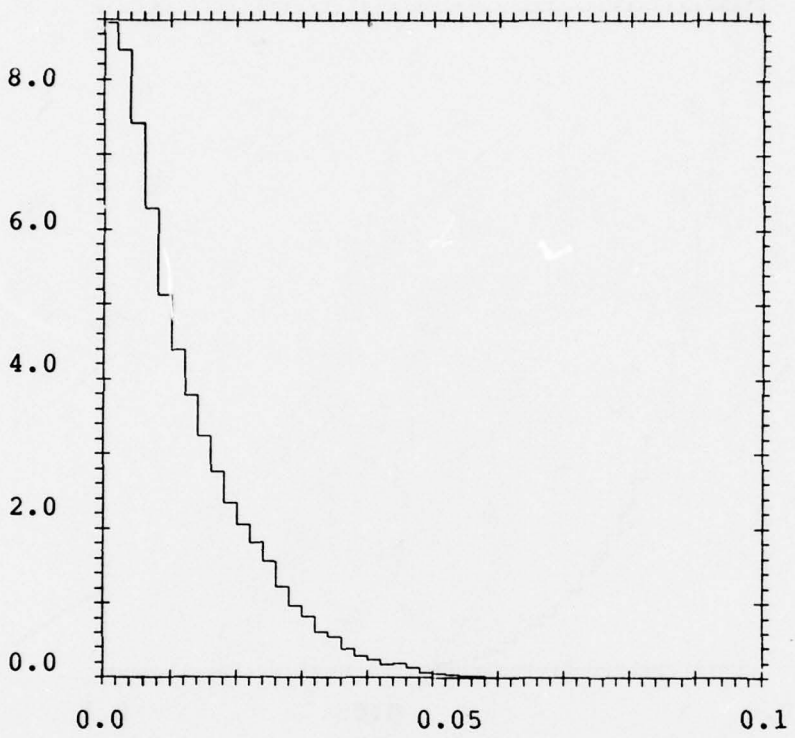
PIEld E Dep. Versus Depth, cos = 0.100E+01, Emean = 0.632E+00

Pulse 4344 into Cermet RHO = 7.9



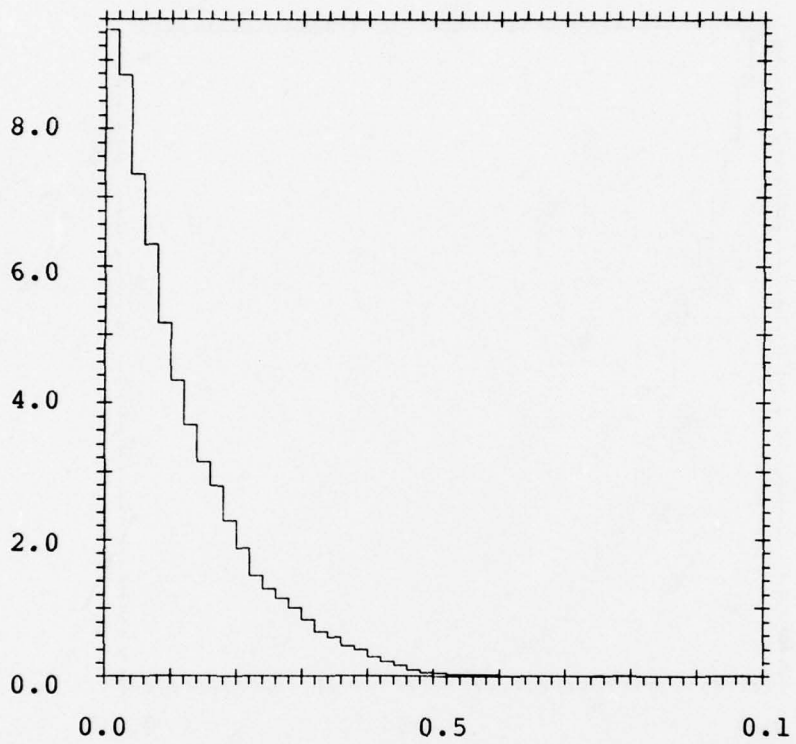
PIElD E Dep. Versus Depth, cos = 0.100E+01, Emean = 0.765E+00

Pulse 4347 into Cermet RHO = 7.29



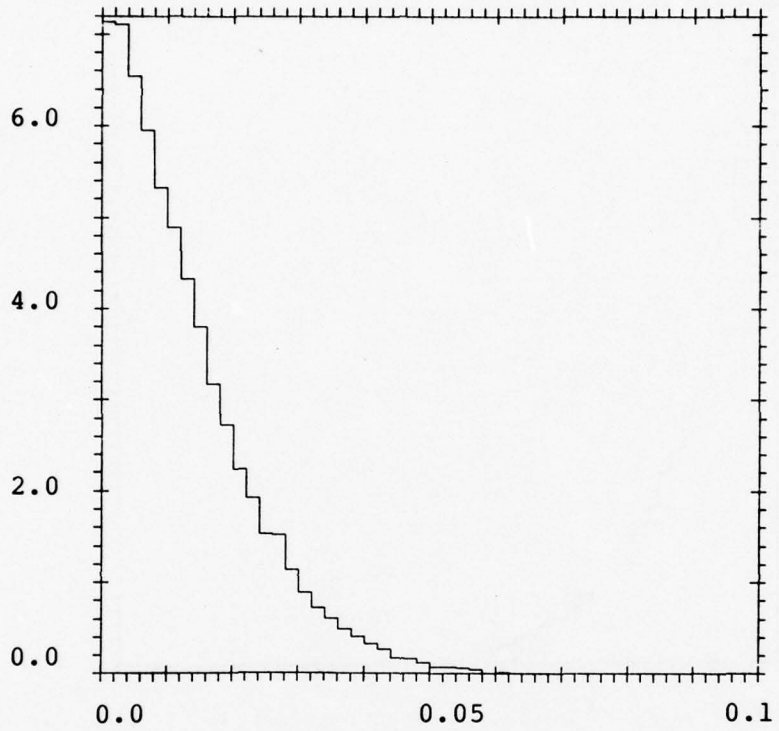
PIEld E Dep. Versus Depth, cos = 0.100E+01, Emean = 0.738E+00

Pulse 4348 into Cermet RHO = 7.29



PIEld E Dep. Versus Depth, cos = 0.100E+01, Emean = 0.686E+00

Pulse 4349 into Cermet RHO = 7.29



PIElD E Dep. Versus Depth, cos = 0.100E+01, Emean = 0.848E+00

APPENDIX D

STRAIN GAUGE RECORDS

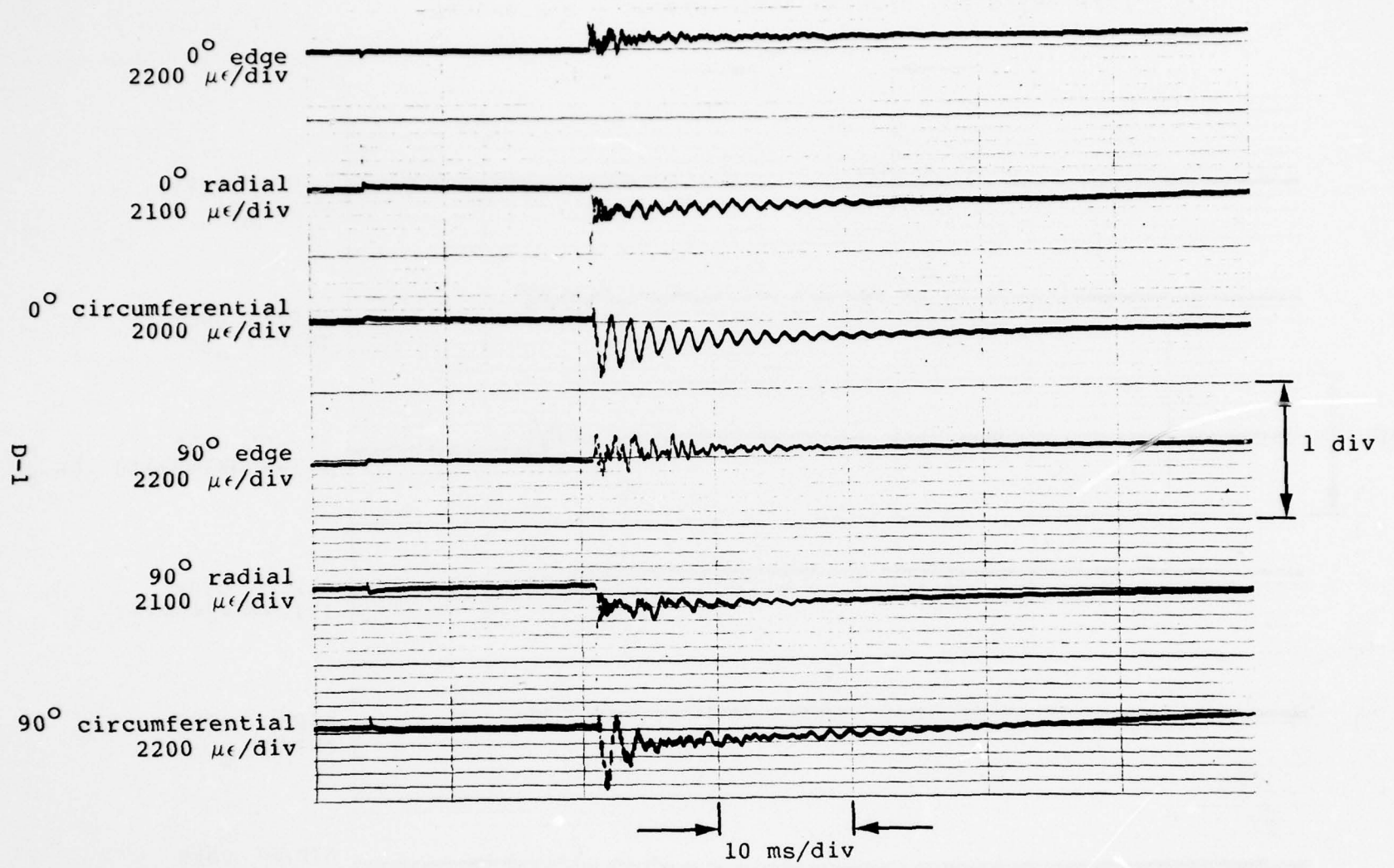


Figure D-1 Strain gauge records for pulse 4312.

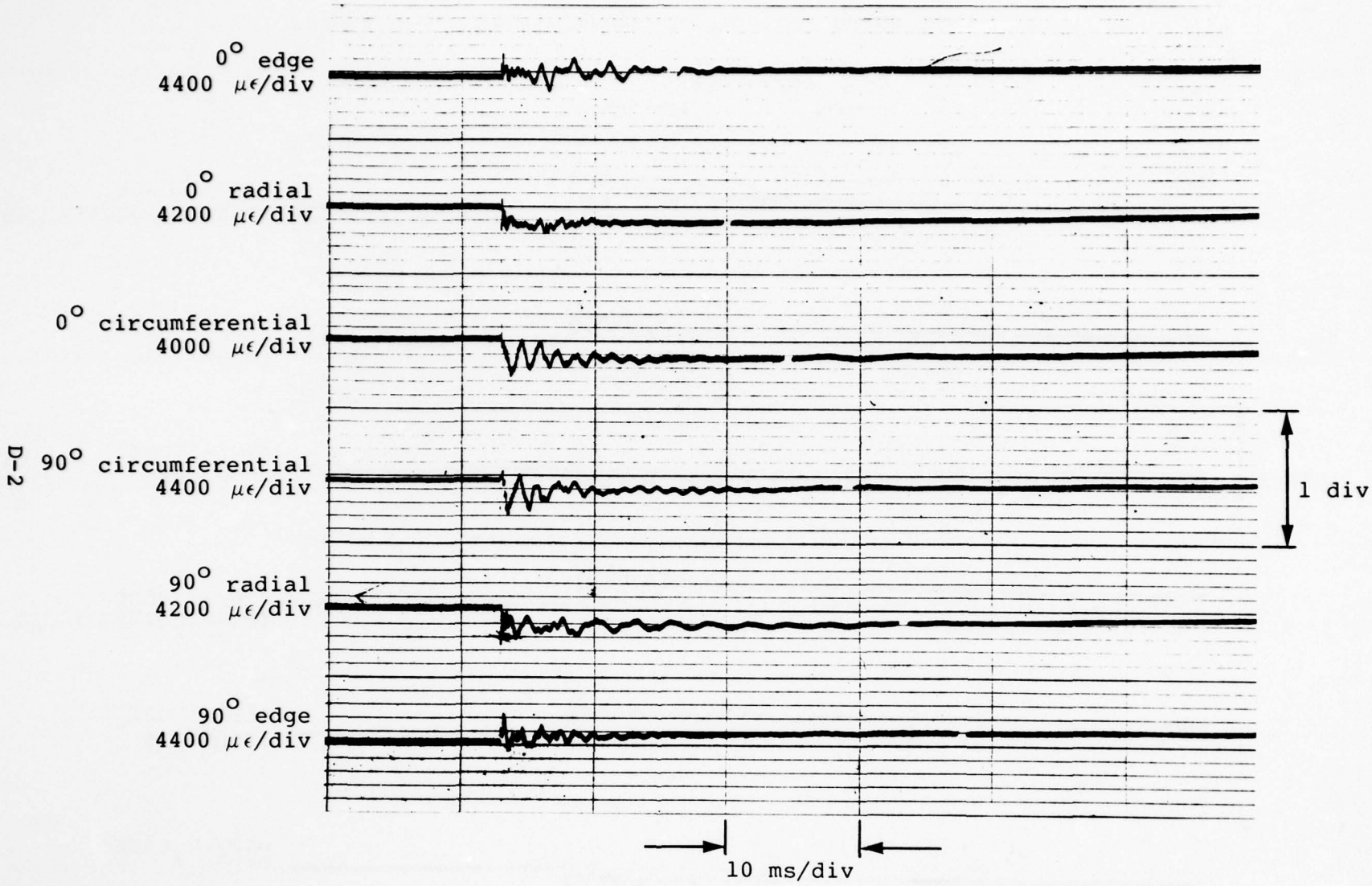


Figure D-2 Strain gauge records for pulse 4327.

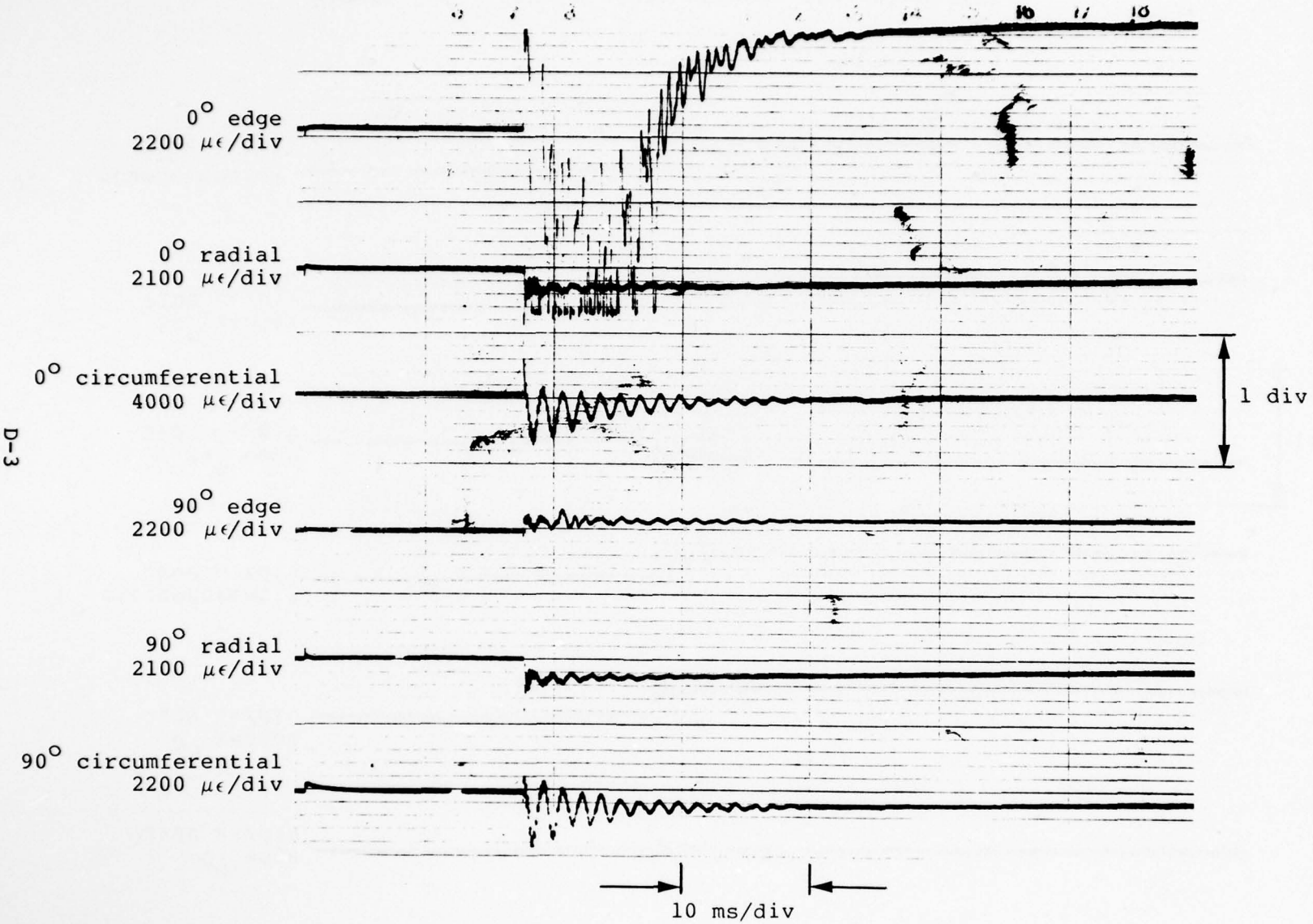


Figure D-3 Strain gauge records for pulse 4334.

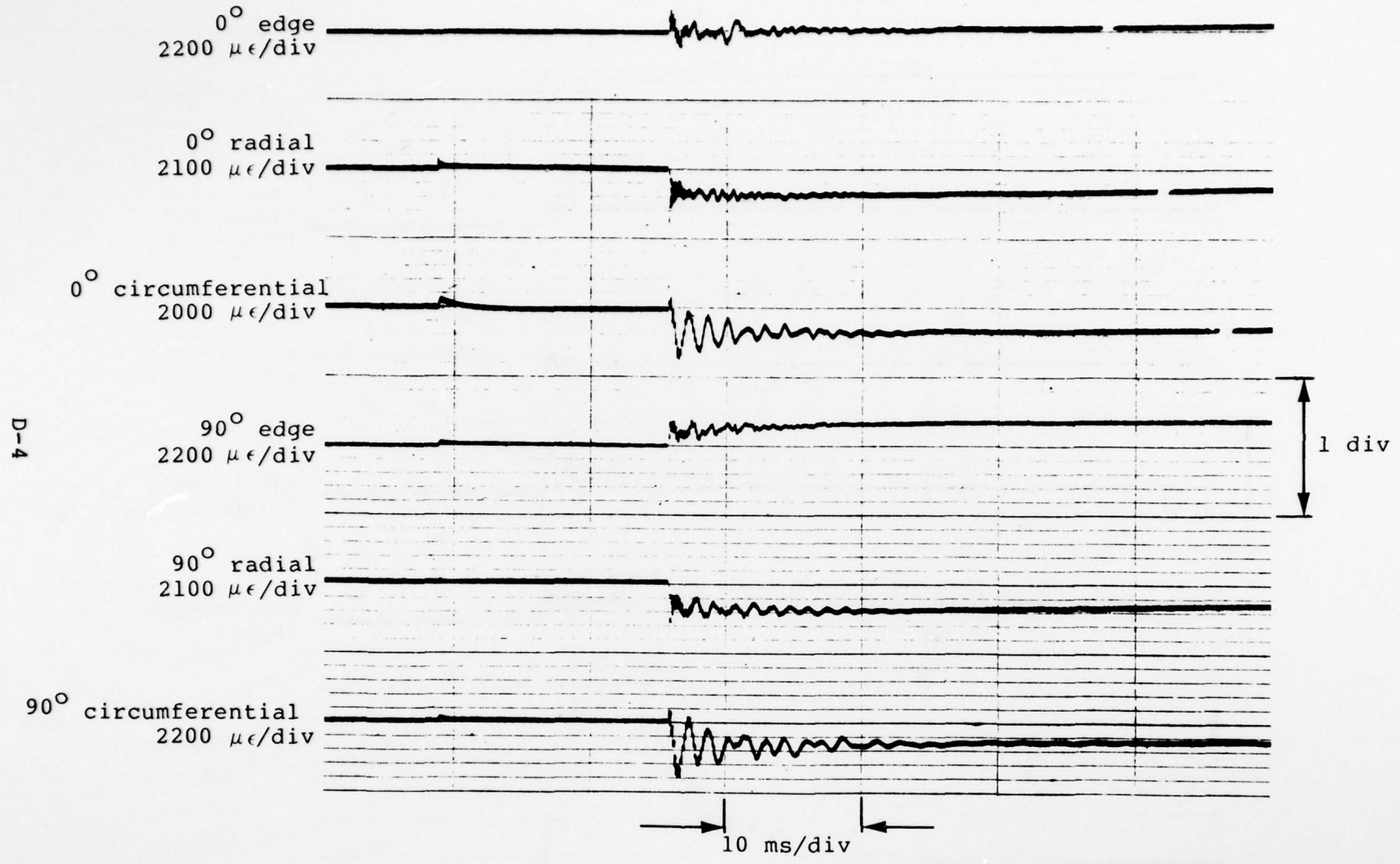
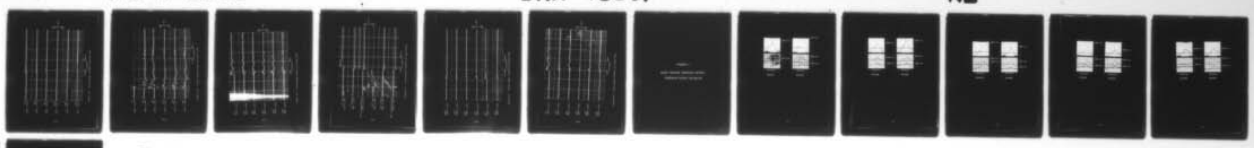


Figure D-4 Strain gauge records for pulse 4335.

AD-A068 496 PHYSICS INTERNATIONAL CO SAN LEANDRO CALIF F/G 11/2
THERMOSTRUCTURAL RESPONSE OF CERMET ANNULI AND RINGS.(U)
NOV 78 E V BUCK, J SHEA DNA001-78-C-0068
UNCLASSIFIED PIFR-1148 DNA-4689F NL

2 OF 2
AD A068496





END
DATE FILMED
6 -79
DDC

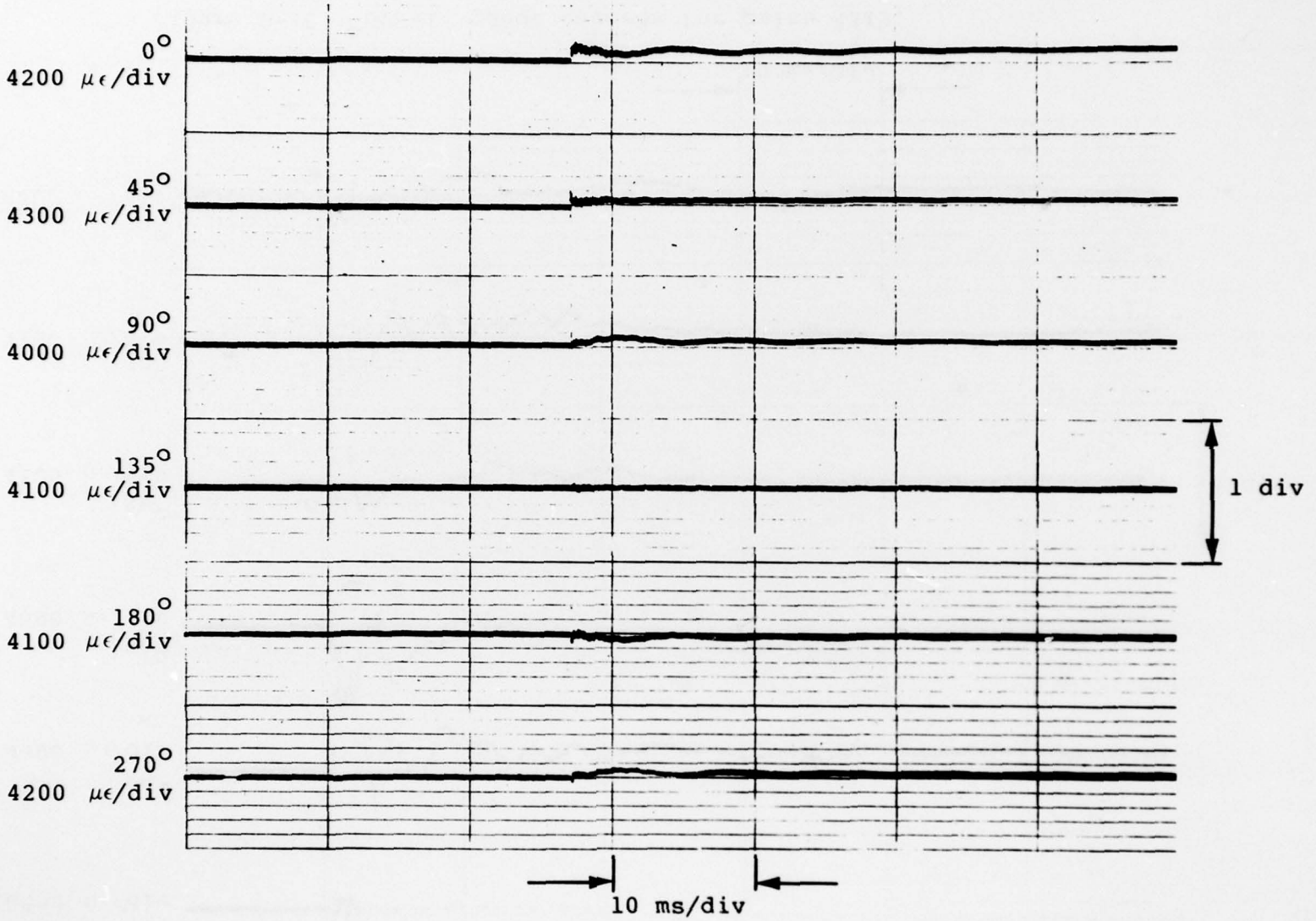


Figure D-6 Strain gauge records for pulse 4343.

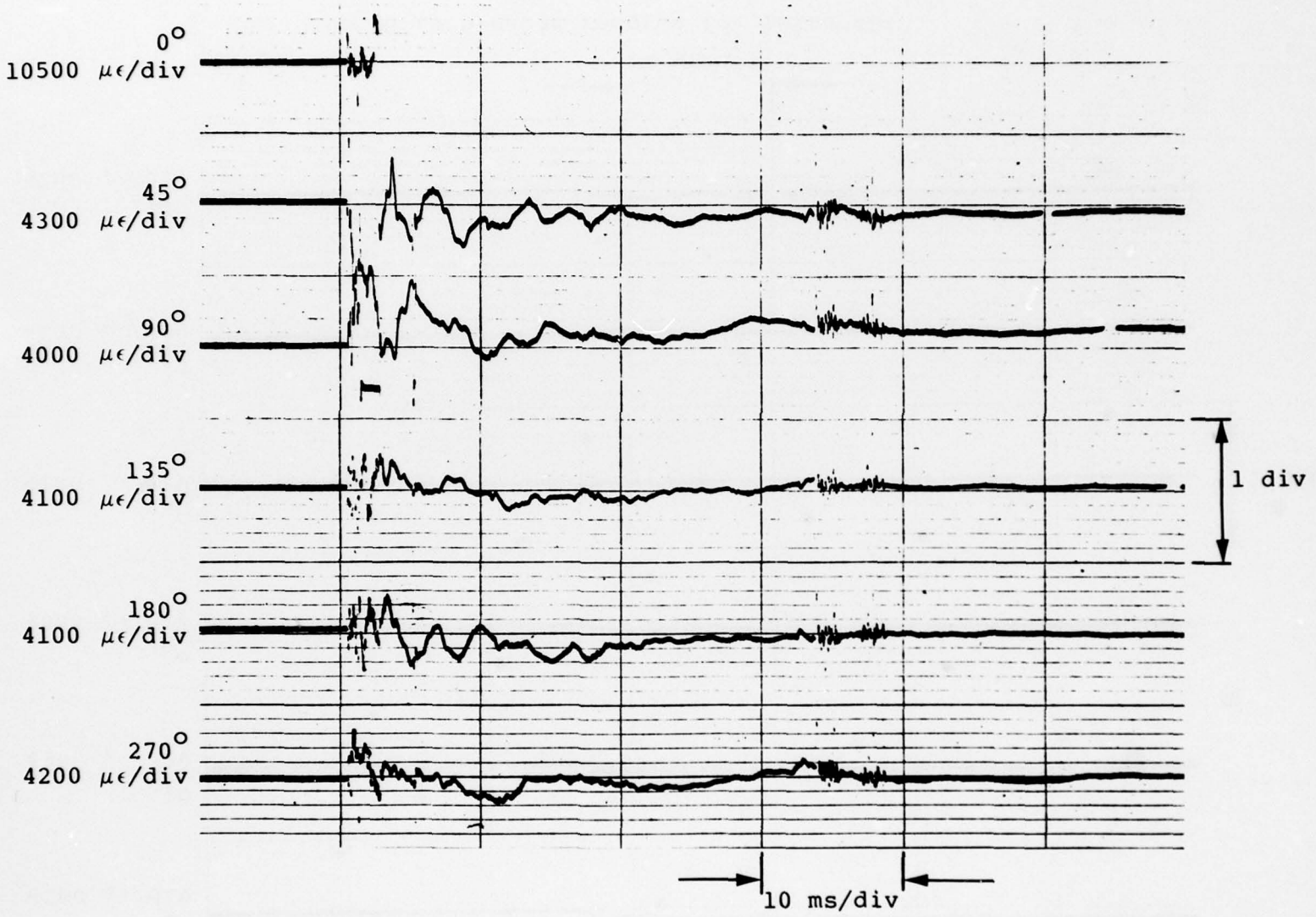


Figure D-10 Strain gauge records for pulse 4349.

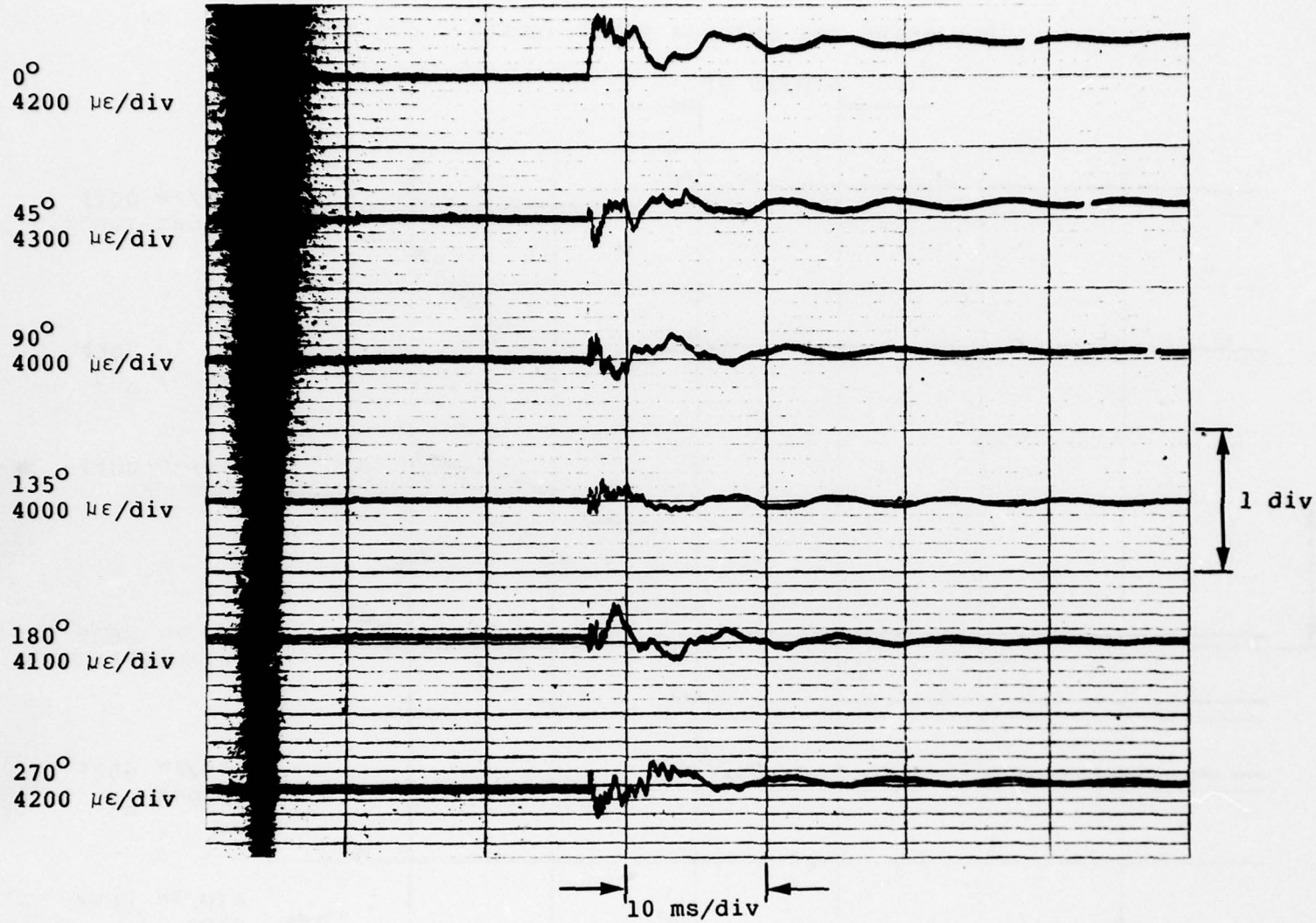


Figure D-8 Strain gauge records for pulse 4347.

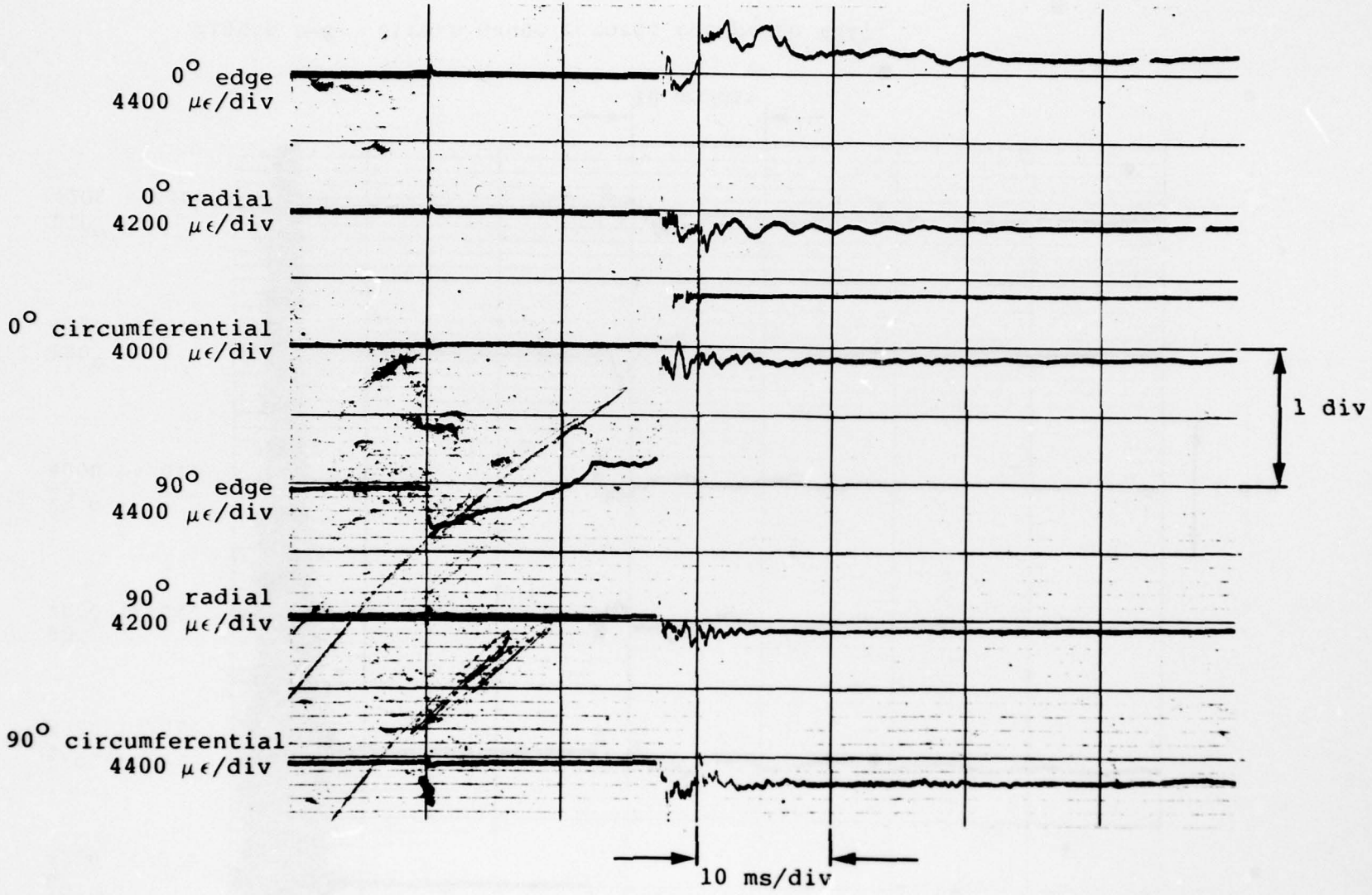


Figure D-5 Strain gauge records for pulse 4338.

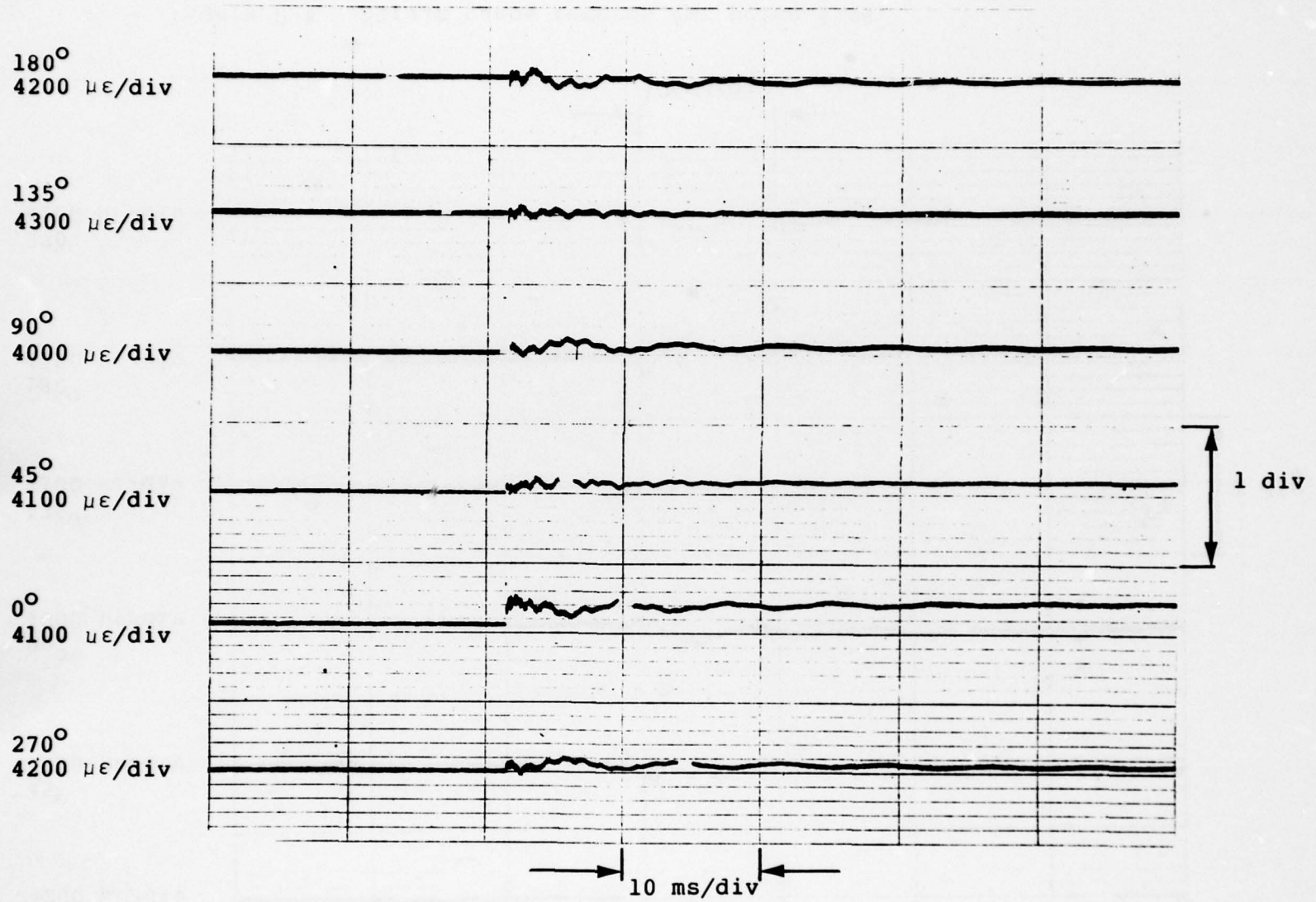


Figure D-7 Strain gauge records for pulse 4344.

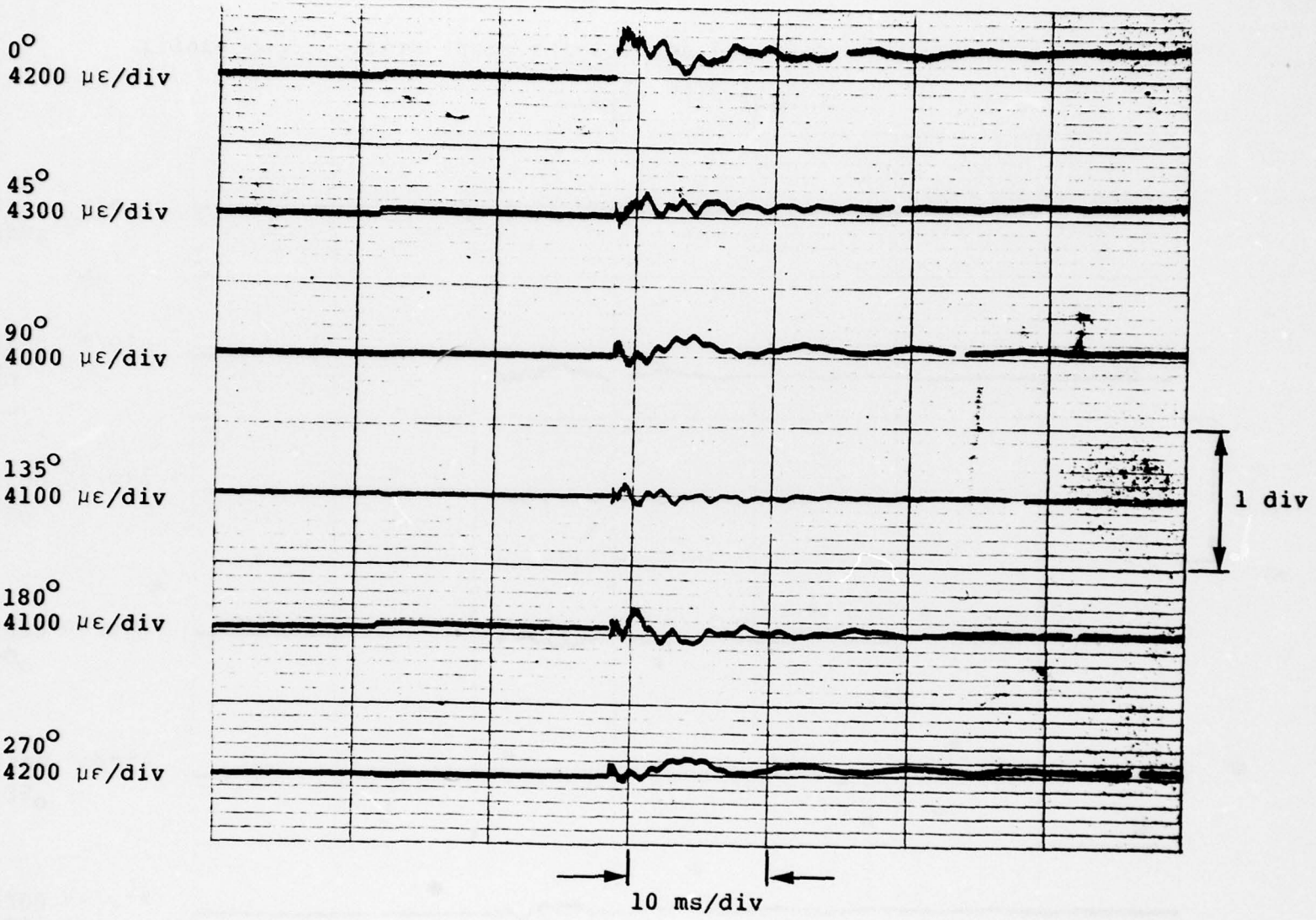
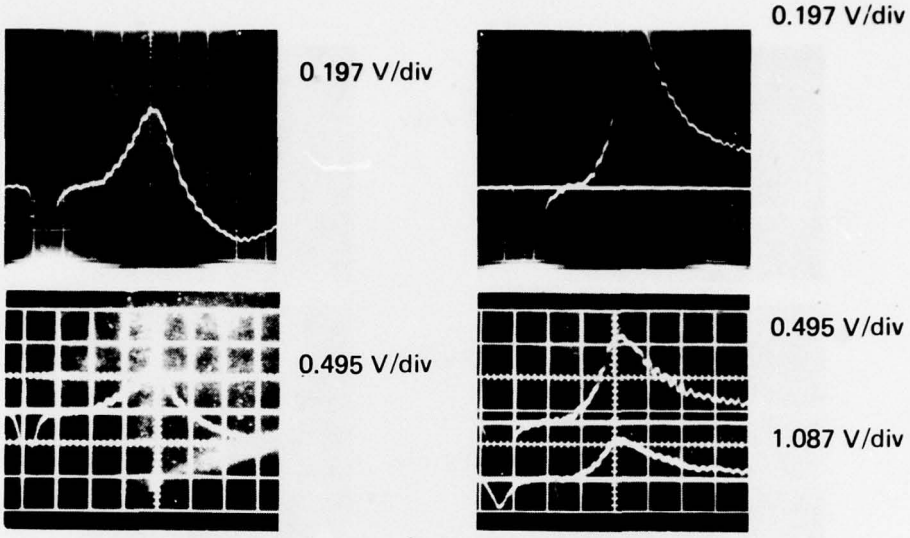


Figure D-8 Strain gauge records for pulse 4348.

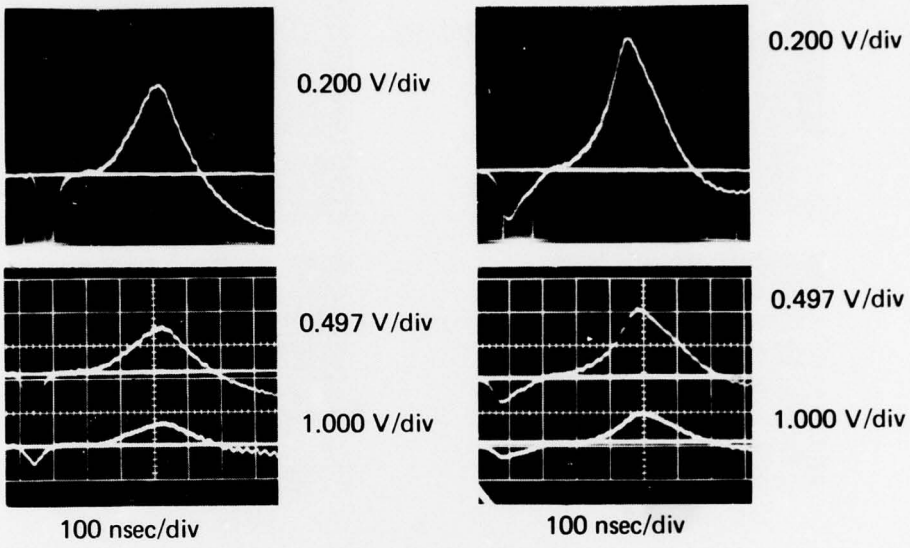
APPENDIX E

QUARTZ PRESSURE TRANSDUCER RECORDS

CONVERSION FACTOR: 0.86 kbar/volt



Pulse 4312 **Pulse 4327**

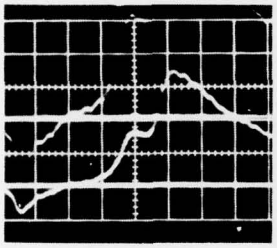


Pulse 4334

Pulse 4335



0.500 V/div

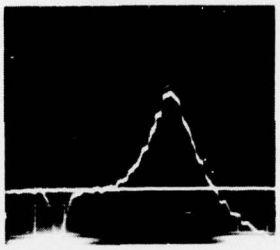


0.497 V/div

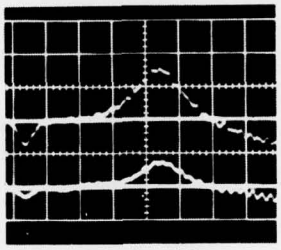
1.000 V/div

100 nsec/div

Pulse 4338



0.200 V/div

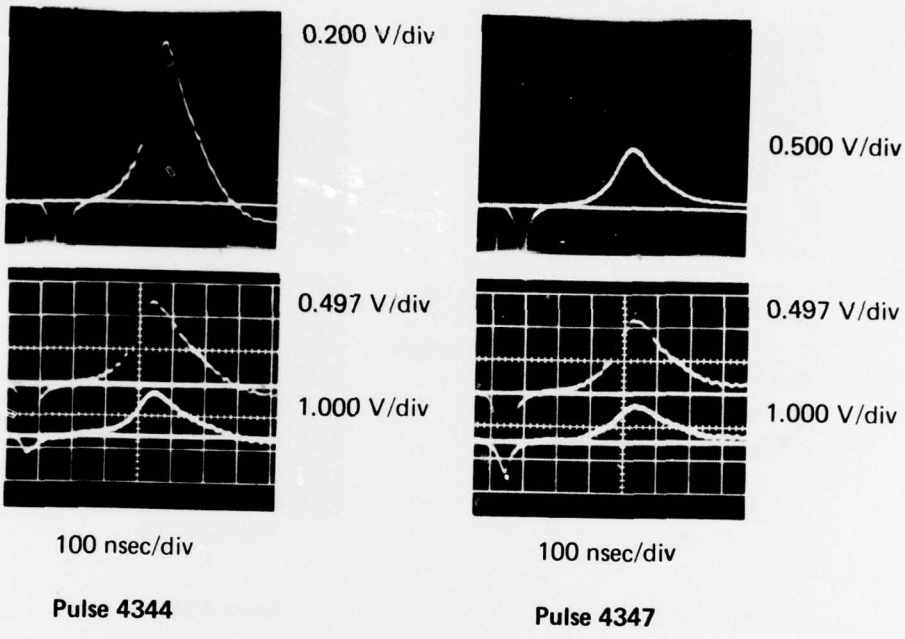


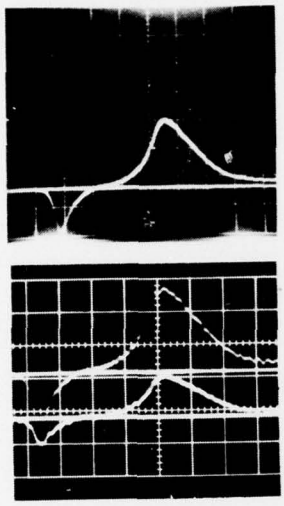
0.497 V/div

1.000 V/div

100 nsec/div

Pulse 4343


0.200 V/div
0.497 V/div
1.000 V/div
100 nsec/div
Pulse 4344
0.500 V/div
0.497 V/div
1.000 V/div
100 nsec/div
Pulse 4347



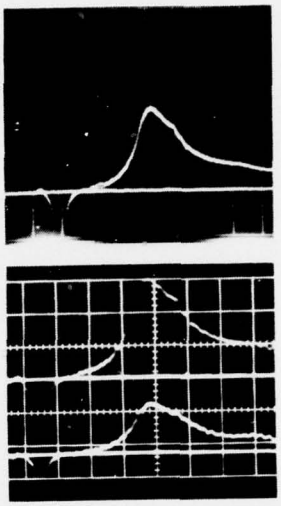
0.500 V/div

0.497 V/div

1.000 V/div

100 nsec/div

Pulse 4348



0.500 V/div

0.497 V/div

1.000 V/div

100 nsec/div

Pulse 4349

DISTRIBUTION LIST

DEPARTMENT OF DEFENSE

Assistant to the Secretary of Defense
Atomic Energy
ATTN: Executive Assistant

Defense Advanced Rsch. Proj. Agency
ATTN: TIO

Defense Documentation Center
12 cy ATTN: DD

Defense Intelligence Agency
ATTN: DT-2

Defense Nuclear Agency
ATTN: SPSS
ATTN: STSP
ATTN: SPTD
ATTN: SPAS
ATTN: DDST
4 cy ATTN: TITL

Field Command
Defense Nuclear Agency
ATTN: FCPR
ATTN: FCTMD

Joint Chiefs of Staff
ATTN: J-5, Nuclear Division
ATTN: SAGA/SFD
ATTN: J-5, Force Planning & Program Div.
ATTN: SAGA/SSD

Joint Strat. Tgt. Planning Staff
ATTN: JPTM
ATTN: JLTW-2

Field Command
Defense Nuclear Agency
Livermore Division
ATTN: FCPRL

Under Secy. of Def. for Rsch. & Engrg.
Department of Defense
ATTN: Strategic & Space Systems (OS)

DEPARTMENT OF THE ARMY

BMD Advanced Technology Center
Huntsville Office
Department of the Army
ATTN: ATC-T, M. Capps

BMD Program Office
Department of the Army
ATTN: Technology Division

BMD Systems Command
Department of the Army
ATTN: BMDSC-H, N. Hurst

Deputy Chief of Staff for Ops. & Plans
Department of the Army
ATTN: Nuclear Plans & Policy

DEPARTMENT OF THE ARMY (Continued)

Deputy Chief of Staff for Rsch. Dev. & Acq.
Department of the Army
ATTN: Nuclear Team

Harry Diamond Laboratories
Department of the Army
ATTN: DELHD-N-P, J. Gwaltney
ATTN: DELHD-N-RBC, D. Schallhorn

U.S. Army Ballistic Research Labs.
ATTN: DRDAR-BLV, W. Schuman, Jr.
ATTN: DRDAR-BLE, J. Keefer
ATTN: DRDAR-BLV, J. Meszaros

U.S. Army Material & Mechanics Rsch. Ctr.
ATTN: DRXMR-HH, J. Dignam

U.S. Army Materiel Dev. & Readiness Cmd.
ATTN: DRCDE-D, L. Flynn

U.S. Army Missile R&D Command
ATTN: DRDMI-TKP, W. Thomas

U.S. Army Nuclear & Chemical Agency
ATTN: Library

U.S. Army Research Office
ATTN: Technical Library

DEPARTMENT OF THE NAVY

Naval Research Laboratory
ATTN: Code 6770, G. Cooperstein
ATTN: Code 2627
ATTN: Code 7908, A. Williams

Naval Sea Systems Command
ATTN: Code 0351
ATTN: 0333A, M. Kinna

Naval Surface Weapons Center
White Oak Laboratory
ATTN: Code F31
ATTN: Code R15, J. Petes
ATTN: Code K06
ATTN: Code K06, C. Lyons

Naval Weapons Evaluation Facility
ATTN: L. Oliver

Office of the Chief of Naval Operations
ATTN: OP-604E, R. Blaise
ATTN: Op-981
ATTN: Op-604

Strategic Systems Project Office
Department of the Navy
ATTN: NSP-273
ATTN: NSP-272

DEPARTMENT OF THE AIR FORCE

Aeronautical Systems Division, AFSC
ATTN: ENFTV

DEPARTMENT OF THE AIR FORCE (Continued)

Air Force Materials Laboratory, AFSC
ATTN: MBC, D. Schmidt
ATTN: MBE, G. Schmitt
ATTN: T. Nicholas

Air Force Rocket Propulsion Laboratory, AFSC
ATTN: LKCP, G. Beale

Air Force Systems Command
ATTN: XRTO
ATTN: SOSS

Air Force Weapons Laboratory, AFSC
ATTN: DYS
ATTN: DYV
ATTN: NT
ATTN: DYT
ATTN: SUL

Deputy Chief of Staff
Research, Development, & Acq.
Department of the Air Force
ATTN: AFRDQSM
ATTN: AFRD

Foreign Technology Division, AFSC
ATTN: TQTD
ATTN: SDBS, J. Pumphrey
ATTN: SDBG

Space & Missile Systems Organization
Air Force Systems Command
ATTN: DYS

Space & Missile Systems Organization
Air Force Systems Command
ATTN: MNNR
ATTN: MNNH

Space & Missile Systems Organization
Air Force Systems Command
ATTN: RSMA
ATTN: RSS
ATTN: RSSE

Strategic Air Command
Department of the Air Force
ATTN: XPQM
ATTN: XPFS
ATTN: DOXT
ATTN: XOBM

DEPARTMENT OF ENERGY

Department of Energy
ATTN: Office of Military Application
(Res & Dev. Branch)

DEPARTMENT OF DEFENSE CONTRACTORS

Acurex Corp.
ATTN: J. Huntington

Aerospace Corp.
ATTN: W. Barry
ATTN: R. Crolius
ATTN: R. Mortensen
ATTN: W. Mann
ATTN: R. Strickler

DEPARTMENT OF DEFENSE CONTRACTORS (Continued)

Avco Research & Systems Group
ATTN: W. Broding
ATTN: J. Gilmore
ATTN: P. Grady
ATTN: J. Stevens
ATTN: G. Weber
ATTN: Document Control

Battelle Memorial Institute
ATTN: M. Vanderlind

Boeing Co.
ATTN: B. Lempriere

California Research & Technology, Inc.
ATTN: K. Kreyenhagen

Effects Technology, Inc.
ATTN: R. Parrise/M. Rosen
ATTN: R. Wengler/R. Bick

Ford Aerospace & Communications Corp.
ATTN: P. Spangler

General Electric Co.
Space Division
ATTN: G. Harrison
ATTN: D. Edelman

General Electric Co.
Re-Entry & Environmental Systems Div.
ATTN: P. Cline

General Electric Co.-TEMPO
Center for Advanced Studies
ATTN: DASIAC

General Research Corp.
Santa Barbara Division
ATTN: R. Rosenthal

Institute for Defense Analyses
ATTN: Classified Library
ATTN: J. Bengston

Ion Physics Corp.
ATTN: R. Evans

Kaman AviDyne
Division of Kaman Sciences Corp.
ATTN: R. Ruetenik

Kaman Sciences Corp.
ATTN: R. Sachs/R. O'Keefe
ATTN: F. Shelton
ATTN: T. Meagher

Lawrence Livermore Laboratory
University of California
ATTN: L-92, C. Taylor
ATTN: L-125, J. Keller
ATTN: D. Hanner
ATTN: L-96, L. Woodruff

Lockheed Missiles & Space Co., Inc.
ATTN: O. Burford
ATTN: R. Walls

DEPARTMENT OF DEFENSE CONTRACTORS (Continued)

Lockheed Missiles and Space Co., Inc.
ATTN: F. Borgardt

Lockheed Missiles and Space Co., Inc.
ATTN: T. Fortune

Los Alamos Scientific Laboratory
ATTN: R. Skaggs
ATTN: J. McQueen/J. Taylor
ATTN: D. Shover
ATTN: R. Dingus

Martin Marietta Corp.
Orlando Division
ATTN: L. Kinnaird

McDonnell Douglas Corp
ATTN: L. Cohen
ATTN: H. Berkowitz
ATTN: M. Schneider
ATTN: J. Peck

Pacific-Sierra Research Corp.
ATTN: G. Lang

Physics International Co.
ATTN: J. Shea
ATTN: V. Buck

Prototype Development Associates, Inc.
ATTN: J. McDonald
ATTN: N. Harrington

R & D Associates
ATTN: W. Graham, Jr.
ATTN: P. Rausch
ATTN: C. MacDonald
ATTN: F. Field

Rand Corp.
ATTN: R. Rapp

DEPARTMENT OF DEFENSE CONTRACTORS (Continued)

Sandia Laboratories
Livermore Laboratory
ATTN: T. Gold
ATTN: H. Norris, Jr.

Sandia Laboratories
ATTN: M. Cowan
ATTN: R. Boade
ATTN: C. Mehl
ATTN: C. Broyles

Science Applications, Inc.
ATTN: O. Nance
ATTN: W. Yengst

Science Applications, Inc.
ATTN: W. Seebaugh
ATTN: W. Layson

Southern Research Institute
ATTN: C. Pears

SRI International
ATTN: H. Lindberg
ATTN: D. Curran
ATTN: G. Abrahamson

Systems, Science & Software, Inc.
ATTN: T. McKinley
ATTN: G. Gurtman
ATTN: R. Duff

Terra Tek, Inc.
ATTN: S. Green

TRW Defense & Space Sys. Group
ATTN: J. Farrel
ATTN: W. Wood
2 cy ATTN: P. Dai/D. Jortner

TRW Defense & Space Sys. Group
San Bernardino Operations
ATTN: L. Berger
ATTN: V. Blankenship
ATTN: W. Polich